A Novel Microscopic Assay of Transient Platelet - von Willebrand Factor Adhesion, Kinetics, Margination, and Blood Rheology

A Thesis

Submitted to the Faculty

of

Drexel University

by

Chang-Beom Kim

in partial fulfillment of the

requirements for the degree

of

Doctor of Philosophy

September 2006

Acknowledgments

I wish to express my hearty gratitude to Dr. David M. Wootton, for his guidance and inspiration during the time of my graduate study and research. I also appreciate to Dr. J. Yasha Kresh for serving as my co-advisor and for his valuable guidance and suggestions on microscope optic system.

I sincerely wish to thank to the committee members of my dissertation, Dr. Gerald Soslau from the College of Medicine, Dr. Young I. Cho and Dr. HongSeok (Moses) Noh from the MEM department. And I deeply appreciate to Dr. Mun Y. Choi who supported and encouraged me when I had difficult time.

I also have wonderful memory with my colleagues who studied and discussed together during my graduate studies, SunJong Kwon, SeulHyun Park, and their family.

I deeply thank my family and my wife's family for their endless support and encouragement. Without their emotional, spiritual, and financial support, accomplishment of PhD degree might be impossible. Last but not least, this thesis is dedicated to my precious family, my wife Ahra and daughter Leah, who have given me their love and concern during my school life.

Table of Contents

List of Tables

List of Figures

Abstract

A Novel Microscopic Assay of Transient Platelet-von Willebrand Facor Adhesion, Kinetics, Margination, and Blood Rheology

Chang-Beom Kim

Professor David M. Wootton and J. Yasha Kresh

Platelets play a central role in hemostasis and arterial thrombosis. At high shear rates, von Willebrand factor (vWF) may recruit passive platelets to a growing thrombus via transient glycoprotein (GP) Ib binding, increasing platelet residence time to allow activation by stress or chemical agonists. Platelet accumulation also depends on dispersive transport driven by shear flow of red blood cells (RBC's), platelet margination (a near-wall enrichment of platelet concentration due to persistent lateral drift), and flow-induced stresses.

A new assay was developed that enables simultaneous measurement of platelet adhesion, platelet margination, wall shear stress, and non-Newtonian flow velocity profile, in blood flow through protein-coated capillaries. Transient platelet adhesion, translation, and embolization are measured by video microscopy. Translating-stage image sequences measure platelet concentration at 3 +/- 1 micron from the capillary surface and centerline flow velocity. The blood velocity profiles are fit to a Casson model based on flow rate, centerline velocity, and pressure gradient.

In capillaries coated with plasma vWF, platelet adhesion was an increasing function of wall shear rate between 126 and 840 /s. Margination increased with shear rate, and decreased on vWF-coated capillaries compared to albumin controls. The characteristic time constant for transient binding on plasma vWF was 1.0 to 1.4 sec. A platelet flux balance was performed on a control volume within 2 μm of the vessel wall using near-wall concentration data, estimated convective flux, and surface net

accumulation rate. Dispersive flux was an order of magnitude faster than the convective flux, meaning stronger contribution of shear-induced dispersion to the contact of platelet with thrombogenic surface, tethering or adhesion, accumulation, and aggregation of platelets than the convective motion. The new assay provides a wealth of data for cell-level computational modeling of platelet adhesion mechanics and kinetics under controlled flow.

CHAPTER 1. INTRODUCTION

1.1 Thrombosis

1.1.1 Human hemostatic system

Humans have an intricate hemostatic system to maintain blood in a fluid state under physiologic conditions, but primed to react to vascular injury to limit blood loss by sealing the defect in the vessel [Goldman, 2000]. The hemostatic system is a complex set of regulated events for the arrest of posttraumatic hemorrhage, consisting of two major contributors to normal hemostasis: the components of the blood vessel wall, and platelets. One important component of the blood vessel wall is the endothelium providing a nonreactive interface between blood and the underlying reactive elements such as von Willebrand factor (vWF) and fibrillar collagen which promote platelet adhesion. The endothelium protects against the formation of intravascular clots, and promotes the degradation of platelet-aggregating agents. Platelets circulate through the blood, surveying the integrity of the vascular system. In normal hemostasis, platelets act in response to traumatic injuries, and adhere to the injury of the vessel within a few minutes and aggregate to one another to form a hemostatic plug [Sixma et al., 1977]. Thus the blood loss is limited by the further clotting sequence of platelets. However, neither platelets nor other components of the hemostatic process can distinguish between traumatic wounds and other lesions developing in the blood vessel.

1.1.2 Role of platelets in hemostatic system

Platelets, also called thrombocytes, are anucleated cells that originate from the cytoplasm of bone marrow megakaryocytes [Italiano et al., 1999], contributing to the maintenance of the normal circulation of blood through the vasculature by taking care of the integrity of the vessel wall and continuously searching the inner lining of the vessel wall for leakage. Platelets immediately respond when the endothelium is injured and rapidly adhere to the exposed subendothelial structures. Platelets are essential for the formation of the primary hemostatic plug at sites of vascular injury and also for the development of pathological thrombi at sites of atherosclerotic plaque rupture. After the adherence of the first layer of platelets, complicated reactions are started that result in the formation of a platelet plug stabilized by an insoluble fibrin network, preventing further loss of blood. The establishment of contact between circulating elements and vessel wall requires sufficient adhesive strength to oppose fluid dynamic forces that would lead to detachment. Platelets provide a relevant paradigm of this biological process since their adhesive functions are necessary to limit blood loss (normal hemostasis) at sites of vascular injury [Sixma, 1977], including areas of the circulation with the highest levels of shear stress [Tangelder, 1988]. Moreover, platelets play a key role in the acute occlusion of atherosclerotic arteries, another event that may involve adhesion under high shear stress [Back et al., 1977; Gibson et al., 1993].

1.1.3 Development of thrombosis

The process of formation of a solid mass inside the blood vessel lumen from the constituents of the blood is known as thrombosis. The resultant mass is called a thrombus which is composed of fibrin and platelets with a few white blood cells and trapped red cells. Thrombus is differentiated from a blood clot; the latter is formed by coagulation of extravascular blood. In response to vascular disease or trauma, platelets interact with exposed subendothelial structures. In high shear flow, platelet thrombus formation develops through four separate stages: tethering, activation, adhesion, and aggregation. (1) vWF from plasma in blood adheres to collagen-coated surface at an injury site through A3-domain. Also another form of vWF is acutely released from endothelial cells under the influence of stimuli associated with an intravascular injury [Ribes et al., 1987]. Plasma vWF plays a central role in tethering of platelets from blood flow through the A1-domain. Specifically, vWF is considered to be indispensable for initial tethering of platelets at high shear rates [Savage et al., 1996]. (2) Tethering to the immobilized vWF by the interaction of platelet membrane glycoprotein GP Ibα with vWF, platelets are activated through stimulation by chemical agonists such as epinephrine, adenosine diphosphate (ADP), thrombin, platelet activating factor (PAF), collagen, or thromboxane. On activation, secretion of vWF from α granules of the platelet is mediated by thromboxane A_2 (TXA_2), phosphorylation of specific proteins (P47-PO_4, MLC-PO_4), and intracellular calcium translocation (Ca^{2+}) inside the platelet. Once activated, platelets bind to adhesive molecules and the platelet surface becomes reactive to recruit further platelets for the aggregation. (3) Adhesion requires more substrates and receptors than

aggregation. Thrombosis initiated by adhesion to extracellular matrix (ECM) involves the synergistic function of four receptors, the glycoprotein Ibα and integrins $\alpha_{IIb}\beta_3$, $\alpha_2\beta_1$, and $\alpha_5\beta_1$ [Savage et al., 1998]. vWF mediates stable surface adhesion of platelets with sequential engagement of GP Ibα and $\alpha_{IIb}\beta_3$ [Ruggeri et al., 1983; Savage et al., 1996]. At high shear rates, the bond between GP Ibα and vWF A1-domain can only initiate tethering of platelets to an injury. But this interactive bond is not stable enough to resist hydrodynamic forces of blood flow. Thus, this short-lived bond can only mediate unstable platelet kinetics such as rolling, translating, flipping, or detachment of platelets on a thrombogenic surface. Following platelet activation, a conformation change allows $\alpha_{IIb}\beta_3$ to interact with fibrinogen or fibrin, $\alpha_2\beta_1$ and $\alpha_5\beta_1$ with collagen and fibronectin, respectively. Spreading of the platelets may follow the firm adhesion. Spreading is an essential step because the flowing blood exerts shear forces on the adhered platelets and the shear forces are proportional to the height of the adhered platelets. The integrin $\alpha_{IIb}\beta_3$ mediates the spreading of the platelets [Weiss et al., 1991]. The activated, spread platelet provides a new surface for the next platelet to adhere to and is the basis of platelet aggregation. (4) Aggregation depends on the GP Ibα and $\alpha_{IIb}\beta_3$ [Ruggeri et al., 1999]. vWF mediates aggregation of platelets [Goto et al., 1998; Ruggeri et al., 1999] and can substitute for fibrinogen as ligand of $\alpha_{IIb}\beta_3$ [De Marco et al., 1986; Fujimoto et al., 1982; Ruggeri et al, 1982 & 1983]. At high shear rates, the indispensable role of vWF – GP Ibα in aggregation highlights the ability to tether flowing platelets to the reactive surface of the platelets already adhered. However, this interaction is also intrinsically short-lived, and not able to yield firm adhesive contact. Thus, additional receptor-ligand interactions

are needed for strong aggregation such as $\alpha_{IIb}\beta_3$ - vWF or $\alpha_{IIb}\beta_3$ - fibrinogen/fibrin shown in Fig. 1-1.

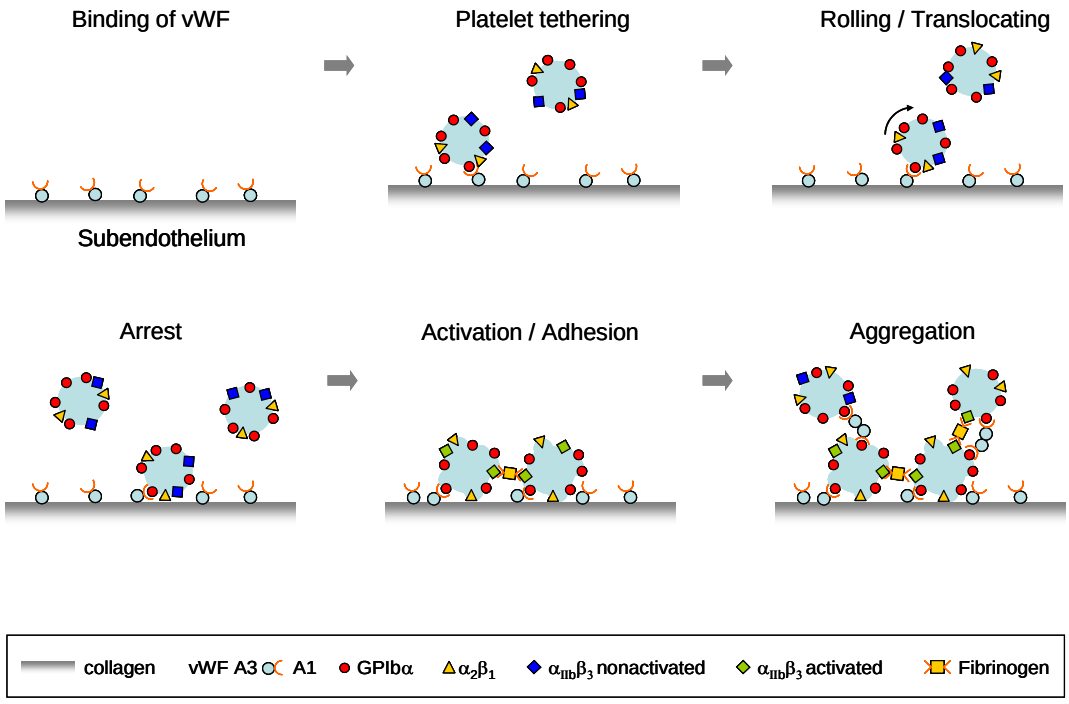

Fig. 1-1. Schematic diagram of simplified biological mechanism of thrombosis.

1.1.4 Clinical effects of thrombosis

Adhesion of platelets to the superficial lesions on the endothelium may be the onset of the formation of a plug in an intact vessel. Subsequently, a mural thrombus is formed that obstructs a blood vessel and prevents the supply of blood to vital organs as an acute cause of ischemic syndromes of the coronary, cerebral, and lower limb circulation in atherosclerosis. These result in a serious pathological condition such as heart attack and stroke. Such a course of events is usually initiated by destabilizing conditions in arteries affected by chronic degeneration, as when an atherosclerotic plaque suddenly ruptures [Fuster et al., 1992 (1) & (2)]. Thrombosis and thromboembolism also cause prosthetic cardiovascular device failure, and can complicate catheter-based intervention. Currently most blood-contacting device design strategies separate design into (1) reducing material thrombogenicity, (2) improvement of flow patterns to remove regions of high shear and high residence time which are associated with thrombosis. (3) Because these first two approaches are usually only partly successful, anticoagulation and/or antiplatelet medication therapy is usually required to prevent device thrombosis. Such therapy is not desirable due to the increased risk of bleeding.

1.2 Atherosclerosis

1.2.1 Structure of blood vessel

Normal blood vessel has a well-developed trilaminar structure: intima, media, and adventitia. The intima lined by endothelium on the inner surface of the vessel is bounded by the internal elastic lamina. The intima consists of a relatively thin layer of connective tissue with smooth muscle cells. The intima is the site at which the lesions of atherosclerosis form by an asymmetrical thickening, and encroach upon the lumen, resulting in a decrease in the flow of blood. The media is located between the internal and external elastic laminae consisting of finestrated sheets of elastic fibers with numerous openings allowing both cells and substances to migrate in either direction. The media is the muscular wall of the artery, consisting mainly of spiraling layers of smooth muscle cells surrounded by basement membrane, collagen fibrils, and proteoglycan. The adventitia is the outmost layer of artery consisting of dense collagenous structure containing numerous bundles of collagen fibrils, elastic fibers, and fibroblasts. Vasa vasorum and nerve endings localize in this layer and the cellular population in the adventitia is sparser than in any other layers.

1.2.2 Pathogenesis of atherosclerosis

The evolution of the atherosclerotic plaque [Braunwald et al, 2001] is briefly introduced in this section. The low-density lipoproteins (LDLs) in blood penetrate

through the gap between endothelial cells and accumulate in the intima. These LDLs are modified by oxidization and glycation, inducing local cytokine elaboration in the intima. The cytokines induce the increased expression of adhesion molecules causing the attachment of leukocytes to endothelial cells and chemoattractant molecules such as monocyte chemoattractant protein 1 (MCP-1) promoting migration of the attached leukocytes into the intima. Those leukocytes encounter some stimuli such as macrophage colony stimulating factor (M-CSF) which increases expression of scavenger receptors from the leukocytes. These scavenger receptors mediate the uptake of modified LDLs and promote the development of macrophage foam cells which are sources of mediators such as further cytokines. Smooth muscle cells in the intima and medial smooth muscle cells migrating into the intima from the media through the openings of the internal elastic lamina can divide and elaborate extracellular matrix. The consequent accumulation of extracellular matrix promotes growing atherosclerotic plaque with calcification, fibrosis, or apoptosis (programmed cell death) in later stages. Finally asymmetrical thickening and encroachment upon the lumen result in a decrease in the flow of blood and an increase of shear rate and stress on the endothelial cells causing an environment for thrombogenesis.

1.2.3 Atherosclerosis and thrombosis

Atherosclerosis is the descriptive term for hardened or thickened lesions occurring within the innermost layer of blood vessel, intima, which is in contrast to arteriosclerosis, the general term describing thickened or stiffened vessels [Goldman, 2000]. Atherosclerosis is largely related to thrombosis which has been considered to be

an important component in the progression of the lesion of atherosclerosis. Once atherosclerosis develops within a layer of blood vessel, it is eccentric in the advanced stages of atherosclerosis and can occlude the lumen of the artery when the injury becomes complicated by thrombosis, causing ischemia and necrosis and clinical sequelae of cerebral infarction (stroke), myocardial infarction (heart attack), or gangrene of the extremities (leading to amputation). Thrombi play key roles in these clinical diseases. Being incorporated into an existing advanced lesion of atherosclerosis, thrombi rapidly cause lumen narrowing and increase the surface of the lesion. Cracks and fissures which might be formed due to the imbalance between the hydrodynamic forces and stresses imposed by pulsatile blood flow and the mechanical strength of the fibrous cap of plaque [Lee et al., 1997], supply the sites for blood platelet adhesion, activation and aggregation. Platelet accumulation may lead to formation of mural occlusive thrombi and coagulation cascade activation [Fuster et al.,1990], causing ischemia (low oxygen) and infarction (death) of downstream tissues [Davies et al, 1984; Friedman et al., 1975; Harker, et al., 1976; More, 1973; Shepard et al., 1971; Stemerman et al.,1972].

1.3 Role of von Willebrand Factor (vWF) in Thrombosis

The role of vWF in platelet thrombus formation and aggregation is primarily the mediation of platelet adhesion to components of the extracellular matrix and to one another. A platelet has two distinct receptors interacting with vWF, the glycoprotein Ibα in the GP Ib-IX-V complex and the integrin $\alpha_{IIb}\beta_3$ (GP IIb-IIIa complex). GP Ibα mainly

contributes to platelet tethering and adhesion, and $\alpha_{IIb}\beta_3$ to aggregation of platelets. GP Ibα binding to immobilized vWF appears to have fast association and dissociation rates as well as high resistance to tensile stress, supporting initial tethering and translocation of platelets on immobilized vWF at high shear rates [Savage et al., 1996]. This eventually reduces platelet velocity relative to free flow and allows activated $\alpha_{IIb}\beta_3$ to arrest platelets on vWF under conditions not permissive of direct binding to fibrinogen. At high shear rates, only the bond between the vWF A1-domain and GP Ibα can initiate the capture and tethering of platelets to a surface. However, this interaction is intrinsically short-lived. By itself, it can only mediate platelet rolling and does not result in firm adhesive contacts, which are typically supported by binding of integrins to vWF or other substrates. vWF appears to be a substitution for fibrinogen as $\alpha_{IIb}\beta_3$ ligand. To form a bridge between platelets, a crucial ligand as a link between platelets in the forming thrombus after a first layer of platelets has been formed. The platelet-bound vWF contributes to platelet recruitment into a growing thrombus.

vWF immediately binds to a site of vascular injury via A3-domain (exposed collagen or exposed subendothelial structures) and subsequently to platelets via A1-domain, thereby helping the platelet adhesion and initiating hemostasis or thrombosis under high shear rates. No spontaneous binding of vWF to platelets occurs in normal circulation. At high shear rates, plasma vWF is required for normal adhesion of platelets to subendothelium as a bridge between platelets and the fibrillar surfaces, however, at low shear rates, platelets can adhere to other proteins substituting for the action of vWF to some extent [De Groot, 2002].

Von Willebrand disease (vWD) is the most common bleeding disorder and is caused by a problem with vWF, is divided into 3 categories: Type 1, Type 2, and Type 3. Type 1 vWD is the most common type in which vWF normally works but vWF concentration is lower than normal, and people have no symptoms until a bad injury. Type 2 vWD is much less common than Type 1 and is divided into several subtypes: 2A, 2B, and 2N. In Type 2A vWD, vWF is less efficient in binding to platelets and does not behave as a glue to hold the platelets at an injury in a blood vessel. In Type 2B vWD, vWF binds to platelets in the bloodstream, instead of the site of an injury to the blood vessel. In Type 2N, vWF does not transport factor VIII, which results in low level in both vWF and factor VIII. Type 3 vWD is the most severe type in which very low level of factor VIII and little vWF exist [Colman et al., 1990].

Whenever vWF mediates stable surface adhesion or aggregation of platelets, it must engage both of its platelet receptors (GP Ibα and $\alpha_{IIb}\beta_3$) sequentially. The synergism between these two receptors occurs irrespective of shear forces and can even be demonstrated under static conditions. In any case, plasma vWF appears to play a central role in thrombus formation under high shear stress conditions, because it can mediate initial steps in the process, even before the release of α-granule or endothelial proteins.

1.4 Effect of Blood Flow on Thrombosis

Platelet accumulation is modulated by the effect of both fluid dynamics and biology. Among the biological factors, platelet membrane receptors are indispensable factors in the formation of thrombosis as described above: GP Ibα-mediated transient binding to vWF for initial tethering, platelet activation through the receptor-ligand interaction of $\alpha_2\beta_1$-collagen, stable adhesion to lesions supported by $\alpha_{IIb}\beta_3$-vWF/fibrinogen/fibrin, $\alpha_2\beta_1$ and $\alpha_5\beta_1$ with collagen and fibronectin, respectively, and recruitment of inactive platelets from the flow onto the reactive surface for the accumulation of platelets via transient binding, chemical agonist and shear-induced activation, and firm binding.

In flow, platelets are transported (1) by convection along flow streamlines, (2) by shear-induced dispersion, random-like motion in the cross-streamline direction, and (3) by persistent drift. Shear-induced dispersion is driven by the motion of red blood cells in shear flow, which may rotate [Wang et al., 1979] or displace one another as they pass [Zydney et al., 1988] in shear flow. Dispersion is an increasing function of shear rate [Turitto et al., 1980]. Persistent drift is migration of platelets from the core of the vessel to the margins, leading to platelet margination, in other words, high platelet concentration profiles skewed toward the vessel wall. An accurate model of platelet accumulation in an arterial flow should include each transport mechanism [Eckstein et al., 1991]: convection and dispersion may increase platelet availability to the thrombus proportional to the shear rate, while platelet margination could increase platelet transport toward the blood vessel by a factor of 1.3 to nearly 10 [Aarts et al., 1988]. Margination is also significant even

under pulsatile flow conditions in arterial flow [Xu & Wootton, 2004], a finding based on a model study of ex vivo platelet aggregation studies [Wootton et al., 2001]. Most studies of margination have been performed in vessels with artificial material walls, but in vivo experiments using intravital microscopy confirm that margination exists over normal vessel wall surfaces [Tangelder et al., 1985].

For the formation of thrombus on the vessel wall, platelets have to be transported toward the wall prior to any biological events. This process is mediated by hemodynamics and rheological factors, such as shear-induced dispersion, margination, or wall shear rates. Platelet adhesion to subendothelium or onto other activated platelets is strongly influenced by wall shear rate [Turitto et al., 1979] and hematocrit [Turitto et al, 1975]. According to Keller (1971), red blood cells rotating in a shear flow induce local stirring and enhance the platelet diffusion. Also, red blood cells migrate toward the core region of the vessel leaving red cell-poor plasma region near the vessel wall. Consequently, platelets are expelled from the core toward near-wall region. High near-wall concentration increases the platelet-wall interaction rate, giving the platelet population more chances to tether or adhere to the subendothelium or other adherent platelets. Furthermore, shear-induced dispersion may work for the platelets in the vicinity of a growing thrombus. An alternative mechanism, hydrodynamic resistance, can be suggested for delaying platelets in the vicinity of a growing thrombus and allowing time for activation. Thus, fluid dynamic events are important factors to enhance the formation of thrombosis and the high near-wall concentration is the basis of the events.

1.5 Overview of Thesis

The broad objective of the present research is to describe the role of hemodynamics in thrombosis. In the work presented here, a new assay was developed that enables simultaneous measurement of platelet adhesion, platelet margination, wall shear stress, and non-Newtonian flow velocity profile, in blood flow through protein-coated capillaries. This novel translating-stage optical method measures (1) non-Newtonian fluid velocity profiles and viscosity, (2) near-wall margination of platelets in a shear flow of blood by using the obtained velocity profiles, (3) kinetics of platelet adhesion on von Willebrand factor coated surfaces. The data from this assay is used in a platelet flux balance for a defined control volume, which showed that lateral platelet flux is the main source of adherent platelets.

CHAPTER 2. OVERVIEW OF THE EXPERIMENTAL DESIGN

2.1 Introduction

In previous studies many researchers understood the fluid mechanical processes governing blood flow by modeling and measuring the velocity profiles [Bishop et al., 2001; Bugliarello et al., 1962 & 1970; Goldsmith et al., 1971 & 1986; Kiserud et al., 1998; Mayrovitz, 1987; Tangelder et al., 1986 & 1988; Wayland et al., 1967]. Blood particles in the median plane of a circular tube were traced along the tube axis by using a traveling microscope stage [Goldsmith et al., 1971] to better examine the detailed motion of blood cells such as lateral diffusive motion as well as convective motion. With this method, the particles remained and were observable in the center of view for a long-time period by setting the speed of the traveling stage to the velocity of the particles at the focal plane, but only low shear rates were observed.

In the present study, the extension of this idea was used to measure the velocity from near-wall to centerline and the concentration of the platelets flowing near the wall based on the measured velocity profiles. A new translating-stage optical method was developed for measuring veloctiy profiles involving non-Newtonian viscosity models and for measuring both surface-adherent and non-adherent near-wall platelet concentrations in shear flow of blood, using an epifluorescence inverted microscope with computer controlled stage (x/z direction) positioning and speed. Fluorescence videomicroscopy technique was used for recording moving images at different shear rates. A flow chamber was designed to employ 50 μm high × 1mm wide × 10 cm long rectangular glass

capillary to create a 2D parallel-plate flow. Capillaries were coated with human plasma vWF, or bovine serum albumin as control. The current study showed that transient platelet binding via GP Ibα-vWF altered platelet concentration in flowing blood near vessel wall and determined the extent to which vWF-mediated transient adhesion may affect near-wall platelet concentration profiles.

2.2 Experimental Setup

2.2.1 Microscope system and optics

A schematic diagram of the experimental setup is shown in Fig. 2-1. An epifluorescence inverted microscope (Nikon) with features of computer-controlled translating stage (x/z-direction, Ludl electronics), computer-controlled focal depth (y-direction), and automatic optical filter wheel (Ludl electronic) was used with a 40× objective (Nikon, oil immersion, numerical aperture 1.3). The translating stage of the microscope was equipped with two stepper motors to control the positioning and speed in both x and z directions. The rotatable filter wheel contained filters for FITC (model DM505, EX465-495, BA515-555) and RHO (model DM575, EX510-560, BA590) fluorescence under epi-illumination.

For the study of velocity profiles of blood suspension at different shear rates, the images were consecutively captured for 4 sec by a high speed camera (125 frames/sec, Encore MAC, Olympus) and directly digitized by an image acquisition board installed in

a computer. The captured images (480 × 420 pixel) corresponded to 190 μm × 166 μm in actual size. For the study of near-wall platelet concentration, a SIT camera (Dage-MTI, 30 frames/sec) was connected to a videocassette recorder (Panasonic) and the images were shown on a monitor. The images (640 × 480 pixel) recorded by SIT camera represented 314 μm × 235 μm in actual size.

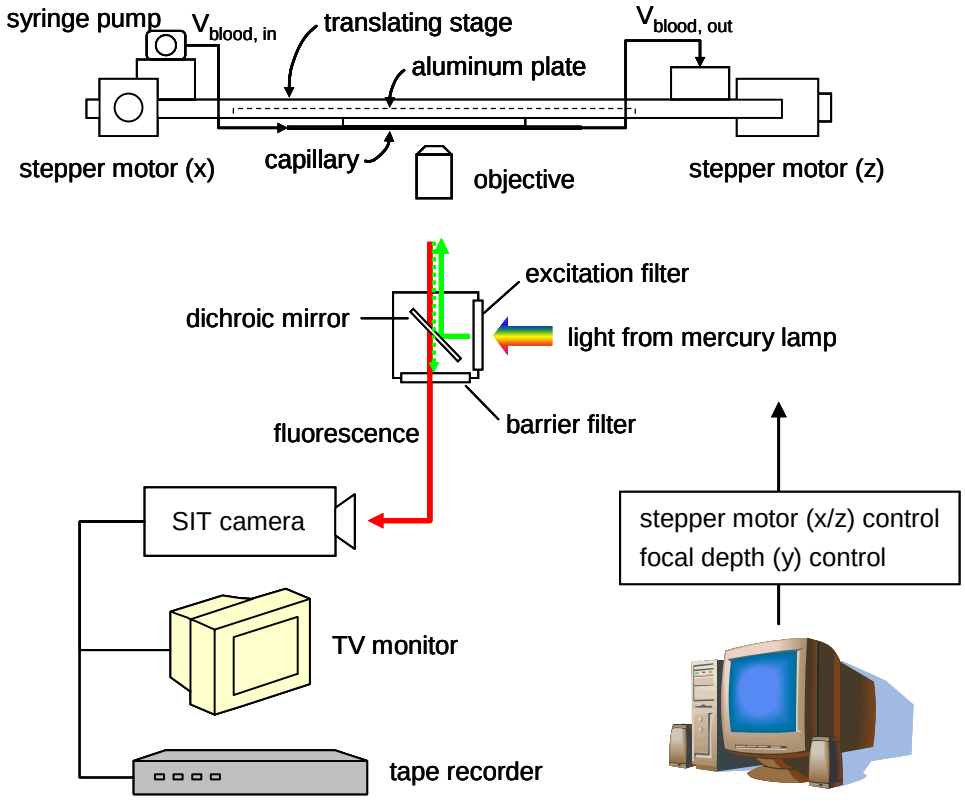

Fig. 2-1. Schematic diagram of the experimental setup.

2.2.2 Flow apparatus

The flow chamber was designed to employ a rectangular cross-sectional borosilicate glass capillary (10cm long × 50μm high × 1mm wide, 50μm wall thickness, VitroCom) into a 2-dimensional parallel-plate flow shown in Fig. 2-2. To avoid optical distortion of images due to the curvature of circular cross-sectional tubes when blood cells are observed by using microscopy, a rectangular cross-sectional channel was used. The high height-to-width ratio (0.05) of the capillary tube was selected so that the cross-lateral velocity profiles across the capillary width would be nearly uniform and the velocity profiles around the center in width which would be recorded for analysis would not be affected by side-walls.

The rectangular capillary tubes were glued with cyanoacrylic adhesive on one side and carefully attached to a surface of a microscope slide (Fisher scientific) whose surface has a very high degree of flatness. Subsequently, the other side of the capillary tube was very flat in longitudinal direction. The working distance between the non-glued side of the capillary tube and the objective of the microscope should keep consistent at every location along the capillary tube during the translating-stage measurements with minimal change of chamber focal plane location (depth) due to stage translation. The microscope slide with an attached capillary tube was glued under an aluminum plate which was positioned and secured on the motorized microscope stage and horizontally aligned with a height-adjustment screw on one side of the aluminum plate so that the working distance could be kept identical while the translating-stage moved along capillary tube. Each end of the capillary tube was carefully inserted in silicone tubing (ID

0.02”, ColeParmer), secured by epoxy glue, and connected to a syringe pump (NE-1000X, New Era Pump) which was stationed and secured on the microscope stage.

Prior to running experiments, the inside surface of the capillary tube was washed with 0.1 M hydrochloric acid and distilled water in this order, and dried with filtered air to completely remove even microscale water particles captured along the side-edges inside the capillary tube, which can otherwise cause microbubbles in the process of vWF and BSA coating. After the washing process, the capillary tubes were coated with 100 μg/ml of human plasma vWF (Heamatologic Technologies, Essex Junction, VT) diluted with phosphate buffered saline (PBS, Sigma), incubated for 2 hours at room temperature, then rinsed and incubated for 30 minutes with PBS with 1% (w/v) bovine serum albumin (BSA, Sigma) to block non-specific interactions of the platelets [Cruz et al., 2000]. Capillaries for negative control experiments were washed, dried, and incubated for 2 hours with 1% BSA in PBS, instead of vWF.

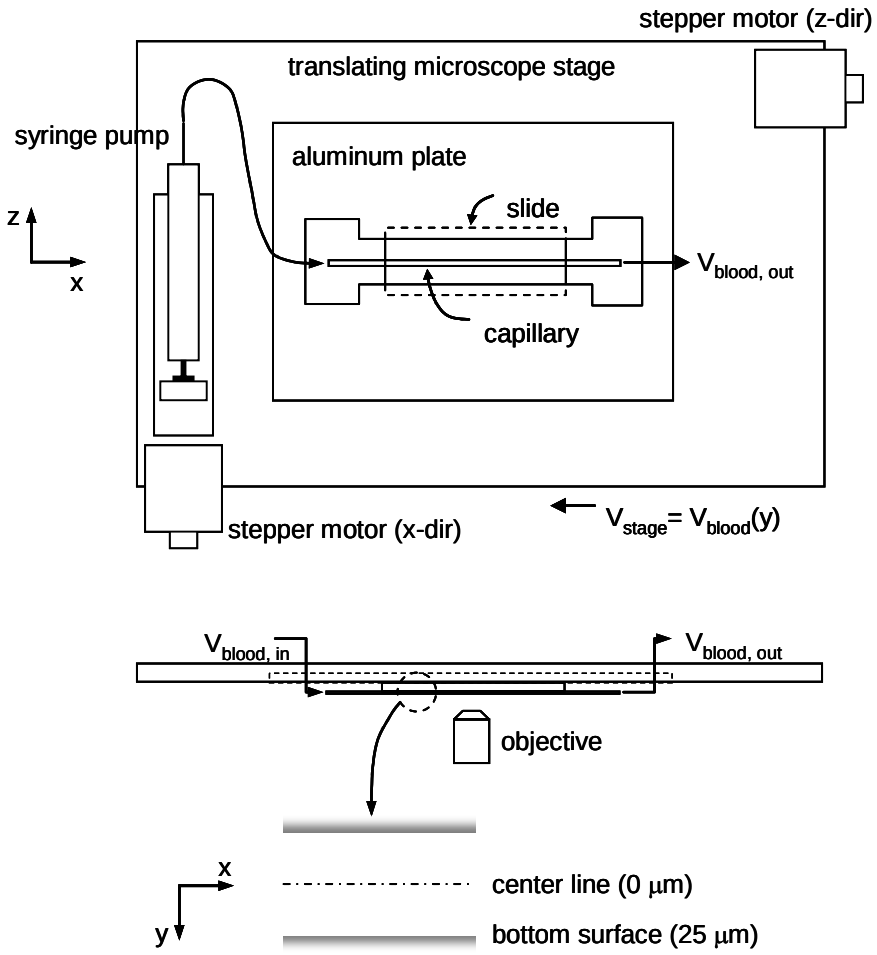

Fig. 2-2. Schematic diagram of the flow apparatus and analysis coordinates.

2.3 Preparation of Blood Suspension

2.3.1 Blood Donors

Blood was drawn from the antecubital vein of healthy adult donors through 21-gauge needle into a syringe containing 3.2% citrate as an anticoagulant. Totally, 30 ml of blood sample, one part of citrate mixed with 9 parts of whole blood, was slowly collected to prohibit shear-induced platelet activation in the process of collection and was immediately transferred into a centrifuge tube. All institutional requirements for human subject protocol review and biohazard control were followed. None of the donors had taken aspirin or blood-thinning medication in the preceding one week.

2.3.2 Blood suspension

Blood suspensions were prepared by modification of a method of Savage *et al*. (2002). On being collected in a centrifuge tube, a blood sample was immediately mixed with prostaglandin E_1 (PGE_1) (final concentration, 10 μM, Calbiochem) to prevent full activation of platelets [Savage et al., 1996] and mixed with EDTA (final concentration, 5 mM, Aldrich) to inhibit integrin receptor function of platelets and coagulation, and supplemented with 5 units/ml of apyrase (grade VII, Sigma) as ADP scavenger [Savage et al., 2002]. The blood sample was also mixed with abxicimab (final concentration, 10 μg/ml, Lilly) to inhibit aggregation of platelets in the whole blood. After incubation for 15min, the blood sample was centrifuged at 280×g for 12 min at 24°C to separate RBCs

from platelet-rich-plasma (PRP). The separated RBCs were gently mixed with 0.9% sodium chloride and centrifuged at 280×g for 12 min at 24°C, and then supernatant sodium chloride was discarded after the centrifugation. This washing procedure was repeated 3 times.

To investigate the velocity profile of flowing blood suspension, 2μl of fluorescent microbeads (d = 1.9μm, Duke scientific) as particle tracking markers in flowing blood suspension was coated with 1% bovine serum albumin (BSA, BD Biosciences) to prevent the microbeads from forming aggregates with blood cells. The BSA-coated fluorescent microbeads and RBCs were resuspended with modified HEPES Tyrodes Buffer (HTB DPX/BSA, NaCl 136.2mM, KCl 2.7mM, NaH_2PO_4 3.8mM, $MgCl_2$ 1.0mM, HEPES sodium salt 3.5mM, Dextrose 2mg/ml, BSA 2mg/ml, pH 7.35) [Basheer et al., 1995]. 0.9ml of the washed RBCs was added to 5ml of HTB DPX/BSA to make 15% hematocrit [Sarelius et al., 1982]. The final concentration of solid BSA-coated fluorescent microbeads in the blood suspension was 0.033% (v/v) to optimize data density and signal to background fluorescence ratio. Particles less than 2.0 μm in diameter may not be considered as a factor for the occurrence of large near-wall excess of small particle during blood flow for the range of shear rates for current study, which is from 120 s^{-1} to 815 s^{-1} [Eckstein et al., 1988], assuming that the microbeads were uniformly distributed in flowing blood suspensions.

For the study of near-wall platelet concentration in flowing blood, PRP was divided into 2 different centrifuge tubes to label platelets with different fluorechromes, one for the stationary images to investigate the dynamics of platelets interacting with surface-bound vWF and the other for motion images to investigate the near-wall (3μm

depth from the surface) concentration of the platelets flowing in blood suspension. Both PRP tubes were centrifuged at 960×g for 12 min at 24°C to separate the platelet pellet from platelet-poor-plasma (PPP), which was discarded after the centrifugation. The platelet pellets in each tube were gently resuspended in PIPES buffer (PIPES 25mM, NaCl 137mM, KCl 4mM, Dextrose 0.1%, pH 7.0) [Frenette et al., 1995], which included calcein green (final concentration, 0.5 μg/ml, Molecular Probes) for the stationary analysis and calcein red-orange (final concentration, 2.0 μg/ml, Molecular Probes) for the motion analysis, followed by the incubation for 30 min at room temperature. PIPES buffer also contained PGE, apyrase (2.5 units/ml), abxicimab (5 μg/ml), and EDTA (5mM) to prevent platelet activation during centrifugation. Both resuspended PRPs were again centrifuged at the same centrifugal force to obtain the labeled platelet pellets and the unbound calcein solutions were removed. The labeled platelet pellets were finally resuspended in HTB DPX/BSA containing 10 μM PGE_1 and 5 mM EDTA, corresponding to the same amount of the original PRP in each centrifuge tube. The number of platelets in the each platelet suspension was counted using a cell counter (Coulter) and adjusted to 180,000 platelets/μl for all analyses. The final platelet-rich-suspension was made with 9 parts of calcein green labeled platelets and 1 part of calcein red-orange labeled platelets. The calcein red-orange labeled platelets were used for moving images to measure platelet concentration. The 10% labeled fraction was selected as a compromise between the number of labeled cells in the focal plane and the background noise due to adherent and out-of-focus platelets. The final blood suspension contained the platelet-rich-suspension and 3 times washed RBCs corresponding to 15% hematocrit [Sarelius et al., 1982].

2.4 Calibration and Measurement

2.4.1 Volume flow rate of syringe pump

It was hard to find a volume flow meter that can measure the lowest range for the present study, which is 0.003 ml/min. A high precision digital scale (precision 10^{-5} g, model XS-105, Metter Toledo) was used to measure the rate of mass accumulation (mass flow rate) instead of volume flow rate. The density of blood suspension was assumed to be 1.06 g/cm^3. The syringe filled with blood suspension was placed on the pump and connected to one end of the capillary tube, and the other end to a small cup on the scale shown in Fig. 2-3 (a). The continuously increasing mass of blood suspension was measured by real-time recording (10 msec, sample period) of the output signal from the scale through an RS-232 port which was plugged into the computer. Data acquisition software was developed using VisualBasic code. The calibration data are shown in Fig. B-1, 2, 3, & 4 in Appendix B for all cases in the present study.

2.4.2 Pressure transducer

In the theoretical estimation of velocity profiles involving non-Newtonian Casson viscosity model for blood suspension, which were compared to the measured velocity profiles, the measurement of pressure drop through the capillary tube was required, as well as the volume flow rate. A solid state pressure transducer (±0.1% accuracy, model NPC-410, GE NovaSensor) based on piezoresistive sensing technology

was used. Calibration was made in the range of 3.5 psi using a manometer, and the output voltage of the pressure transducer was directly obtained through a data acquisition board (model Daq-801, Omega) and transferred into the computer in real time (5.7 msec, sample period) by data acquisition software programmed in VisualBasic. The calibration data are shown in Fig. B-5 in Appendix B.

Pressure drop through the capillary tube was obtained using the same data acquisition system as shown in Fig. 2-3 (b). Microbubbles captured in capillary tube were removed prior to the measurement because they can induce flow disturbance and yield improper pressure drop data. Even though both sides of the capillary tube were connected to silicone tubings (ID 0.02”), pressure drop in the outlet tubing was negligible compared to that in capillary because pressure drop in capillary was theoretically 157 times larger than that in outlet tubing as shown in Table 2-1.

Table 2-1. Comparison of pressure drop in capillary and outlet tubing (unit: Pa/10cm).

flow rate (ml/min)	shear rate (s^{-1})	capillary	outlet tubing
0.0204	815	3260	21
0.0148	590	2360	15
0.0088	350	1400	9
0.0030	120	480	3

2.4.3 Translating speed of microscope stage

The speed of the translating stage was calibrated and was a linear function with respect to the various stage speed settings (data are shown in Fig. B-6 in Appendix B).

This process was performed by a macro program of ImagePro, a commercial image analysis software, which controls the operation of the stepper motors. Start time was recorded at the onset of the translation of microscope stage, and end time at the termination of the translation along some traveling distance. This process was repeated for every 5th speed setting from 5 to 80, and setting 1. The stage speed was obtained by division of the translating distance by the elapsed time. To minimize the effect of acceleration and deceleration at the start and end of the stage motion, respectively, on the calibration data, the maximum traveling distance available for the microscope stage was used.

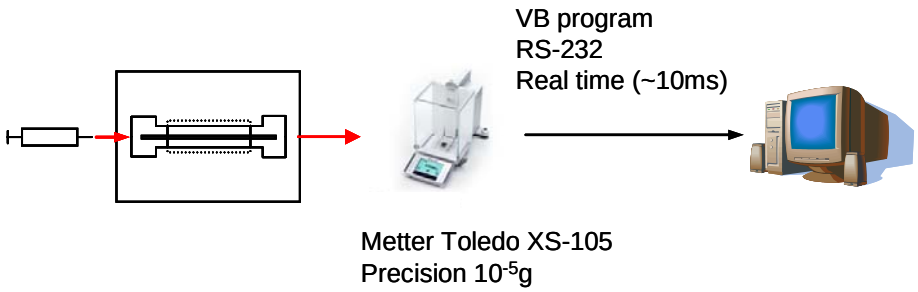

Fig. 2-3. (a) Calibration of volume flow rate of syringe pump.

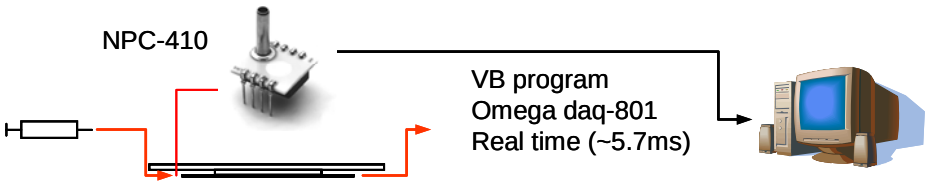

Fig. 2-3. (b) Measurement of pressure drop along capillary tube.

2.5 Experiment Protocol

2.5.1 Measurement of velocity profiles

Once a test-section consisting of a microscope slide, a capillary tube, and two silicone tubes extended from each end of the capillary tube was attached under the aluminum plate shown in Fig. 2-2, the aluminum plate was positioned and secured on the motorized microscope stage. The starting point of the observation zone was set approximately 3 cm from the entrance of the channel and ending point 3cm from the exit. The total distance traveled by the translating stage was approximately 4cm. To check that the working distance was consistent while the translating stage was traveling along the capillary tube, the bottom surface inside the capillary tube at the starting point of the observation zone was brought into focus by adjusting the objective in y-direction, and then, the ending point of the observation was focused on by manipulating a height-adjustment screw installed on the aluminum plate, which might make the starting point to be out of focus again, but the degree of deviation from focus became smaller. By repeated cycles of adjustment, eventually both the starting and ending points were brought into focus. Once the focus was set for both locations, several other locations between starting and ending point were randomly chosen and examined to confirm that the entire capillary was in focus.

The syringe pump mounted on the translating stage began pumping the blood suspension composed of RBCs and fluorescent microbeads through the channel. Four different flow rates of 0.003, 0.0088, 0.0147, and 0.020 ml/min were selected for this

study, corresponding to the nominal wall shear rate of 120, 350, 590, and 815 s^{-1}, respectively. A total of 9 focal depths were selected to be recorded for each shear rate between the bottom surface (25 μm) and the center (0 μm) of the capillary tube, every 3 μm from the bottom surface up to 4 μm, and 2 and 0 μm. Starting with the focal depth of 22 μm, recordings were made for every selected focal depth while the translating stage was traveling in the opposite direction to the blood flow with speed similar to that of water, corresponding to the focal depth for a flow rate, which was proven to be parabolic. Sedimentation of the blood cells occurs at rates of about 10^{-4} cm/sec, which is 100 times smaller than the lowest mean velocity for this study so that particles do not sediment out of the focal plane. Water velocity profiles were also examined using the translating-stage method for the same flow rates for validation of the velocity profile measurement method.

2.5.2 Near-wall concentration of platelets in flowing blood suspension

Based on the obtained velocity profile above, the near-wall (22 μm) concentration of platelets in flowing blood suspension was investigated for vWF- and BSA-coated surface using the translating-stage method. Blood suspension composed of RBCs, fluorescently labeled platelets, and HTB buffer was pumped out of a syringe placed on a syringe pump on the translating stage. To avoid settlement of RBCs in the syringe during experiments, a miniature magnetic bar smaller than the syringe diameter was inserted and gently stirred every 1 min for uniform distribution of all blood cells in the syringe. The same flow rates were selected as in the velocity profile measurements, but only one focal depth (22 μm) near the wall was swept by the translating stage to

investigate the concentration of the platelets. Also stationary images at 3 different locations were recorded for 3 sec to quantitatively analyze the interaction of the platelets with vWF-coated wall such as adherent, translocating, incoming from the main flow, and leaving to the main flow. A macro program of an image analysis software, ImagePro, was developed to automatically control the whole process whose one cycle was programmed to conduct the translation of the motorized stage for recording each stationary image of the lower surface at 3 different locations, and then sweep to record a moving image at the stage speed corresponding to the blood suspension at 22 μm focal plane.

CHAPTER 3. VELOCITY PROFILE AND VISCOSITY ESTIMATION

3.1 Introduction

3.1.1 Background

Detailed knowledge of the velocity distribution over the cross-sectional area of a microvessel is important for several reasons: (1) Information about the flow field velocity gradients can suggest an adequate description of blood flow. In the past 30 decades, *in vitro* studies in glass tubes have measured the velocity profiles of ghost (erythrocyte membrane) cells [Goldsmith et al., 1979] or blood [Baker et al., 1974; Bishop et al., 2001; Bugliarello et al.,1963 & 1970; Goldsmith, 1971; Wayland et al., 1967]. The shapes of the velocity profiles were dependent on the shear rates: flat at extremely low shear rates, parabolic at high shear, or blunted at moderate shear rates. *In vivo* studies in a microvessel were also performed. Even though the geometry of a real blood vessel affected the shape of velocity profiles and the profiles did not exactly satisfy no-slip condition at wall, the profiles were flattened as compared to a parabola, both in systole and diastole [Tangelder et al., 1986 & 1988]. (2) Transport of blood components is determined by the concentration of the cells over the cross-sectional area and the velocity profiles. Knowledge of concentration of blood platelets and velocity profiles was used to estimate the rate of platelet delivery to thrombus formation [Tangelder et al., 1985]. Eckstein *et al*. (1991) added a drift term to convective diffusion equation for platelet transport so that near-wall excesses of platelets could be described. This issue will be

more discussed in Chapter 4. (3) The velocity profile is required to investigate volume flow rate as well as wall shear rate and shear stress. Wall shear rate is an important parameter in describing the interaction between blood cells and the vessel wall. The significance is that the adhesion of platelets to subendothelial structures was determined by wall shear rates because both the transport of the platelets toward the vessel wall and the chemical reactions involved in the binding depend on the shear rate [Turitto et al., 1979]. However, shear rate is not directly measurable, especially in microvessels, due to scarce information on velocity profiles, thus shear rate has been calculated based on the assumption of Newtonian parabolic velocity profile. However, the velocity profiles in arterioles differ significantly from a parabolic distribution because the profiles are blunt in both diastole and systole [Tangelder et al., 1986]. Tangelder *et al*. (1988) could estimate the shear rate from the velocity profile in arterioles obtained by the *in vivo* observation of fluorescence-labeled platelets as natural markers using intravital fluorescence microscopy. The velocity profiles were modeled and compared with parabolic profiles, concluding that the wall shear rates were at least 1.46-3.94 times higher than parabolic distribution for the same volume flow rate.

3.1.2 Goals and experimental end points

The present study has not been confined to the qualitative measurement of non-Newtonian velocity profiles in a microscale capillary tube, but extended to the application of the observed and theoretical profiles to determination of the location of platelets flowing in a zone near the wall, representing the near-wall platelet concentration.

Thrombogenesis must require transport of blood components to the blood vessel wall by two principal mechanisms in the fluid mechanical point of view: convection and shear-induced dispersion. The transversely diffusive behavior of red blood cells strongly contributes to the complex interaction between the red blood cells and platelets (in fact, all other cells). The RBCs tend to be more highly concentrated at the vessel center in shear flow, along with random lateral fluctuations in position due to their high concentration. These motions, perhaps combined with the tendency of rigid particles to concentrate away from the tube center, induce migration of the platelets toward the vessel wall, and consequently a radial concentration distribution of platelets develops in shear blood flow, with high concentration skewed toward the blood vessel wall. The enriched near-wall concentration is often called “platelet margination”. The high near-wall concentration of the platelets has been primarily treated as a prerequisite of adhesion, aggregation, and thrombus formation in an intravascular injury. Many trials to measure the spatially skewed distribution of platelets or platelet-sized microspheres in a shear flow of blood have been made *in vivo* and *in vitro*. They made a focus on the median plane at maximum diameter of vessel or a tube and made consecutive photographs of flowing platelets from centerline to the wall. Possible errors in the concentration observation could occur by the fact that some platelets observed might travel along rather lower streamline than that of the centerline and some platelets along rather higher streamline. Detection of the microparticles as fluorescence-labeled tracer markers in flowing blood suspension represents the acquisition of the two-dimensional projection of a real three-dimensional flow. However, once a velocity profile in a flow field is accurately defined, the location of the particles flowing in the flow field can be exactly

defined, because the velocity profile is obviously a function of lateral dimension such as radius for circular tube or height for rectangular duct. Thus, accurate determination of velocity profile needs to be done prior to investigation of concentration of platelets.

One more issue is that Newtonian velocity profile has been well known to be a parabola, but blood is a non-Newtonian fluid which has a plug flow region at the centerline due to yield shear stress. Also blood has thixotropic (time-dependent) [Barnes, 1997; How, 1996] characteristics and its viscoelastistic properties can change with the level of strain [Fung, 1993, Munson, 1998]. Thus, accurate wall shear rate need to be estimated, which is higher than Newtonian case and is an important parameter in describing the interaction between blood components and vessel wall.

The experiments in this section are briefly described as follows:

1. Measurement of velocity profiles of water using a translating microscope stage method to verify the applicability of this method to velocity profile measurement by comparing the experimental results to theoretical profiles for the same flow conditions in section 3.3.
2. Derivation of theoretical non-Newtonian general flow equations in a rectangular capillary tube using Casson and Power-law non-Newtonian viscosity models in sections 3.4.1 and 3.5.1, respectively.
3. The numerical calculation of velocity profiles based on the theoretical equations obtained in section 3.4.1 & 3.5.1, measurement of three experimental parameters (volume flow rate, maximum velocity, and pressure drop), and best fit to the Casson and Power-law viscosity models in section 3.4.2 and 3.5.2, respectively.

4. Comparison of the experimentally measured velocity profiles by the translating microscope stage method with the theoretical non-Newtonian velocity profiles in section 3.4.3 and 3.5.3: these velocity profiles were used for the determination of the location of flowing fluorescence-labeled platelets, and consequently used for the investigation of the near-wall platelet concentration in Chapter 4.
5. Estimation of accurate wall shear rate and shear stress based on these velocity profiles for different flow rates.

3.2 Experimental Determination of the Location and Velocity of Fluorescent Microbeads flowing in a Capillary

3.2.1 Criteria for the detection of focused particles

In this section, the optical method for identification of focused fluorescent microbeads at a given focal distance in flow is described. To visualize velocity profiles, a small amount of FITC-labeled fluorescent microbeads (1.9 μm in diameter) as tracer markers were added in water or blood suspension. The visually captured images of the fluorescent microbeads in water or blood suspension represent two-dimensional projections of three-dimensional flow. Many fluorescent microbeads were out of focus; some of those were located above the focal layer and some below. To determine criteria for locating particles in the focal layer based on image intensity distribution and magnitude, a simple test was performed. A rectangular capillary tube filled with blood

suspension including fluorescent microbeads was placed on the microscope stage. The blood suspension was essentially stationary, but microbeads were slowly moving around due to the motion of RBCs and Brownian motion, except a few microbeads stuck to the lower or upper surface inside the capillary tube. To determine the line intensity profiles of the stationary microbead images with varying focal depth with respect to a microbead stuck to the lower surface, the lower surface was focused first and the objective was raised by 0.95 μm to focus at the centroid of the microbead because the diameter of the microbead is 1.9 μm, and an image was captured at the centroid of the microbead. More images focused at +3 and +6 μm with respect to the centroid of the microbead were also captured by raising the objective. For a microbead adhering to the upper surface of the capillary tube, the same process was performed by lowering the objective from the top surface. Line intensity analysis was performed by an image analysis software, ImageJ. The x-axis (horizontal) of the image represents flow direction and y-direction perpendicular to the image indicates the direction of capillary height. The z-direction line crossing centroid of microbead image was analyzed, to avoid possible effects of microbead motion on pixel intensity, such as instant acceleration or deceleration of microbead in flow direction (x-direction). Fig. 3-1 shows the captured images and corresponding line intensity profiles for the z-direction (perpendicular to the flow) with ± 3 μm vertical shifts of the microscope objective. This figure demonstrates two criteria:

(i) Intensity: the pixel intensity of the microbead focused at the centroid has a maximum value.

(ii) Intensity distribution: the location of 30% of the maximum value corresponds to 8 pixels in diameter.

Even though the negative 3μm-focused microbead has an almost maximal-intense image, the intensity distribution shape represented in the second criteria can distinguish a centroid-focused microbead from a negative 3μm-focused microbead. With the use of this method, it was possible to differentiate the centroid-focused microbeads from out-of-focus microbeads in the flowing blood suspension. Others have neither maximum intensity, nor 8 pixels in diameter for 30% of the maximum intensity.

3.2.2 Determination of the location and velocity of fluorescent microbeads

Based on the above criteria, the microbeads flowing at a focal depth could be recognized by a VisualBasic program which was developed to investigate velocity profile at a fixed flow rate. This program reads and memorizes pixel values of all images for 4 sec (number of x-pixel × number of z-pixel × number of images during 4 second; 480 × 420 × 512 = 103,219,200 data). Once this program detects a pixel intensity value which is larger than 95% of the maximum intensity (8-bit image, pixel intensity values ranging from 0 to 255, representing black and white, respectively) in an image, two pixels located at ± 5^{th} and two pixels located at ± 4^{th} from the centroid of the detected pixel in z-direction are examined. If the detected point is the centroid of the microbead image, the intensity values of the two ± 5^{th} pixels should have intensity values smaller than 30% of the maximum intensity value, and the intensity values of the two ± 4^{th} pixels larger than 30% of the maximum pixel. If the detected point is satisfied by intensity (95% of maximum intensity value) but not by size (8 pixels), the point could be slightly deviated

from the centroid and this program continues to examine the adjacent x-position particle intensity distribution. If the detected point is satisfied by two constraints in pixel intensity and size, the particle at that point is considered to be at the focal depth.

Once a centroid is considered to be at a focal depth in a frame, the relative velocity (defined as the displacement of the centroid between the frame and the next frame divided by time between two frames; Δt = 0.008 sec/frame) was computed by examining the displacement on the track of the centroid within proceeding 10 frames (Δt = 0.08 sec), during which the consecutive motions of the centroid are assumed to represent an instant motion. In the next frame, a rectangular observation zone was set surrounding the centroid within ± 5 pixels from the previous (x, z) coordinates as shown in Fig. 3-2. No focused particles moved farther than 5 pixels between frames (0.39548 μm/pixel, Δt = 0.008 sec/frame), in other words, relative velocity of any microbeads between continuing frames did not exceed 0.02472 cm/s even for the case of the highest flow rate. Fortunately, no microbeads overlapped each other within 10 frames. In the rectangular observation zone, all points were searched to find a point satisfying the criteria. The distance between centroid at the initial frame and the next frame indicates the displacement during 0.008 sec. Thus, the relative velocity of the microbead between two consecutive frames was computed by dividing the displacement by the elapsed time. This computing process continued up to 10^{th} frame from the first frame. The actual velocity of the microbead in flowing blood suspension is sum of the relative velocity of the microbead and the translating stage speed, which was already calibrated. The sign of relative velocity could be negative (‘moving backward’ in the images), corresponding to microbeads below the zero-velocity plane in the translating stage. On the other hand,

particles moving forward in the images have positive relative velocity, and are slightly above the zero-velocity plane.

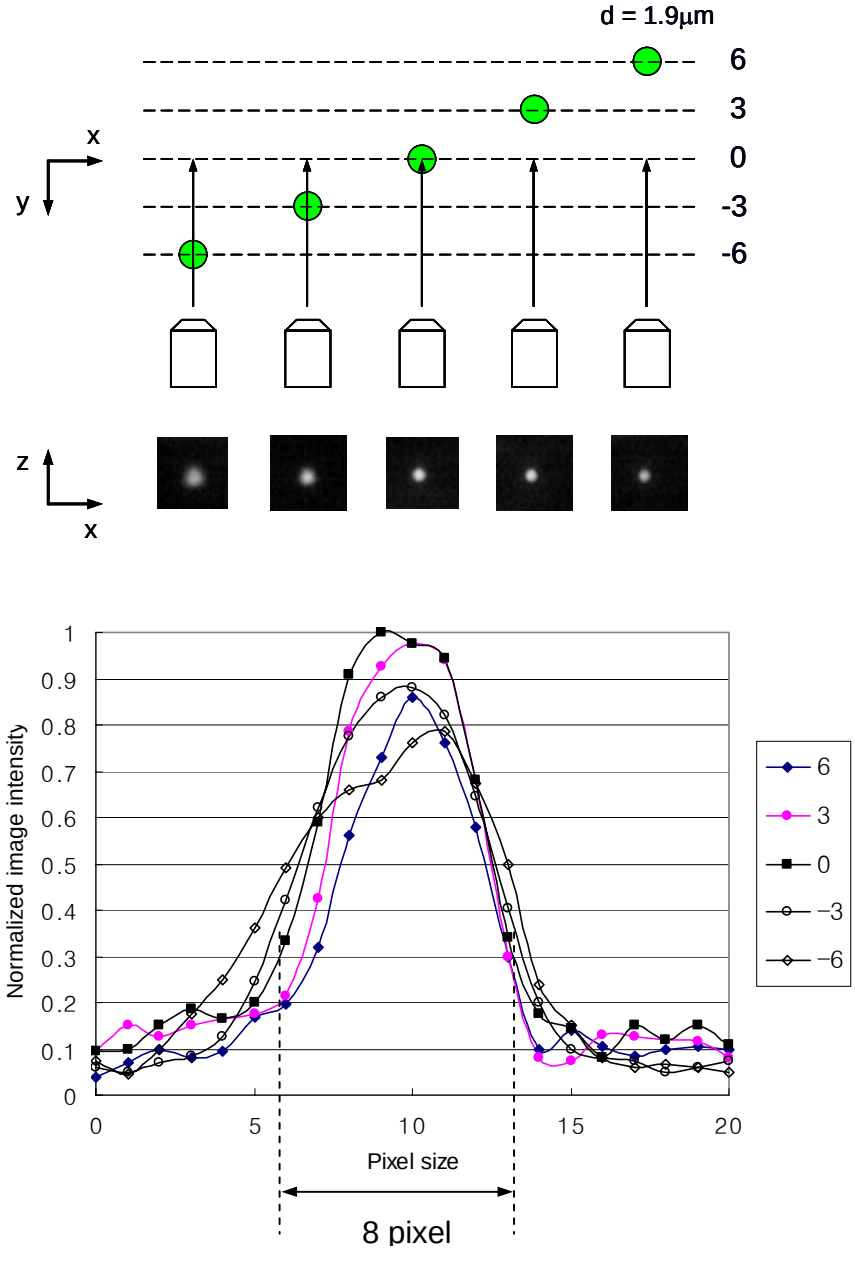

Fig. 3-1. Calibration of captured microbead image and line intensity profiles.

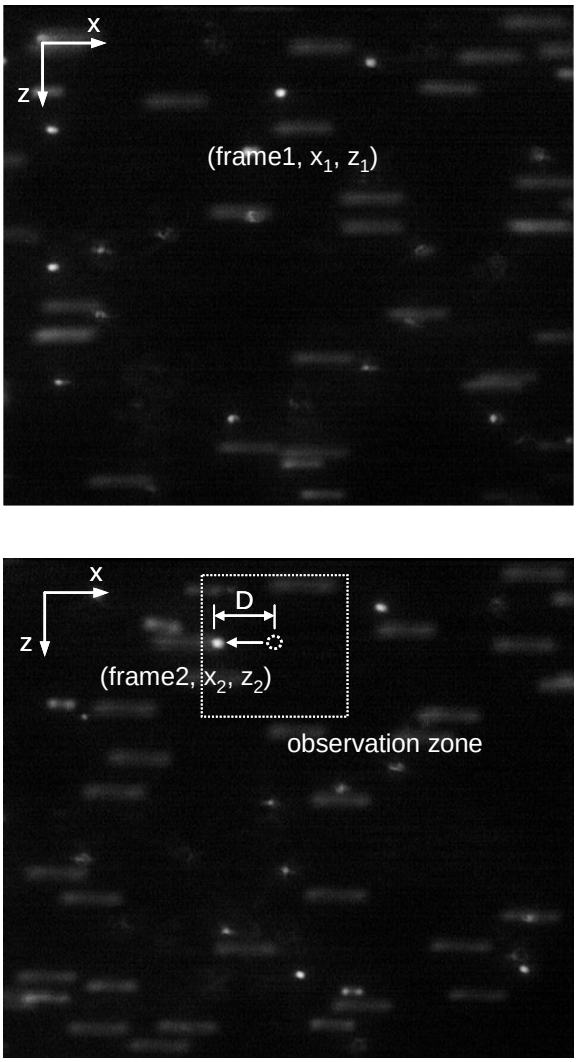

Fig. 3-2. Measurement of the relative velocity of a focused microbead.

3.3 Velocity Profile of Newtonian Fluid flowing in a Rectangular Capillary Tube

In this section, the flow of water was considered to derive the theoretical equation of the velocity profile in a rectangular capillary tube and to check that the translating-stage assay used for this study was applicable to measure the parabolic features of Newtonian fluid velocity profile, comparing the often-observed theoretical parabolic velocity profiles with experimental results at four different flow rates. Final concentration of fluorescent microbeads as tracer markers in the water was 0.033% (v/v) to optimize data density and signal to background fluorescence ratio. Nine focal depths in flow field were experimentally examined between the centerline and the bottom surface of the capillary tube. For the theoretical derivation, several assumptions were made. Flow is assumed to be laminar, steady, and fully developed, so that the conditions of flow change neither with the time nor the axial location along the tube. Also, the ratio of height to width of the tube was small (H/W=0.05) enough to ignore the side-wall effect on the velocity profile at the centerline (in width) of the tube. The above assumptions are mathematically expressed as follows,

$$\frac{du}{dt} = a_x = 0, \qquad \frac{du}{dx} = 0, \qquad \frac{du}{dz} = 0,$$

where u is the velocity in the x-direction.

3.3.1 Mathematical derivation for the general equations of motion

Since the flow has uniform boundary conditions in the flow direction and is also symmetric across the x axis, only the half volume under the centerline of the flow field

was considered. Let us consider a control volume of fluid of height y, length *dx* in the flow direction, and unit length in z-direction as shown in Fig. 3-3. The body is subjected to a pressure P from the left end and $P+\frac{\partial P}{\partial x}dx$ from the right end. It is also subjected to the shear stress τ on the bottom surface. Shear force on the side surface is ignored due to the assumption, $\frac{du}{dz}=0$, and shear force on the upper (y = 0) surface due to symmetry. Newton's second law was applied to this body,

$$\sum \vec{F}_x = M\cdot\vec{a}_x \ : \ P\cdot(y\cdot 1)-\left(P+\frac{\partial P}{\partial x}dx\right)\cdot(y\cdot 1)-\tau\cdot(dx\cdot 1)=0,$$

$$\tau(y)=-y\frac{\partial P}{\partial x}=-y\frac{dP}{dx}\ . \tag{3-1}$$

By the definition of Newtonian viscosity,

$$\tau=\mu\dot{\gamma}=-\mu\frac{du}{dy}, \tag{3-2}$$

where

μ = Newtonian fluid viscosity,

$\dot{\gamma}$ = shear rate.

Substitution of Eq. (3-1) into Eq. (3-2) yields

$$\frac{du}{dy}=\frac{1}{\mu}\frac{dP}{dx}y\,. \tag{3-3}$$

Therefore, one can integrate Eq. (3-3) with respect to y to obtain the theoretical velocity profile,

$$u(y)=\frac{1}{2\mu}\frac{dP}{dx}\left(y^2-h^2\right)=\frac{h^2}{2\mu}\left(-\frac{dP}{dx}\right)\left[1-\left(\frac{y}{h}\right)^2\right], \tag{3-4}$$

where

h = height between centerline and bottom surface of capillary tube.

This equation is obviously a parabola with respect to y. Maximum velocity occurs at the centerline (y=0) of a rectangular capillary tube,

$$u_{\max} = u(0) = \frac{h^2}{2\mu}\left(-\frac{dP}{dx}\right). \tag{3-5}$$

The rate of flow through the tube can be obtained by integrating the velocity profile over the cross-sectional area of the tube,

$$Q = 2\int_0^h \frac{1}{2\mu}\frac{dP}{dx}\left(y^2 - h^2\right)\cdot(w\cdot dy) = -\frac{2}{3}\frac{wh^3}{\mu}\frac{dP}{dx}, \tag{3-6}$$

where

w = width of capillary tube.

The shear rate can be obtained by differentiating the velocity profile with respect to y, representing a linear profile over the flow field,

$$\dot{\gamma}(y) = -\frac{du}{dy} = -\frac{1}{\mu}\frac{dP}{dx}y. \tag{3-7}$$

Therefore, wall shear rate and wall shear stress can be expressed as follows,

$$\dot{\gamma}_w = \dot{\gamma}(h) = -\frac{h}{\mu}\frac{dP}{dx}. \tag{3-8}$$

$$\tau_w = \tau(h) = -h\frac{dP}{dx}. \tag{3-9}$$

3.3.2 Experimental results and discussion

As previously described, water velocity profiles at four different flow rates were experimentally examined to check the applicability of the present translating microscope stage method for investigation of non-Newtonian blood velocity profiles. At least n = 3 particles were analyzed at each *y* position. Experimental results (mean and standard deviation of particle velocity) were compared to theoretical profiles as shown in Fig. 3-4 (a), (b), (c), and (d). The pressure drop and volume flow rate through the capillary tube were measured as shown in Fig. 2-3 in Chapter 2, and the viscosity of water was measured by using a cone-plate digital rheometer [model DV-III, Brookfield]. These data were used in Eq. 3-4 to plot the theoretical velocity profiles (see Table 3-1).

Figure 3-4 (a) shows the comparison of the average values of measured velocity data with the theoretical velocity profile for flow rate 0.003 ml/min and statistical standard deviation (see Table 3-2), indicating good agreement of the average experimental data with theoretically obtained profiles based on the measured pressure drop across capillary tube and viscosity. Figure 3-4 (b) also shows good agreement of experiment and theory for flow rate 0.0088 ml/min, and Figure 3-4 (c) and (d) for 0.0149 ml/min and 0.0203 ml/min, respectively. The plots of raw data of the measured velocity are shown in Fig. C-1, 2, 3, and 4 in Appendix C. Therefore, we concluded that the present translating microscope stage method is applicable to the measurement of velocity profiles in the rectangular capillary.

Table 3-1. Measured properties of water through a rectangular capillary.

Shear rate (s^{-1})	120	350	590	815
Viscosity (cP)	0.9	0.9	0.9	0.9
Pressure drop (Pa/m)	4300	12500	21300	29000
u_{max} (cm/s)	0.149	0.434	0.740	1.007
Flowrate (ml/min)	0.0030	0.0088	0.0149	0.0203
Wall shear stress (Pa)	0.1075	0.3125	0.5325	0.7250

Table 3-2. Standard deviation of measured velocity data at different shear rates.

y (m)	Shear rate (s^{-1})			
	120	350	590	815
0.000000	0.003	0.005	0.007	0.010
0.000002	0.003	0.005	0.008	0.012
0.000004	0.004	0.003	0.009	0.011
0.000007	0.005	0.005	0.011	0.012
0.000010	0.005	0.007	0.009	0.011
0.000013	0.006	0.010	0.015	0.009
0.000016	0.006	0.012	0.009	0.010
0.000019	0.008	0.011	0.010	0.010
0.000022	0.007	0.026	0.011	0.019

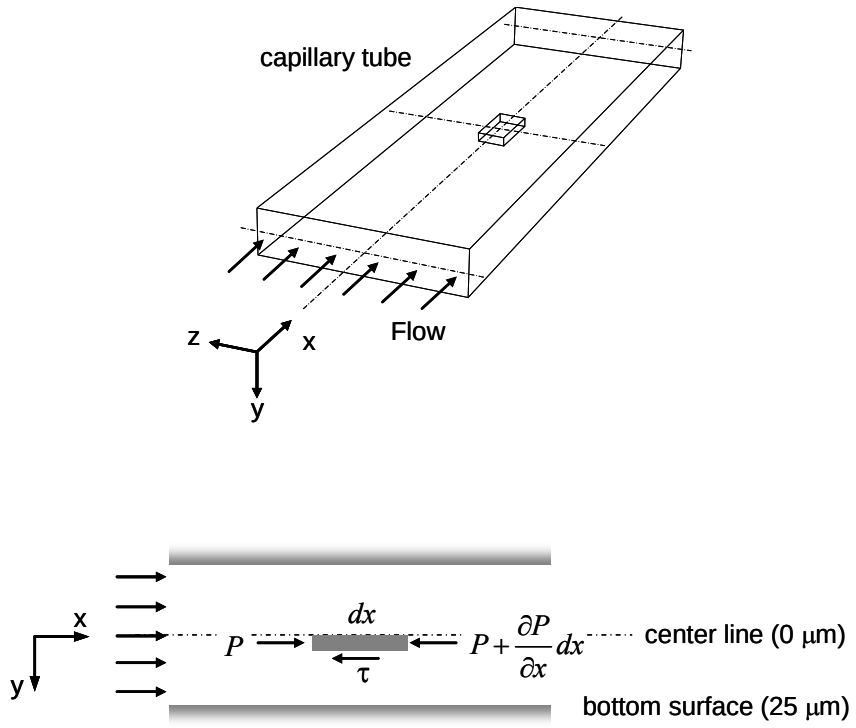

Fig. 3-3. An isolated small body of fluid derive general flow equations.

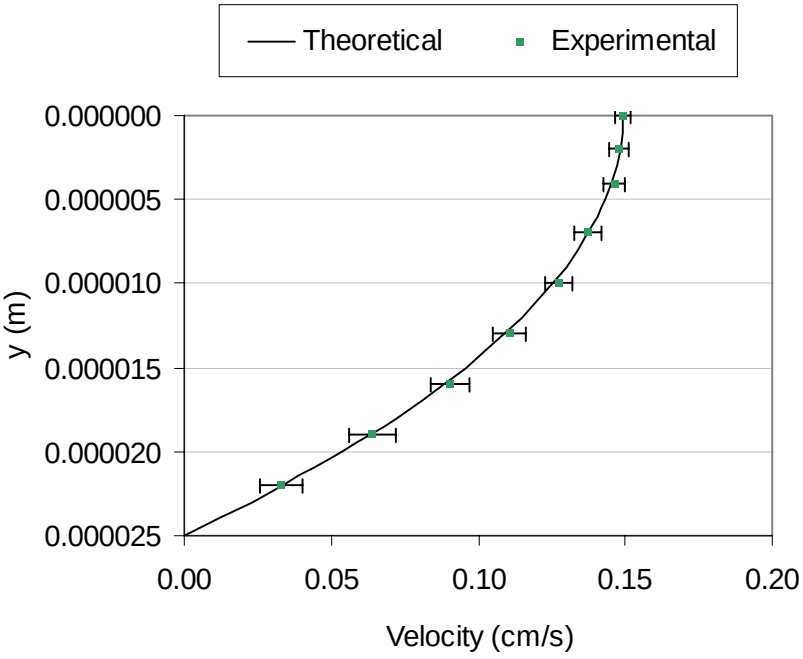

Fig. 3-4. (a) Water velocity profile at wall shear rate 120 s^{-1}.
Points are experimental measurements (mean ± STDev; n = 3).

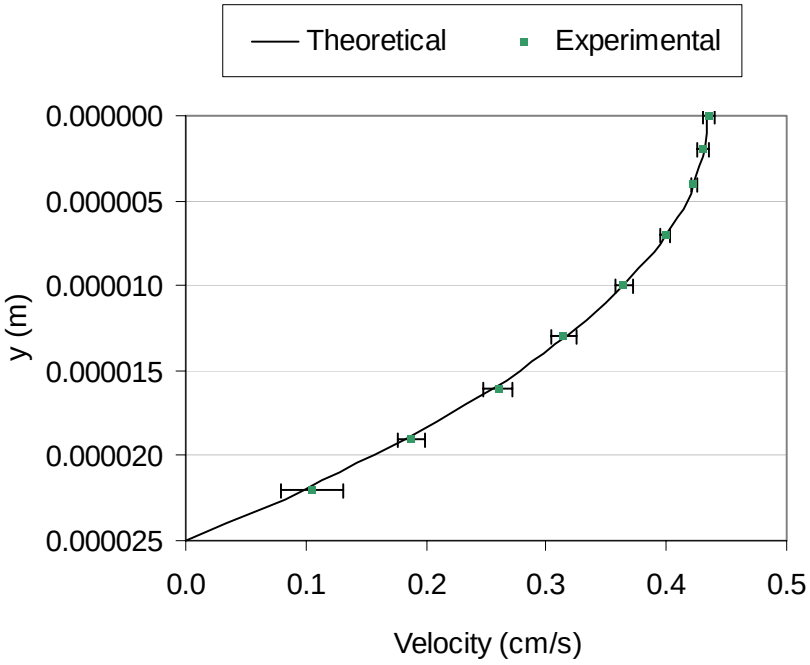

Fig. 3-4. (b) Water velocity profile at wall shear rate 350 s^{-1}.
Points are experimental measurements (mean ± STDev; n = 3).

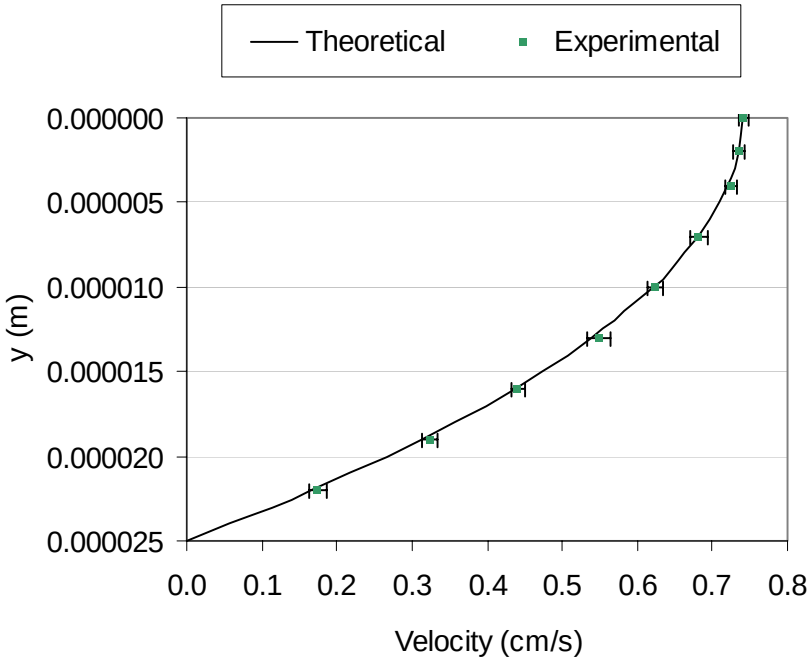

Fig. 3-4. (c) Water velocity profile at wall shear rate 590 s^{-1}.
Points are experimental measurements (mean ± STDev; n = 3).

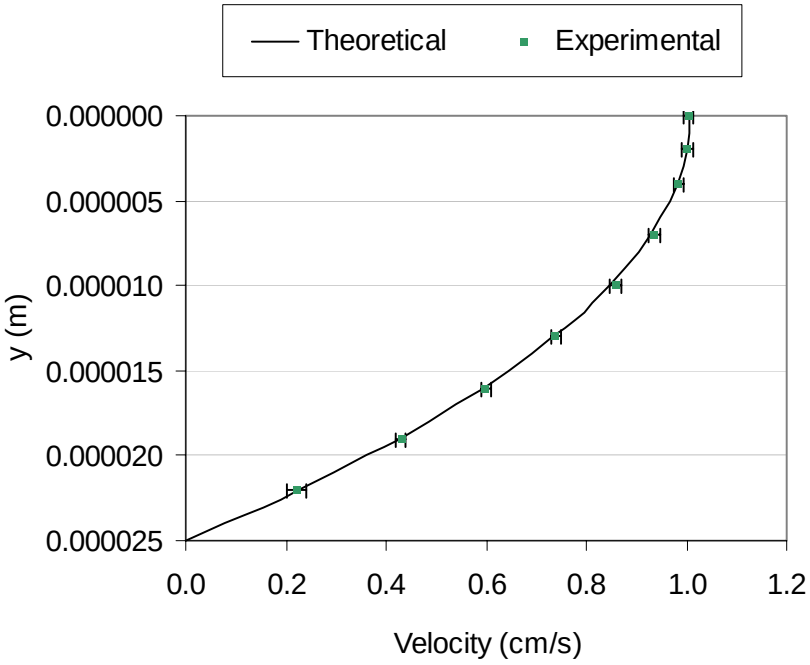

Fig. 3-4. (d) Water velocity profile at wall shear rate 815 s^{-1}.
Points are experimental measurements (mean ± STDev; n = 3).

3.4 Velocity Profile for Non-Newtonian Fluid with Casson Viscosity Model flowing in a Rectangular Capillary Tube

In this section, the Casson viscosity model was used to derive a theoretical equation for the velocity profile in a rectangular capillary tube, and the flow of blood suspension (Hct 15%) was considered to measure the blunted feature of non-Newtonian fluid velocity profile, comparing the theoretical velocity profiles with experimental results at four different flow rates. Final concentration of fluorescent microbeads as tracer markers in the blood suspension was 0.033% (v/v) to optimize data density and signal to background fluorescence ratio. Nine focal depths in the flow field were experimentally examined between the centerline and the bottom surface of the capillary tube. For the theoretical derivation, the same assumptions as Newtonian case were made:

$$\frac{du}{dt} = a_x = 0, \qquad \frac{du}{dx} = 0, \qquad \frac{du}{dz} = 0.$$

3.4.1 Mathematical derivation for the general equations of motion

Since the blood flow is axisymmetric, only the half volume under the centerline of the flow field was considered. The same control volume as in the Newtonian fluid case was considered to apply Newton's second law (Fig. 3-3). The body is subjected to a pressure P from the left end and $P + \frac{\partial P}{\partial x} dx$ from the right end. It is also subjected to the shear stress τ on the bottom surface, but no shear stress on the side surface due to the assumption, $\frac{du}{dz} = 0$. The Newton's second law was applied to this body,

$$\sum \vec{F}_x = M \cdot \vec{a}_x \ : \ P \cdot (y \cdot 1) - \left(P + \frac{\partial P}{\partial x} dx \right) \cdot (y \cdot 1) - \tau \cdot (dx \cdot 1) = 0 ,$$

$$\tau(y) = -y \frac{\partial P}{\partial x} = - y \frac{dP}{dx} \ . \tag{3-1}$$

Introducing a constitutive equation, Casson viscosity model, which can handle both yield stress and shear thinning characteristics of blood, one can describe as follows [Barbee et al., 1971; Benis et al., 1971; Reinhart et al.,1990];

$$\sqrt{\tau} = \sqrt{\eta \dot{\gamma}} + \sqrt{\tau_y} \qquad \text{when} \quad \tau \geq \tau_y , \tag{3-10}$$

$$\dot{\gamma} = 0 \qquad \text{when} \quad \tau \leq \tau_y , \tag{3-11}$$

where

τ and $\dot{\gamma}$ = shear stress and shear rate, respectively,

τ_y = yield stress, and

η = viscosity at very high shear stress $(\tau >> \tau_y)$.

Substitution of Eq. (3-1) into Eq. (3-10) yields

$$\sqrt{-y \frac{dP}{dx}} = \sqrt{\eta \left(- \frac{du}{dy} \right)} + \sqrt{\tau_y} \ : \ \frac{du}{dy} = - \frac{1}{\eta} \left(\sqrt{-y \frac{dP}{dx}} - \sqrt{\tau_y} \right)^2 . \tag{3-12}$$

Therefore, one can integrate Eq. (3-12) with respect to *y* to obtain the theoretical velocity profile,

$$u(y) = \frac{1}{2\eta} \frac{dP}{dx} y^2 - \frac{4\sqrt{y_c}}{3\eta} \frac{dP}{dx} y^{\frac{3}{2}} + \frac{y_c}{\eta} \frac{dP}{dx} y$$

$$+ \left(- \frac{1}{2\eta} \frac{dP}{dx} h^2 + \frac{4\sqrt{y_c}}{3\eta} \frac{dP}{dx} h^{\frac{3}{2}} - \frac{y_c}{\eta} \frac{dP}{dx} h \right), \tag{3-13}$$

where

y_c = half-width of the plug flow zone.

Equation (3-13) specifies a blunted profile shape around core region where the shear rate is zero because the shear stress is less than the yield stress. Maximum velocity is equal to the core velocity as follows,

$$u_c = u(y_c) = \frac{1}{6\eta}\frac{dP}{dx}{y_c}^2 + \left(-\frac{1}{2\eta}\frac{dP}{dx}h^2 + \frac{4\sqrt{y_c}}{3\eta}\frac{dP}{dx}h^{\frac{3}{2}} - \frac{y_c}{\eta}\frac{dP}{dx}h \right). \tag{3-14}$$

The rate of flow through the tube can be obtained by integrating velocity profile over the cross-sectional area of the tube,

$$Q = 2\cdot\left[u_c \cdot (w\cdot y_c) + \int_{y_c}^{h} u(y)\cdot(w\cdot dy) \right]$$

$$= -\frac{2w}{3\eta}\frac{dP}{dx}h^3 + \frac{8w\sqrt{y_c}}{5\eta}\frac{dP}{dx}h^{\frac{5}{2}} - \frac{wy_c}{\eta}\frac{dP}{dx}h^2 + \frac{w}{15\eta}\frac{dP}{dx}{y_c}^3. \tag{3-15}$$

The shear rate can be obtained by differentiating the velocity profile with respect to y,

$$\dot{\gamma}(y) = -\frac{1}{\eta}\frac{dP}{dx}\left(\sqrt{y} - \sqrt{y_c}\right)^2, \qquad y > y_c \tag{3-16}$$

Therefore, wall shear rate, wall shear stress, and yield stress can be expressed as follows,

$$\dot{\gamma}_w = \dot{\gamma}(h) = -\frac{1}{\eta}\frac{dP}{dx}\left(\sqrt{h} - \sqrt{y_c}\right)^2, \tag{3-17}$$

$$\tau_w = \tau(h) = -h\frac{dP}{dx}, \tag{3-18}$$

$$\tau_y = \tau(y_c) = -y_c\frac{dP}{dx}. \tag{3-19}$$

3.4.2 Numerical method to fit experimental data to theoretical profiles

The general flow equations for the Casson viscosity model were obtained in the previous section. Now, a specific theoretical velocity profile satisfying best agreement with a measured velocity profile needs to be obtained. Basic form of the theoretical velocity profile is as follows,

$$u(y) = f(\frac{dP}{dx}, \eta, y_c, h, y) = C_1 y^2 + C_2 y^{3/2} + C_3 y + C_4 . \quad (3\text{-}20)$$

This equation is a function of pressure drop along the capillary tube, viscosity of a blood suspension, radius of plug flow, and geometry, and can be simply described as a polynomial type with four coefficients, C_1, C_2, C_3, and C_4. Best agreement requires the optimized estimation for these four coefficients.

The pressure drop dP/dx is easily measured and height, h, between the centerline and surface of a capillary tube is a known geometrical value. But, for non-Newtonian fluid, viscosity η is a fluid property when shear rate is infinite, in other words, $\eta = \mu(\dot{\gamma} \to \infty)$. Unlike a Newtonian fluid which has a constant viscosity for all range of shear rates, viscosity of a non-Newtonian fluid is a nonlinear function of shear rate, thus, simple substitution of a viscosity value in Eq. (3-13) does not yield a correct velocity profile. Furthermore, Eq. (3-13) is a function of the radius of plug flow, y_c, which is not easy to measure, and radius of plug flow depends on both flow rate and viscosity. Thus, three easily-measured experimental parameters were chosen to obtain the best optimized four coefficients in Eq. (3-20), which are the (1) pressure drop through the

capillary tube, (2) volume flow rate, and (3) maximum velocity at the centerline obtained by the translating stage method.

A numerical process for optimizing the flow profile to the experimental measurements was developed (Fig. 3-5). The pressure drop was measured and plugged into Eq. (3-13) as an input parameter. The geometry *h* and *w* were also plugged into the velocity equation. This numerical process totally consists of three iteration loops: the biggest outside iteration loop is for the radius of plug flow y_c with an increment $\Delta y_c = 0.01$ μm, and the middle iteration loop is for the viscosity parameter η with an increment $\Delta\eta$ = 0.00001 Pa·s, and the smallest inner iteration is for the velocity profile $u(y)$ calculated between the centerline and the capillary surface with an increment $\Delta y_c = 0.01$ μm. The radius of plug flow y_c varied from 0 μm meaning no plug flow to 4 μm which is sufficient for the range of flow rates considered. The viscosity η varied from 1 to 4 centiPoise (cP) for the middle iteration loop, and *y* from 0 (centerline) to 25 μm (surface of capillary tube) for the velocity. For a specific value of y_c and η, velocity was calculated for every 0.01 μm from the centerline to surface and total volume flow rate was calculated for the velocity values using trapezoid rule integration. The total volume flow rate is the sum of core region and shear region. The maximum velocity is the velocity at the centerline when $y_c = 0$, otherwise, $u_{\max} = u_c = u(y_c)$. Here, the measured flow rate played a role as a constraint to limit the result of this numerical process: only the calculated flow rates within 0.5% in error were accepted when those were compared with the measured flow rate. After this calculation processes, all data satisfied two out of the three parameters: pressure drop and flow rate within 0.5% in error.

The last parameter, maximum velocity, varied within maximum $\pm 10\%$ with respect to the measured maximum velocity. Some data similar to the measured maximum velocity at centerline were chosen, but the corresponding y_c and η were different for each case. To obtain the optimized values of y_c and η, and consequently the four coefficients in Eq. (3-20), root mean square (RMS) method was applied to get a data set for (y_c, η, $u_{\max}$), which finds the minimum value for the combined normalized error of both $u_{\max}$ and flow rate as follows,

$$RMSerror = \sqrt{\left(\frac{u_{\max,m} - u_{\max,cal}}{u_{\max,m}}\right)^2 + \left(\frac{Q_m - Q_{cal}}{Q_m}\right)^2} \tag{3-21}$$

where

$u_{\max,m}$ = measured maximum velocity at the centerline,

$u_{\max,cal}$ = calculated maximum velocity,

Q_m = measured flow rate, and

Q_{cal} = calculated flow rate.

Finally, the four coefficients, C_1, C_2, C_3, and C_4, of the theoretical velocity profile could be determined so that the velocity profile based on Casson viscosity model could accomplish the best fit to experimental data obtained by the translating microscope stage method. Furthermore, once the optimized values for y_c and η were obtained, wall shear rate, wall shear stress, and yield shear stress could be calculated from Eq. (3-17), (3-18), and (3-19), respectively.

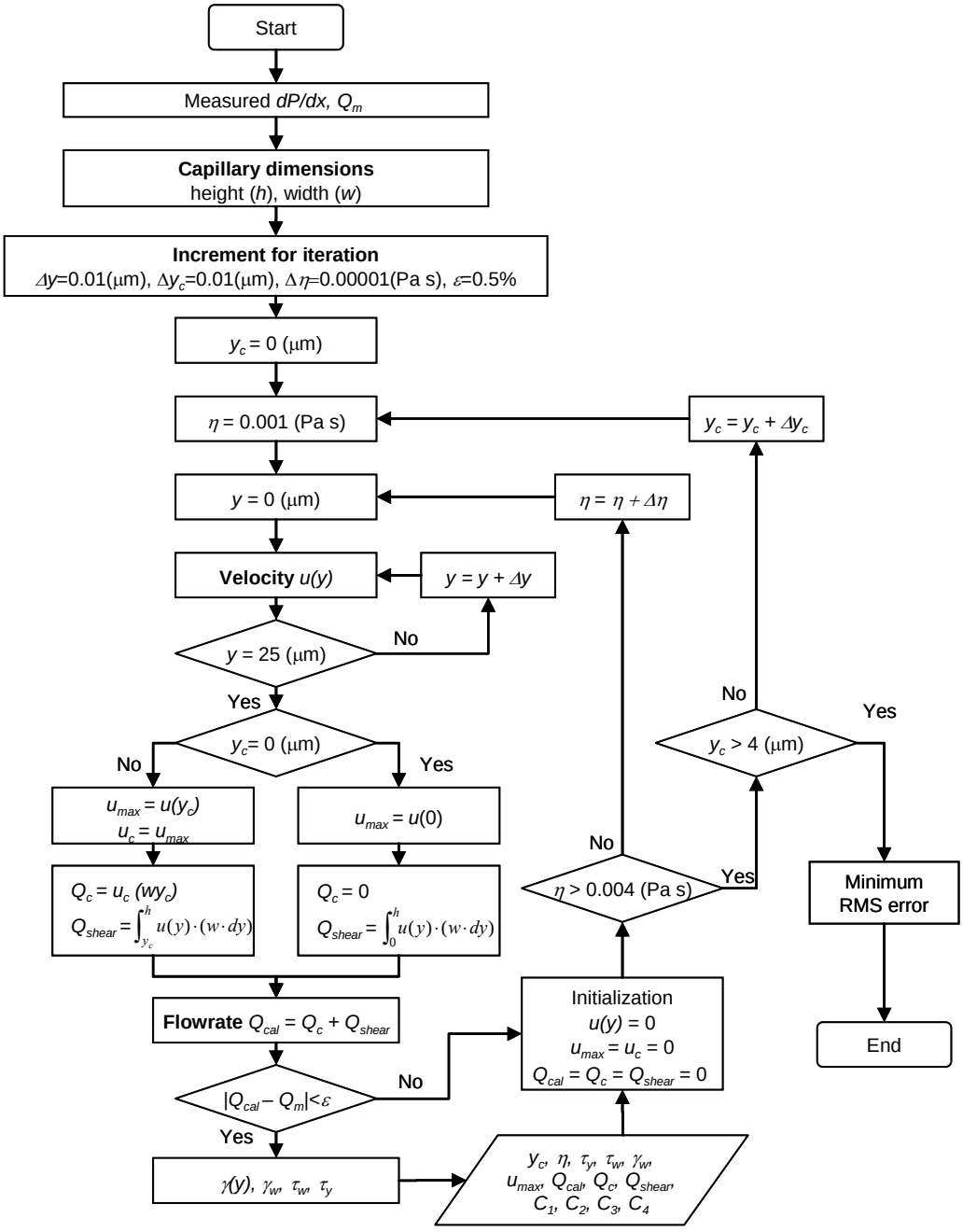

Fig. 3-5. Flow chart describing numerical method to obtain optimized velocity profiles for Casson non-Newtonian viscosity model.

3.4.3 Experimental results and discussion

The results obtained for platelet velocity profiles are presented in Tables 3-3 and 3-4. Table 3-3 shows values of the optimized coefficients for Casson velocity profiles at different nominal shear rates (nominal shear rates are calculated using Newtonian parabolic profile assumption), based on the numerical method. The estimate of experiment shear rate was obtained by the differentiation of the resulting theoretical velocity equation. Thus the intercept of the profile and vessel wall almost satisfied no-slip conditions on the wall. But actually, the velocity at the wall varied from -0.00002 to 0.00005 cm/s, which were negligible compared to that of the remainder of the vessel. Based on these velocity profiles, other properties were estimated and compared with the measured values as shown in Table 3-4. The estimates of the calculated wall shear rate ranged from 126 to 840 s^{-1}, and centerline velocity varied from 0.141 to 1.004 cm/s. The wall shear rates were 1.03-1.05 times higher than expected in Newtonian parabolic velocity profiles (nominal shear rates). The reason that there are no big differences in wall shear rates might be caused by the facts that 1) natural plasma was not used in the blood suspension sample used, making the suspension less viscous than whole blood and reducing the tendency of RBCs to aggregate, 2) with this blood suspension, hematocrit was not as much as normal large-artery value, 3) even the lowest shear rate range doesn't bring the blunted characteristics of non-Newtonian fluid around the core region. Here, the assumption of a parabolic velocity profile for a shear flow of blood may cause a significant error in consideration of wall shear stress, one of significant factors involving the effect of hydrodynamic forces on the kinetics of tethered platelets to an intravascular

injury, endothelial cells, or thrombogenetic surfaces. Even though the radius of plug flow looks smaller than expected for a non-Newtonian fluid, there is an obvious effect on the velocity profiles and its influence on the wall shear rates should not be neglected a priori. The viscosity and yield stress of the blood suspension were calculated for four different shear rates and had good agreement to each other, which is supposed to be same because same blood suspension was used in the experiment.

Adequate descriptions of the shape of both the experimental and theoretical profiles based on the Casson viscosity model were presented in Fig. 3-6 (a), (b), (c), and (d) at different shear rates. The maximum velocity measured by translating stage method is less than that of parabolic profile of Newtonian case. The averages of raw data at each observed focal depth are presented with statistical standard deviations. The raw data are also presented in Fig.C-5, 6, 7, and 8 in Appendix C. Based on this maximum velocity, the theoretical velocity profile was fitted to experiment data by the iteration seeking for y_c and η pursuing the optimized profile with the least RMS error in both total volume flow rate and maximum velocity. The averages of measured data slightly deviate from the theoretical fit, but stayed well within the range of standard deviation as shown in Table 3-5. As the observed focal depth reaches the surface, the standard deviation values increase relative to that of core region, meaning that motions of the particles flowing in a thin layer of fluid near wall have stronger effect of the neighboring layer of fluid compared to the core region because the near wall velocity gradient is steeper than in the remainder of the vessel. In conclusion, the measured microbead velocities showed good agreement with the theoretical profiles at different flow rates. Thus the theoretical profiles can be used to investigate the location of flowing platelets, if the speed of platelets is measured

from the consecutive images using the translating stage microscopy method in section 4.3. In addition, the local concentration of platelets in shear flow of blood can be estimated, as well as the concentration profile over the entire flow field. The shear rate and shear stress at the wall could be estimated, and fluid properties such as viscosity and yield stress were also obtained.

Table 3-3. The optimized coefficients for Casson velocity profiles.

Coeff	Nominal Shear rate (s-1)			
	120	350	590	815
C_1 (m^{-1} s^{-1})	-3493492.03	-8853342.33	-14292353.54	-19138945.41
C_2 ($m^{-1/2}$ s^{-1})	6971.44	11073.56	14260.56	16139.38
C_3 (s^{-1})	-3.913	-3.895	-4.002	-3.828
C_4 (m/s)	0.001410	0.004247	0.007250	0.010040

Table 3-4. Comparison of the measured and calculated flow and fluid properties.

	Nominal Shear rate (s^{-1})			
	120	350	590	815
Calculated				
η (cP)	2.51	2.57	2.54	2.57
y_c (μm)	0.56	0.22	0.14	0.10
γ_w (s^{-1})	126	364	612	840
τ_w (Pa)	0.4384	1.1377	1.8151	2.4594
τ_y (Pa)	0.0098	0.0100	0.0102	0.0098
u_{max} (cm/s)	0.1409	0.4246	0.7250	1.0040
Q_{core} (ml/min)	0.0001	0.0001	0.0001	0.0001
Q_{shear} (ml/min)	0.0028	0.0086	0.0147	0.0203
Q (ml/min)	0.0029	0.0087	0.0148	0.0204
Measured				
dP/dx (Pa/m)	-17537	-45506	-72605	-98374
Q (ml/min)	0.0029	0.0088	0.0148	0.0204

Table 3-5. Standard deviation of the measured velocity data at different shear rates.

y (m)	Shear rate (s-1)			
	120	350	590	815
0	0.0024	0.0040	0.0068	0.0124
0.000002	0.0030	0.0055	0.0065	0.0090
0.000004	0.0038	0.0041	0.0084	0.0130
0.000007	0.0046	0.0068	0.0139	0.0118
0.000010	0.0040	0.0077	0.0117	0.0115
0.000013	0.0056	0.0093	0.0165	0.0106
0.000016	0.0069	0.0135	0.0110	0.0089
0.000019	0.0082	0.0113	0.0093	0.0089
0.000022	0.0113	0.0236	0.0101	0.0219

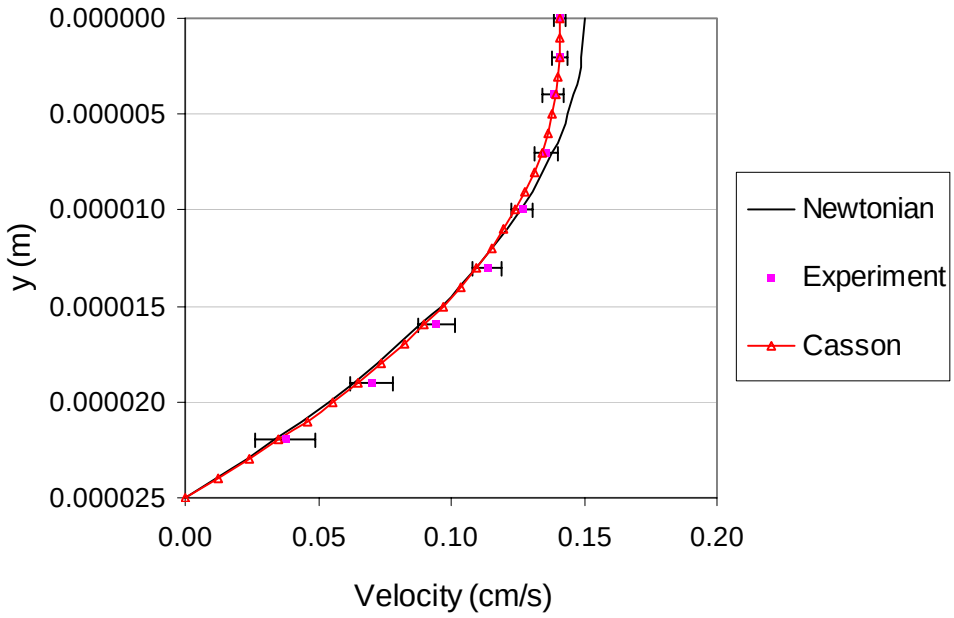

Fig. 3-6. (a) Non-Newtonian Casson velocity profiles at wall shear rate 126 s^{-1} compared to experimental measurements (n = 3).

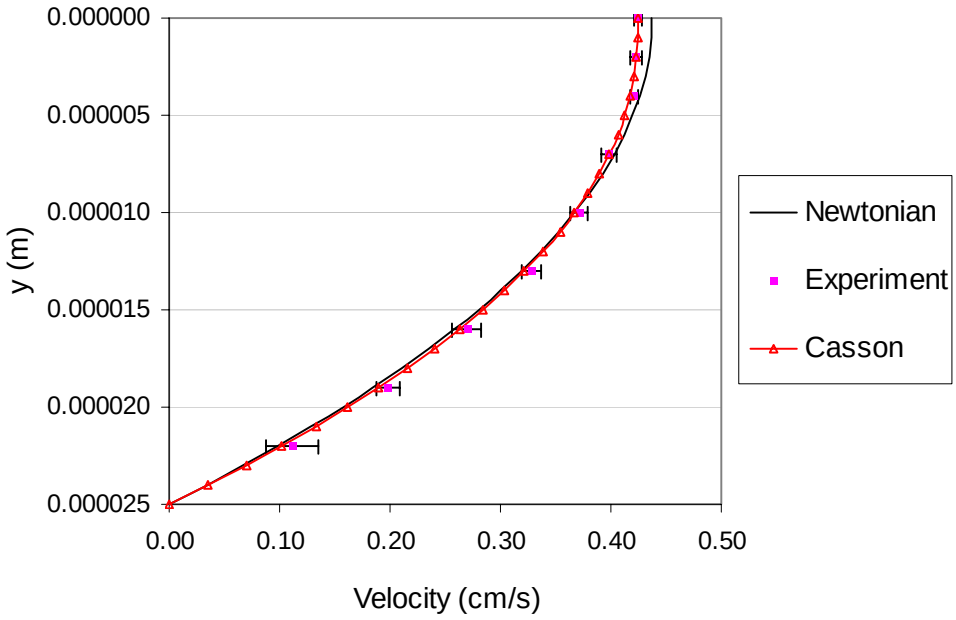

Fig. 3-6. (b) Non-Newtonian Casson velocity profiles at wall shear rate 364 s^{-1} compared to experimental measurements (n = 3).

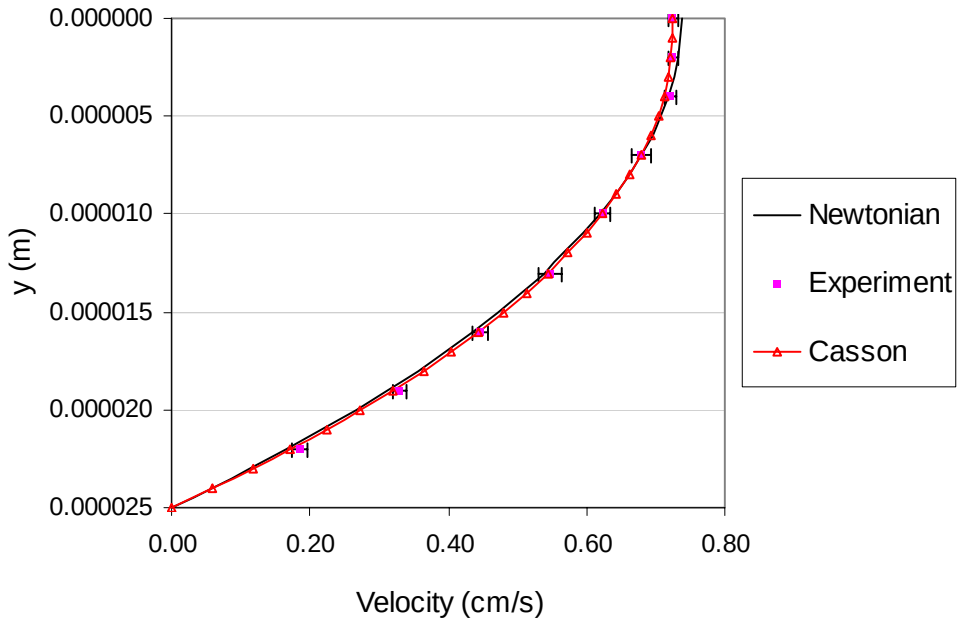

Fig. 3-6. (c) Non-Newtonian Casson velocity profiles at wall shear rate 612 s^{-1} compared to experimental measurements (n = 3).

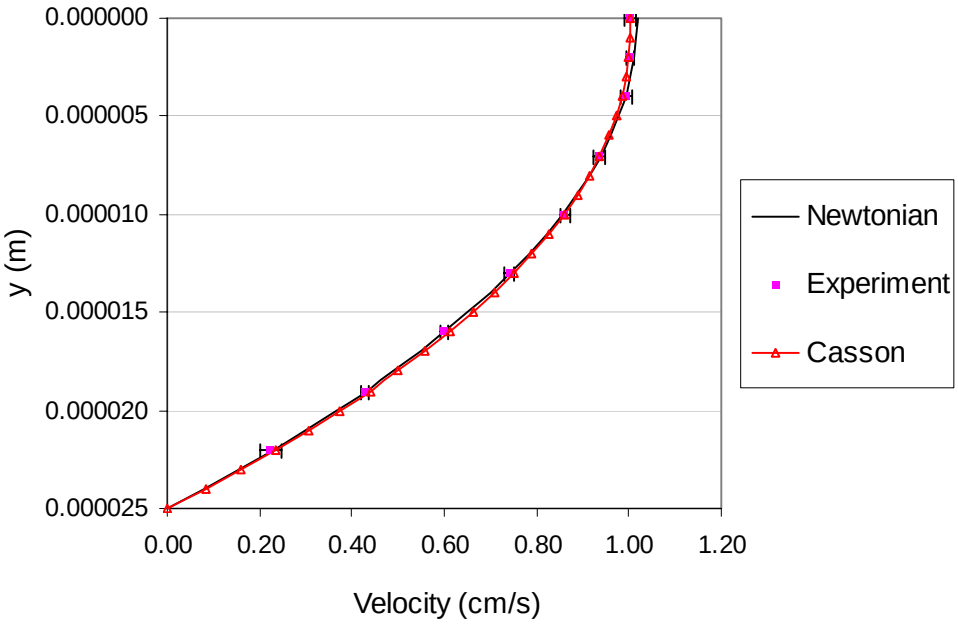

Fig. 3-6. (d) Non-Newtonian Casson velocity profiles at wall shear rate 840 s^{-1} compared to experimental measurements (n = 3).

3.5 Velocity Profile for Non-Newtonian Fluid with Power-law Viscosity Model flowing in a Rectangular Capillary Tube

In this section, the Power-law viscosity model was used to derive a theoretical equation for the velocity profile in a rectangular capillary tube, and the flow of blood suspension (Hct 15%) was used to compare the theoretical velocity profiles with experimental results at four different flowrates. Final concentration of fluorescent microbeads as tracer markers in the blood suspension was 0.033% (v/v) to optimize data density and signal to background fluorescence ratio. Nine focal depths in the flow field were experimentally examined between the centerline and the bottom surface of the capillary tube. For the theoretical derivation, the same assumptions as Newtonian or Casson model case were made:

$$\frac{du}{dt} = a_x = 0\,, \qquad \frac{du}{dx} = 0\,, \qquad \frac{du}{dz} = 0\,.$$

3.5.1 Mathematical derivation for the general equations of motion

The same control volume in section 3.3 or 3.4 was considered to apply Newton's second law as shown in Fig. 3-3. The Newton's second law was applied to this body,

$$\sum \vec{F}_x = M \cdot \vec{a}_x \;:\; P \cdot (y \cdot 1) - \left(P + \frac{\partial P}{\partial x} dx \right) \cdot (y \cdot 1) - \tau \cdot (dx \cdot 1) = 0\,,$$

$$\tau(y) = -y \frac{\partial P}{\partial x} = -y \frac{dP}{dx}\,. \tag{3-1}$$

Introducing a constitutive equation, the Power-law viscosity model, which contains two parameters: m (with units of $\mathrm{Pa}\cdot\mathrm{s}^{n}$), and n (dimensionless), one can describe as follows,

$$\mu = m\dot{\gamma}^{n-1}. \tag{3-22}$$

When $n=1$ and $m=\mu$, the Newtonian fluid is recovered. If $n<1$, the fluid is said to be "pseudoplastic" or "shear-thinning", and if $n>1$, the fluid is considered "dilatant" or "shear-thickening" [Bird et al, 1987]. The relationship between shear stress and shear rate is as follows,

$$\tau = \mu\dot{\gamma}. \tag{3-23}$$

Substitution of Eq. (3-1) and (3-22) into Eq. (3-23) yields

$$-y\frac{dP}{dx} = m\dot{\gamma}^{n} = m\left(-\frac{du}{dy}\right)^{n} : \quad \frac{du}{dy} = -\left(-\frac{1}{m}\frac{dP}{dx}\right)^{\frac{1}{n}} y^{\frac{1}{n}}. \tag{3-24}$$

Therefore, one can integrate Eq. (3-24) with respect to y to obtain the theoretical velocity profile,

$$u(y) = \frac{n}{1+n}\left(-\frac{1}{m}\frac{dP}{dx}\right)^{\frac{1}{n}}\left(-y^{1+\frac{1}{n}} + h^{1+\frac{1}{n}}\right). \tag{3-25}$$

The rate of flow through the tube can be obtained by integrating the velocity profile over the cross-sectional area of the tube,

$$Q = 2\cdot\int_0^h u(y)\cdot(w\cdot dy) = \frac{2n}{1+2n}\left(-\frac{1}{m}\frac{dP}{dx}\right)^{\frac{1}{n}} h^{2+\frac{1}{n}} w. \tag{3-26}$$

The velocity profile can be described in terms of flow rate,

$$u(y) = \frac{1+2n}{2(1+n)}\frac{h^{-2-\frac{1}{n}}}{w}\left(-y^{1+\frac{1}{n}} + h^{1+\frac{1}{n}}\right)Q. \tag{3-27}$$

The maximum velocity occurs at the centerline,

$$u_{\max} = u(0) = \frac{1+2n}{2(1+n)}\frac{Q}{hw}. \tag{3-28}$$

The shear rate can be obtained by differentiating the velocity profile with respect to y,

$$\dot{\gamma}(y) = \frac{1+2n}{2n}\frac{h^{-2-\frac{1}{n}}}{w} y^{\frac{1}{n}} Q. \tag{3-29}$$

Therefore, wall shear rate, wall shear stress, and yield stress can be expressed as follows,

$$\dot{\gamma}_w = \dot{\gamma}(h) = \frac{1+2n}{2n}\frac{Q}{wh^2}, \tag{3-30}$$

$$\tau_w = \tau(h) = -h\frac{dP}{dx}. \tag{3-31}$$

The power-law parameter, m, can be described in terms of flow rate and pressure drop,

$$m = -\frac{dP}{dx}\left(\frac{1+2n}{2n}\frac{Q}{w}h^{-2-\frac{1}{n}}\right)^{-n}. \tag{3-32}$$

3.5.2 Numerical method to fit theoretical profiles to experimental data

The general flow equations for the Power-law viscosity model were obtained in the previous section. Now, a specific theoretical velocity profile satisfying best agreement with a measured velocity profile needs to be obtained. The basic form of the theoretical velocity profile shown in Eq. (3-27) is as follows,

$$u(y) = f(Q, h, w, n, y). \tag{3-33}$$

The velocity profile is a function of flow rate, geometry, and a power-law parameter. Flow rate was measured and geometrical dimensions are given values. One of the power-

law parameters n is the only unknown in this equation while y is independent variable. If n is given as an input constant, the theoretical profile can be directly estimated over the flow field. Thus a numerical process was developed to estimate the optimized value of n which could yield the best fit of a theoretical profile to experimental data (Fig. 3-7). The pressure drop was measured and used to calculate the other power-law parameter m in Eq. (3-32). The geometry *h* and *w* were also plugged into the velocity equation. The numerical process consists of two iteration loops: the outside iteration loop is for a power-law parameter n with an increment $\Delta n = -0.0001$, running in a way of decreasing n. The inner iteration is for the velocity $u(y)$ between the centerline and surface of capillary with an increment $\Delta y = 0.01$ μm. The Power-law parameter n varied from 1.0 to 0.1 for the outer iteration, and *y* from 0 (centerline) to 25 μm (surface of capillary tube) for the velocity. For a power-law parameter n, velocity was calculated for every 0.01 μm from the centerline to the surface, and maximum velocity was considered as $u_{\max} = u(0)$. Here, the measured centerline velocity played a role as a constraint to limit the result of this numerical process: only the calculated $u_{\max}$ within 0.5% in error was accepted when it was compared with the measured centerline velocity. After the whole iteration processes, the calculated maximum velocity varied within $\pm 0.5\%$ with respect to the measured maximum velocity. Some data similar to the measured maximum velocity were chosen, but corresponding m and n were different for each case. To obtain the values of m and n for the optimized velocity, the normalized error of the calculated maximum velocity was examined. Finally, the theoretical velocity profile could be determined so that the velocity profile based on the power-law viscosity model could accomplish best fit to experimental data obtained by the

translating microscope stage method. Furthermore, once optimized values for m and n were obtained, wall shear rate and wall shear stress could be calculated using Eq. (3-30) and (3-31), respectively.

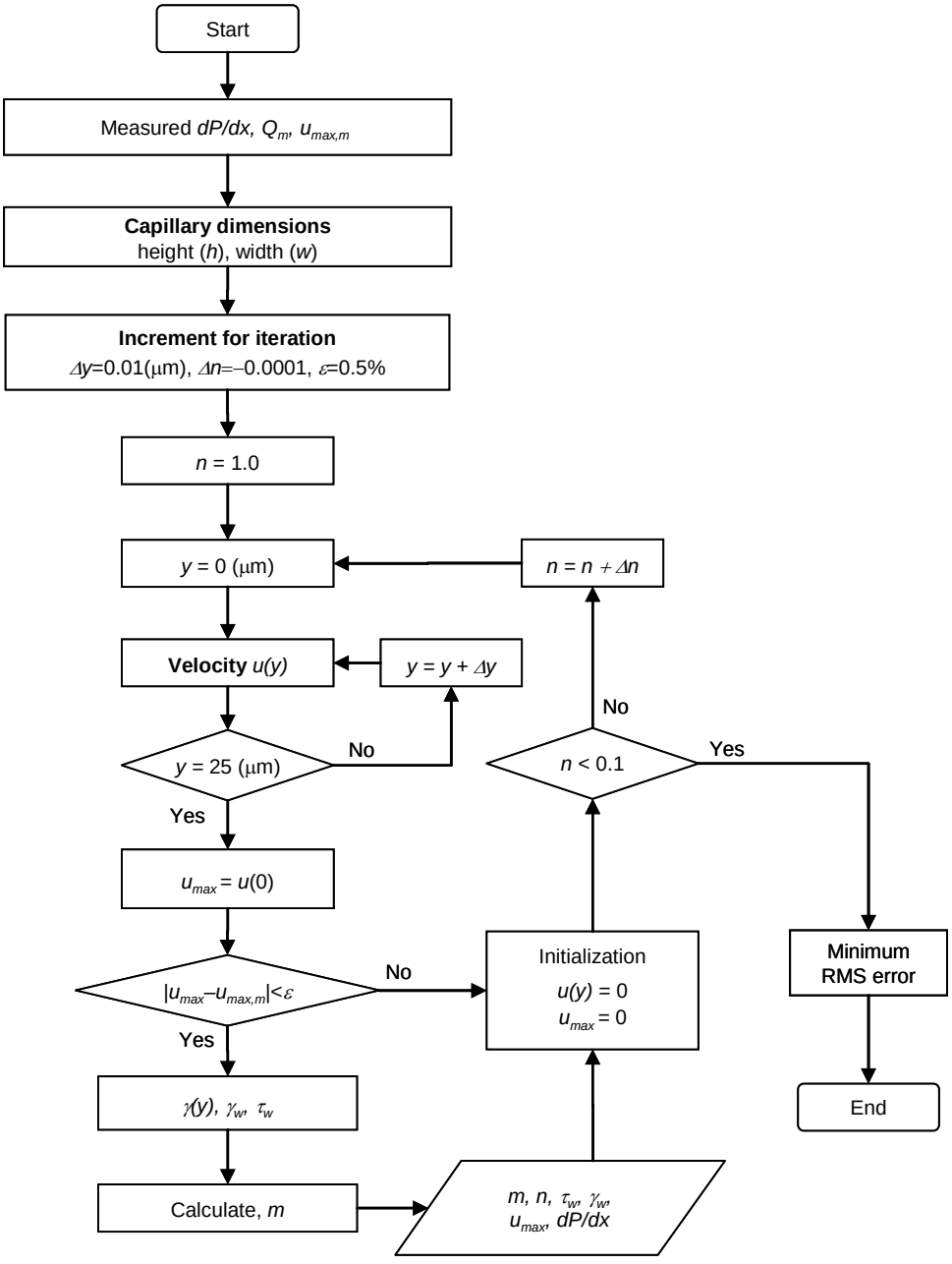

Fig. 3-7. Flow chart describing numerical method to obtain optimized velocity profiles for Power-law non-Newtonian viscosity model.

3.5.3 Experimental results and discussion

The velocity equation shown in Eq. (3-25) or (3-27) was on the basis of theory, and the estimation of shear rate was obtained by the differentiation of the velocity equation. The intercept of the profile and vessel wall exactly satisfied no-slip conditions on the wall. Based on these velocity profiles, other properties were estimated and compared with the measured values as shown in Table 3-6. The estimates of the calculated wall shear rate ranged from 127 to 827 s^{-1}, and centerline velocity varied from 0.141 to 1.010 cm/s. The wall shear rates were 1.02-1.06 times higher than expected in Newtonian parabolic velocity profiles (nominal shear rates). Here, the assumption of a parabolic velocity profile for a shear flow of blood may cause a significant error in consideration of wall shear stress, one of significant factors involving the effect of hydrodynamic forces on the kinetics of platelets.

Adequate descriptions of the shape of both the experimental and theoretical profiles based on the power-law viscosity model are presented in Fig. 3-8 (a), (b), (c), and (d) at different shear rates. The maximum velocity measured by the translating stage method is similar to that of the parabolic profile of the Newtonian case. The averages of raw data at each observed focal depth are presented with statistical standard deviations. The raw data are also presented in Fig. C-9, 10, 11, and 12 in Appendix C. Based on the maximum velocity, the theoretical velocity profile was fitted to experimental data by an iteration method seeking the value of y_c and η to give an optimized profile with the least RMS error in both total volume flow rate and maximum velocity. The averages of measured data slightly deviate from the theoretical fit, but the theoretical fit stayed well

within the range of standard deviation. In conclusion, the measured platelet velocities showed good agreement with the theoretical profiles at different flow rates. Thus the theoretical profiles can be used to investigate the location of flowing platelets, if the speed of platelets is measured using the translating stage microscopy method. In addition, the local concentration of platelets in a shear flow of blood can be estimated, as well as whole concentration profile over the flow field. The shear rate and shear stress at the wall can also be estimated.

Table 3-6. Comparison of the measured and calculated flow and fluid properties.

	Nominal Shear rate ($s^{-}1$)			
	120	350	590	815
Calculated				
m (Pa s^n)	0.00905	0.00807	0.00564	0.00397
n (N/A)	0.8007	0.8358	0.9000	0.9571
γ_w (s^{-1})	127	363	612	827
τ_w (Pa)	0.4384	1.1377	1.8151	2.4594
u_{max} (cm/s)	0.1414	0.4245	0.7246	1.0113
Q (ml/min)	0.0029	0.0087	0.0148	0.0204
Measured				
dP/dx (Pa/m)	-17537	-45506	-72605	-98374
Q (ml/min)	0.0029	0.0088	0.0148	0.0204

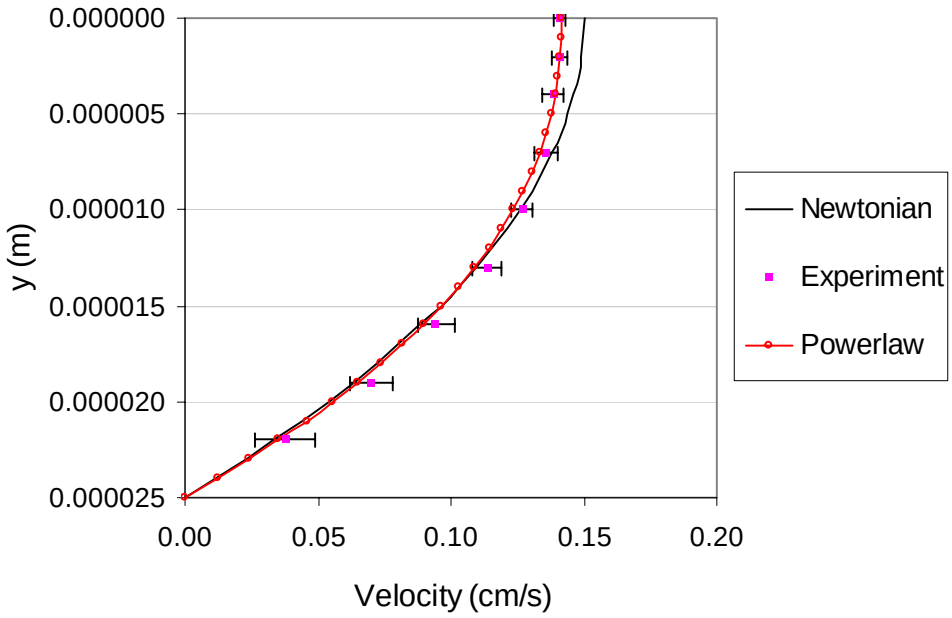

Fig. 3-8. (a) Non-Newtonian Power-law velocity profiles at wall shear rate 127 s^{-1} compared to experimental measurements (n = 3).

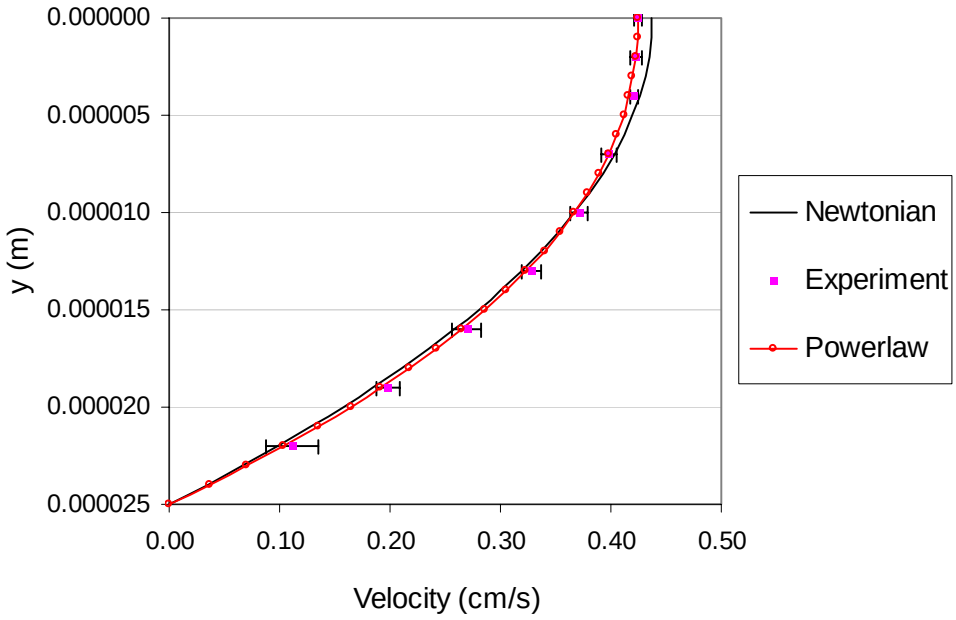

Fig. 3-8. (b) Non-Newtonian Power-law velocity profiles at wall shear rate 363 s^{-1} compared to experimental measurements (n = 3).

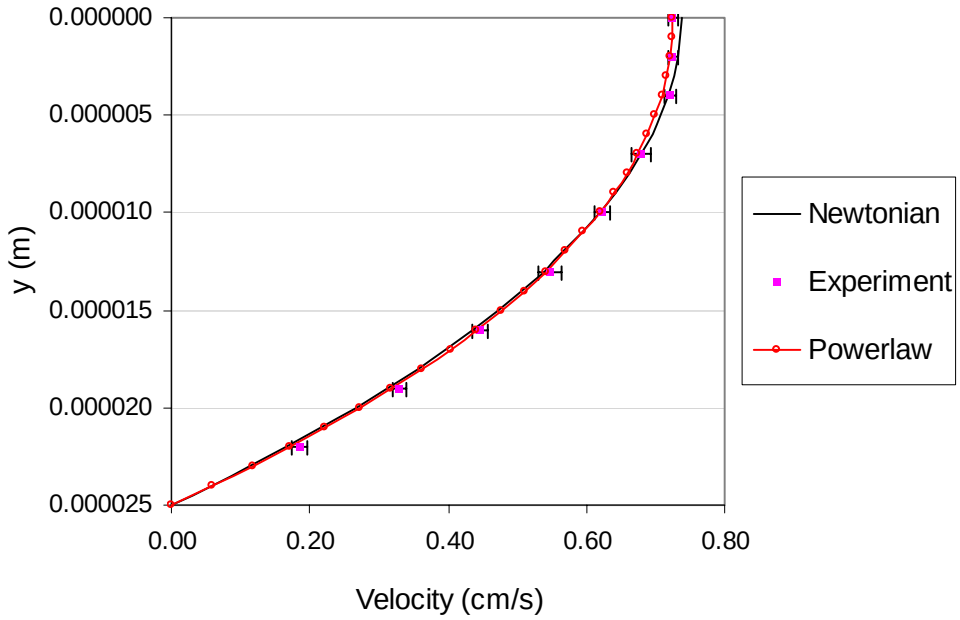

Fig. 3-8. (c) Non-Newtonian Power-law velocity profiles at wall shear rate 612 s^{-1} compared to experimental measurements (n = 3).

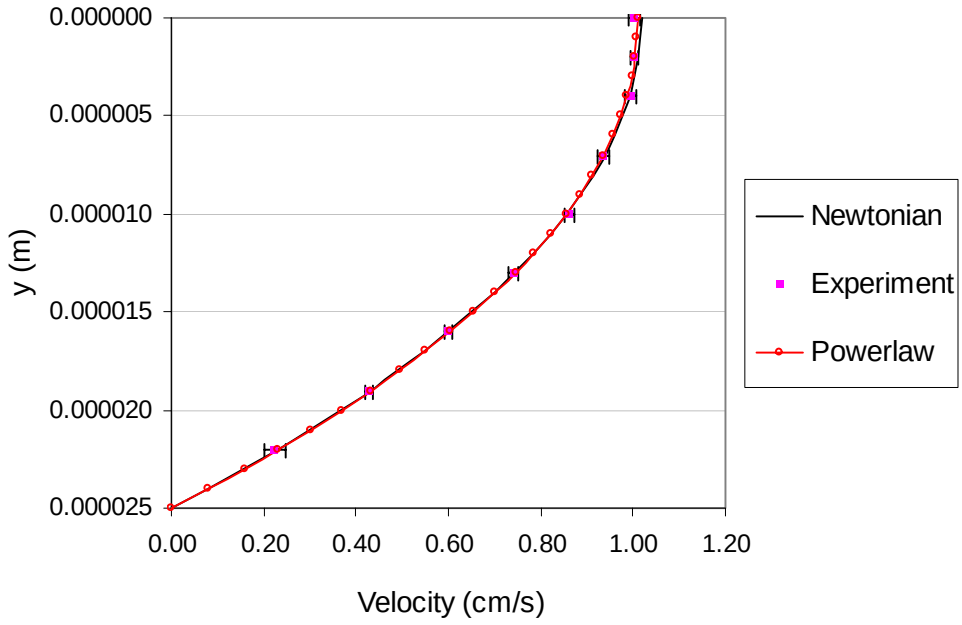

Fig. 3-8. (d) Non-Newtonian Power-law velocity profiles at wall shear rate 827 s^{-1} compared to experimental measurements (n = 3).

CHAPTER 4. PLATELET MARGINATION AND vWF ADHESION KINETICS

4.1 Introduction

4.1.1 Background

A prerequisite step prior to molecular thrombogenic adhesion events is the physical contact of platelets to protein-adsorbed surfaces. The contact requires transport of platelets to the vessel wall. Three principal mechanisms of platelet transport have been described: convection, shear-induced dispersion, and persistent drift. More distinctly, the transversely diffusive behavior of red blood cells strongly contributes to the complex interaction between the red blood cells and platelets (in fact, all other cells), and induces migration of the platelets toward the vessel wall. Consequently flowing blood develops a radial distribution of concentration of platelets, skewed toward the blood vessel wall, known as "platelet margination." Many *in vivo* [Tangelder et al., 1982 & 1985; Woldhuis et al., 1992] and *in vitro* [Aarts et al., 1988; Bilsker et al., 1989; Corattiyl et al., 1986; Eckstein et al., 1988 & 1989; Koleski et al., 1991; Tilles et al., 1987; Turitto et al., 1972; Waters et al., 1990; Xu & Wootton, 2004: Yeh et al., 1994] trials to measure the spatially skewed distribution of platelets or platelet-sized microspheres in a shear flow of blood have been made. A phenomenological computational method has been developed with a drift term added to the convective diffusion equation for platelet transport so that situations with near-wall excesses of platelets could be described [Eckstein et al., 1991; Yeh et al., 1994]. The mathematical relationship between the drift and the fully

developed, steady state platelet concentration profile was obtained, and the functional form of the drift led to concentration profiles similar to experimentally determined profiles.

After establishment of contact of flowing platelets with the blood vessel wall, sufficient adhesive strength to overcome hydrodynamic forces is needed. The extent of a platelet's ability to resist flow depends on the interactive forces between platelet receptors and ligands. $\alpha_{IIb}\beta_3$-fibrinogen can support interaction of both platelet-surface adhesion and platelet-platelet aggregation [Bennett et al., 1982; Coller, 1980; Gogstad et al.,1982; Mustard et al., 1978; Nachman et al., 1982; Ruggeri, 2000]. GP Ibα-vWF is indispensable for platelet tethering at high shear rates, and $\alpha_{IIb}\beta_3$-vWF appears to have similar functions to $\alpha_{IIb}\beta_3$-fibrinogen. Savage *et al*. (1996) observed two distinct mechanisms initiating the adhesion of flowing platelets to thrombogenic surfaces. A receptor, $\alpha_{IIb}\beta_3$, considered to be efficient for stable adhesion and aggregation, promoted immediate arrest onto fibrinogen at shear rate less than 900 s^{-1}, but reduced adhesion at higher shear rate. This limitation might be due to the slow rate of bond formation or weak resistance to the blood flow. In contrast, GP Ibα-mediated binding to immobilized vWF showed transient motion of platelets on the protein-coated surface at high shear rates. These phenomena might be caused by fast association and dissociation rates of platelet interaction with multimeric vWF. Furthermore, this bonding appeared to be strongly resistive to tensile stress at the surface.

4.1.2 Goals and experimental end points

The broad objectives of the present research are to describe the role of flow and cellular kinetics in thrombosis. Experimental in vitro and ex vivo models of arterial thrombosis demonstrate that platelet accumulation is modulated by both fluid mechanics and biology, particularly platelet aggregation involving GP Ibα, $\alpha_{IIb}\beta_3$, vWF, and platelet activation. In this chapter we developed the translating stage microscope as a novel in vitro assay of vWF-mediated platelet adhesion in shear flow of blood cell suspensions, which for the first time allows simultaneous imaging of platelets adhering to the vessel wall, and platelets flowing in near-wall layers of blood. In this system we have observed enhanced platelet margination (near-wall platelet concentration increases) with increasing wall shear rate, and a significant decrease of platelet margination in vWF-coated surfaces.

The experimental end points in this section are briefly described as follows:

1. Quantitative evaluation of shear rate dependence of platelet adhesion with immobilized vWF and the effect of time on platelet adhesion in section 4.2.
2. Near-wall concentration of platelets in shear flow and development of image analysis tool in section 4.3.
3. Surface kinetics of platelet transient binding on immobilized vWF and development of image analysis tool in section 4.4.

4.2 Shear Rate Dependence of Platelet Adhesion with Immobilized vWF

The experiments in this section were planned to obtain a quantitative evaluation of vWF-coated surface coverage by platelets in terms of shear rate or time because vWF has essential functions in the very first stage of hemostasis or thrombosis. vWF is an adhesive protein circulating in plasma, being synthesized by the subendothelium and also secreted from α-granules of platelets. At the site of vascular damage, vWF binds immediately to exposed subendothelium, thereby facilitating the initial tethering of platelets. After a first layer of platelets has been formed, vWF is crucial as a link between platelets in the formation of thrombosis. Based on a theoretical model of platelet transport, activation, and aggregation, during thrombus growth there should be some mechanism that detains platelets long enough to be activated for $\alpha_{IIb}\beta_3$-mediated binding. Transient GP Ibα-vWF binding is one possible delay mechanism.

Blood containing 3.2% citrate as an anticoagulant and treated with the fluorescent dye calcein green for platelet visualization was perfused over a surface coated with 100 μg/ml of human plasma vWF in a rectangular capillary tube at room temperature, and over a surface coated with 200 μg/ml of bovine serum albumin as control. The blood sample was mixed with prostaglandin E_1 (PGE_1) (final concentration, 10 μM, Calbiochem) to prevent full activation of platelets [Savage et al., 1996] and mixed with EDTA (final concentration, 5 mM, Aldrich) to inhibit integrin receptor function of platelets, and supplemented with 5 units/ml of apyrase (grade VII, Sigma) as an ADP scavenger [Savage et al., 2002]. The blood sample was also mixed with abxicimab (final concentration, 10 μg/ml, Lilly) to inhibit aggregation of platelets in the whole blood. The

flow rate was set to produce wall shear rate 126, 364, 612, and 840 s^{-1}. Images of transiently adherent platelets were acquired using a silicon intensified target (SIT) camera (MTI Dage) with automated gain and were recorded on a tape using a videomicroscopy system described in Chapter 2. The individual images do not contain any information regarding stability of adhesion. Actually, these images contain all kinds of interaction of platelets such as stationary on the surface, leaving the surface, newly coming onto the surface, and translocating over the surface during experiments. However, the interactions of platelets that result in the instantaneously captured image are also strongly influenced by the combination of hemorheological factors such as shear-induced dispersion, persistent drift, and wall shear rates.

4.2.1 Shear rate effect

Figure 4-1 shows the image sequences of the interaction of platelets with immobilized vWF or BSA-coated surface. Each image corresponds to an area of 0.000402 cm^2. Platelets in flowing blood suspension attached to immobilized vWF even at high wall shear rate and in spite of treatment with platelet activation inhibitors. The number of platelets interacting with vWF is obviously greater at higher shear rate for the same time frame, and the surface is nearly saturated at the higher shear rate. However with the presence of four inhibitors for platelet activation, there is no formation of large thrombi. In contrast, the interaction with BSA-coated surface does not show clear effect of shear rate on the accumulation of platelets. Surface-bound BSA, unlike vWF, fails to recruit platelets at all shear rate range in this study. Figure 4-2 shows quantitative

evaluation of the number of platelets interacting with vWF-coated surface with pre-perfusion for 1min. The number of adherent platelets is a significantly ($p<0.05$) increasing function of shear rate, except for wall shear rates between 612 and 840 s^{-1} at 5 and 20 min. At high shear rates, quite strong dispersive motion of RBCs in flow might cause the similar adhesive interaction of platelet with vWF even at 5 min after perfusion. Savage *et al.* (1996) showed a qualitatively similar platelet interaction with plasma vWF: the number of platelets adherent to immobilized vWF was not significantly different under the shear rates ranging from 630 to 1500 s^{-1} after perfusion for 5 min. Figure 4-3 shows adhesion values normalized with respect to the number of platelets at the lowest shear rate (126 s^{-1}). After 1 min perfusion of blood suspension, the number of platelets for the highest shear rate is almost 7 times larger than that for the lowest shear rate. However, after 20 minutes the number of platelets for the highest shear rate is only 2.6 times larger than that for the lowest shear rate. The effect of shear rate on the number of platelet is gradually decreasing with time as the surface is saturated, with bound platelets

4.2.2 Time effect

Figure 4-1 also shows that the number of platelets interacting with vWF is a function of time for each shear rate. The time course of platelet adhesion demonstrates progressive accumulation onto vWF-coated substrate as opposed to the rapid attainment of a plateau in the number of platelets interacting with vWF [Savage et al, 1996]. This difference may be caused by the hematocrit of blood suspension, which is 15% for the present study. Lower hematocrit may cause weaker shear-induced dispersive motion of

flowing platelet near wall, subsequently slow rate of accumulation onto vWF. However, the interaction of platelets with vWF appears to be crucial to platelet adhesion in high shear flow. Figure 4-2 shows quantitative evaluation of the number of platelets interacting with vWF-coated surface with pre-perfusion for 1min. This figure shows that the number of adherent platelets is a significantly increasing function of time ($p<0.05$). Figure 4-4 shows normalized values with respect to the number of platelets at 1 min for each shear rate. The number of platelets at 20 min for shear rate 840 s^{-1} is almost 2 times larger than at 1min: in contrast, it is 5.2 times larger for shear rate 126 s^{-1}. The effect of time on the platelet adhesion is gradually decreasing with shear rates, representing the trend of more rapid attainment of steadiness at higher shear rate, due to more active transport of platelets.

4.2.3 Photo activation effect

Photoactivation is a chemical reaction to light and is caused by photosynthesis in molecules due to high energy from light source. To allow visualization, platelets were labeled by direct incubation with fluorescent dye mepacrine [Mazzucato et al., 1999], and to prevent photoactivation by the irradiating UV light, neutral density filters were used. Two tests, one which examines for the effect of incident light on platelet adhesion and one which checks for sufficient light for accurate observation of cells, have been tried, and evaluations were made of the adhesion of platelets labeled with the fluorescent dyes mepacrine and acridine orange [McClung et al., 1992]. Vascular injury and thrombus formation in rat mesenteric vessels was induced by photoactivation [Kulkarni et al.,

2000]. The platelet photoactivation may play an important role in the initiation of early vascular damage.

To prevent photoactivation of platelets in the present study, the neutral density filter (ND8) was used between light source and test section. Final concentration of calcein green as fluorechrome was adjusted to 0.5 μg/ml as low as possible with some trials and errors. Figure 4-5 (a) and (b) show the effect of photo activation on platelet adhesion at shear rate 126 and 840 s^{-1}, respectively. Loc 1, 2, and 3 indicate the positions in capillary where the fluorescent light was exposed for 3 sec at each measuring cycle (every 1 min, totally 20 min measuring). On the other hand, Loc 4, 5, and 6 were the positions where the light was exposed for less than 100 msec for each time. Longer exposure of light yielded a little more platelet adhesion on the immobilized vWF (final concentration 200 μg/ml), which means the platelets were slightly affected by photoactivation.

4.2.4 Conclusion

The first step of the process of platelet adhesion to vWF, mediated by interaction with GP Ibα, was evaluated by blocking activation with four inhibitors (PGE_1, EDTA, apyrase, and abxicimab) to prevent possible changes due to the secondary engagement of vWF-related receptor such as $\alpha_{IIb}\beta_3$, and subsequent aggregation. The higher the wall shear rate, the more and faster the platelets accumulated on the immobilized vWF surface. The interaction of platelets with vWF appears to be crucial to platelet adhesion especially in high shear flow, and is central to the intriguing phenomena of shear-induced platelet

adhesion. This fast rate of bond formation between GP Iβα and vWF A1 domain allows establishment of initial contact even when platelets move at high hydrodynamic speed.

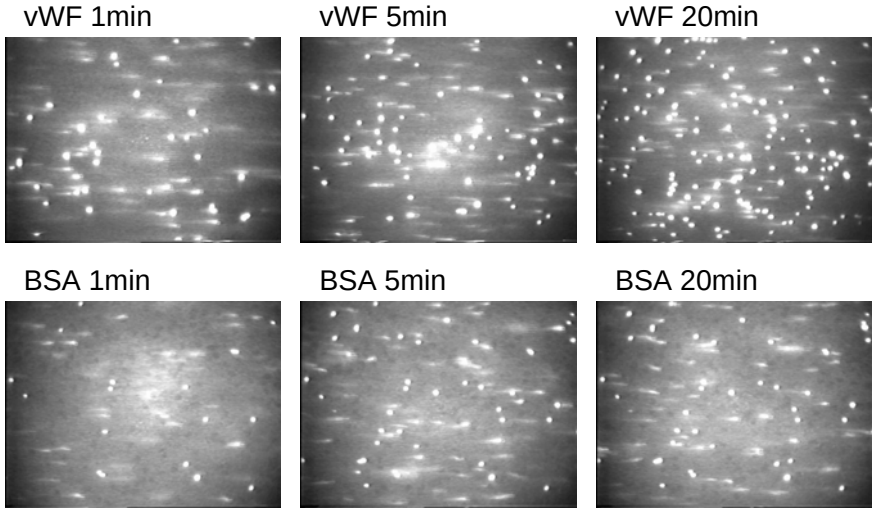

Fig. 4-1. (a) Dynamics of platelet adhesion on immobilized vWF at wall shear rate 126 s^{-1}.

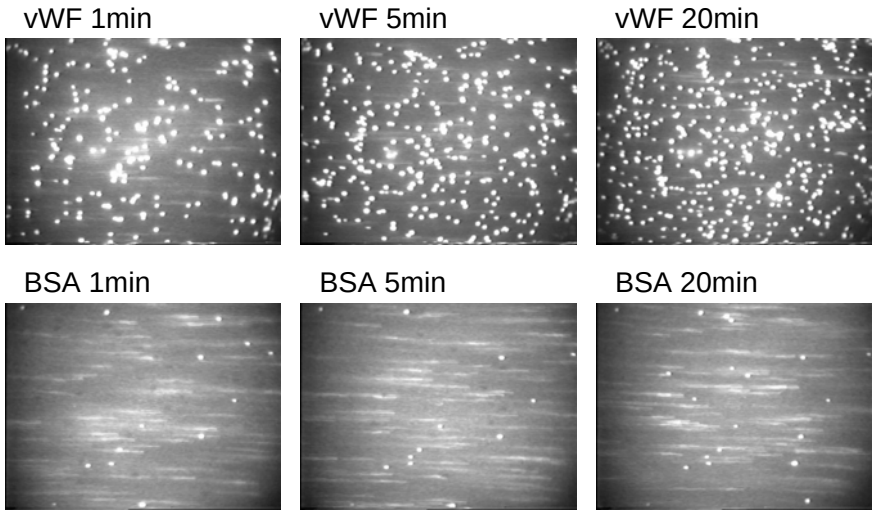

Fig. 4-1. (b) Dynamics of platelet adhesion on immobilized vWF at wall shear rate 364 s^{-1}.

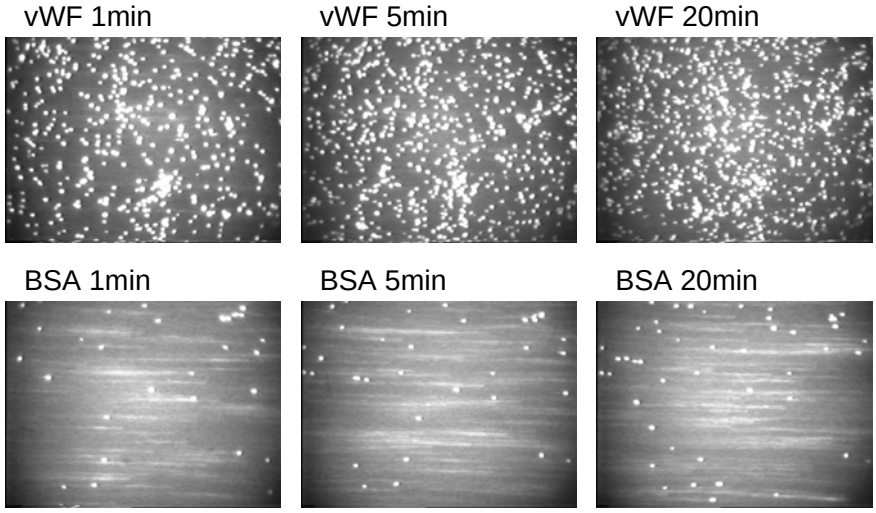

Fig. 4-1. (c) Dynamics of platelet adhesion on immobilized vWF at wall shear rate 612 s^{-1}.

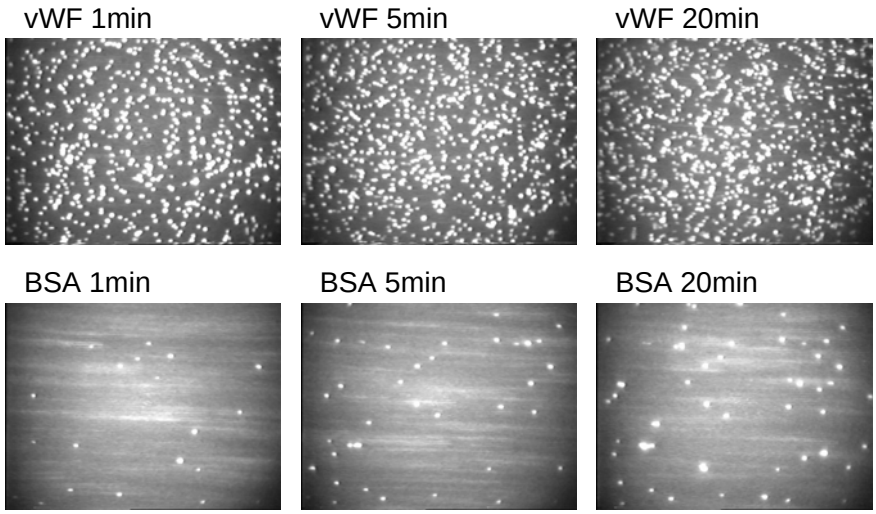

Fig. 4-1. (d) Dynamics of platelet adhesion on immobilized vWF at wall shear rate 840 s^{-1}.

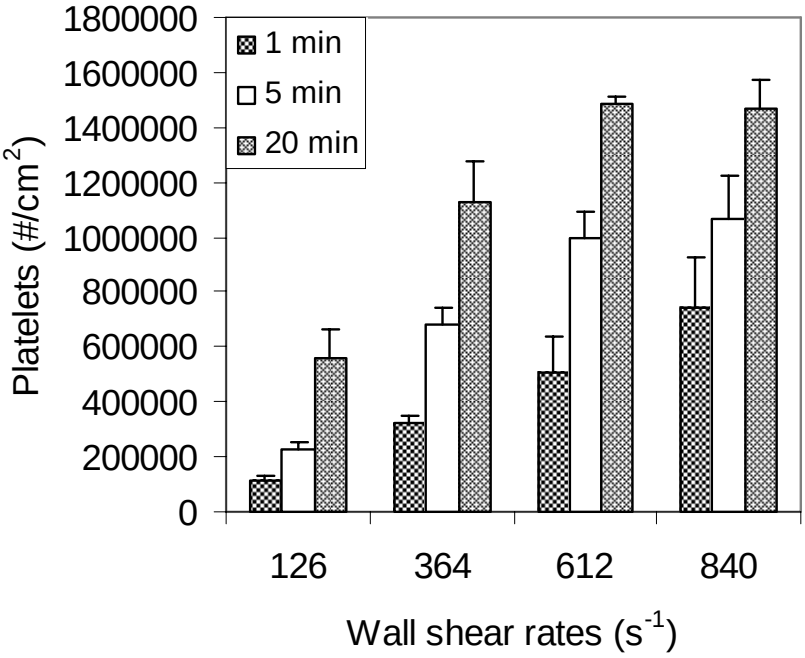

Fig. 4-2. Shear dependent platelet adhesion on immobilized vWF under various shear rates at different time frame.

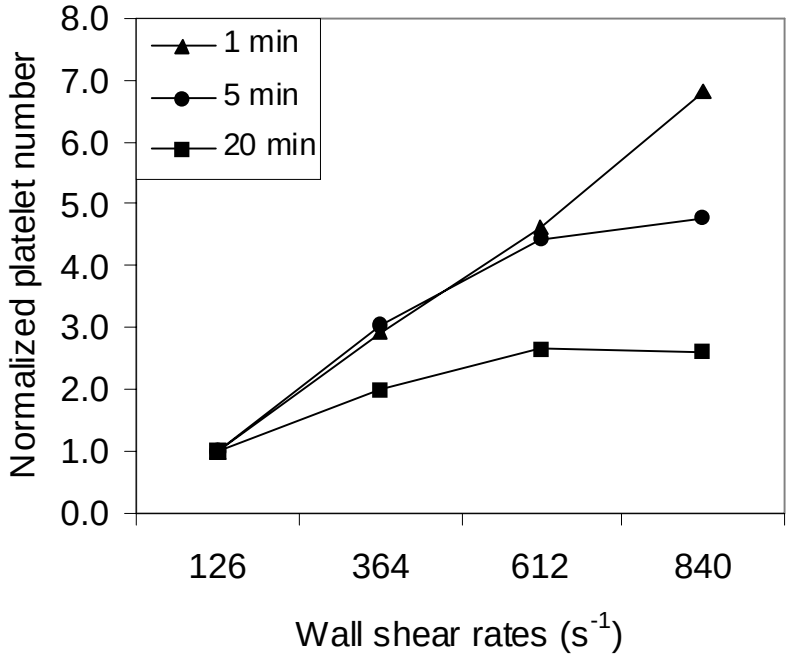

Fig. 4-3. The effect of shear rate on shear dependent platelet adhesion on immobilized vWF at different time frame.

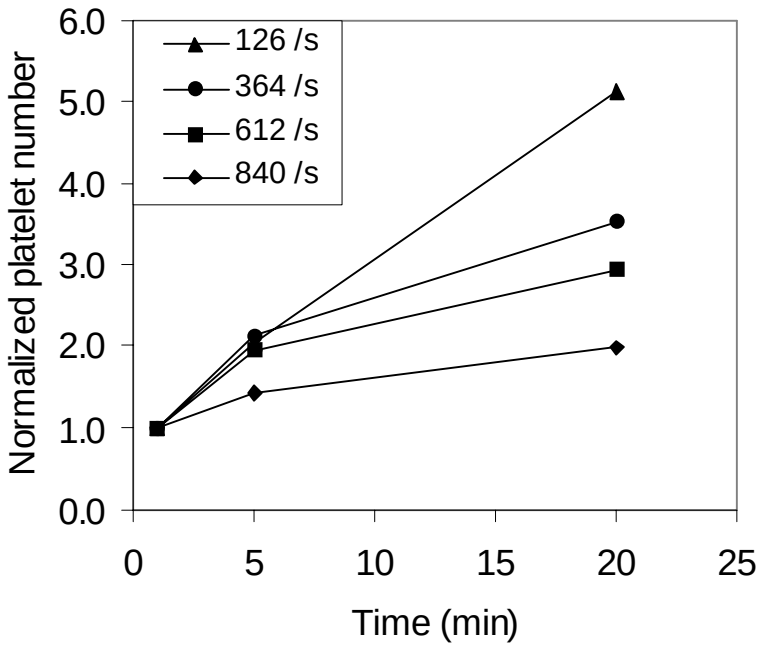

Fig. 4-4. The effect of time on shear dependent platelet adhesion on immobilized vWF under different shear rates.

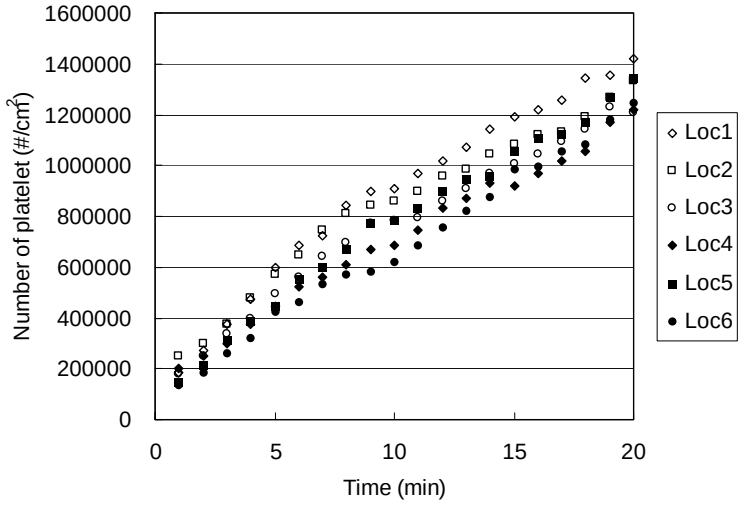

Fig. 4-5. (a) Effect of photoactivation on platelet adhesion at shear rate 126 s^{-1}. Location 1, 2, & 3 were exposed to fluorescence for 3 sec, location 4, 5, & 6 for 100 msec.

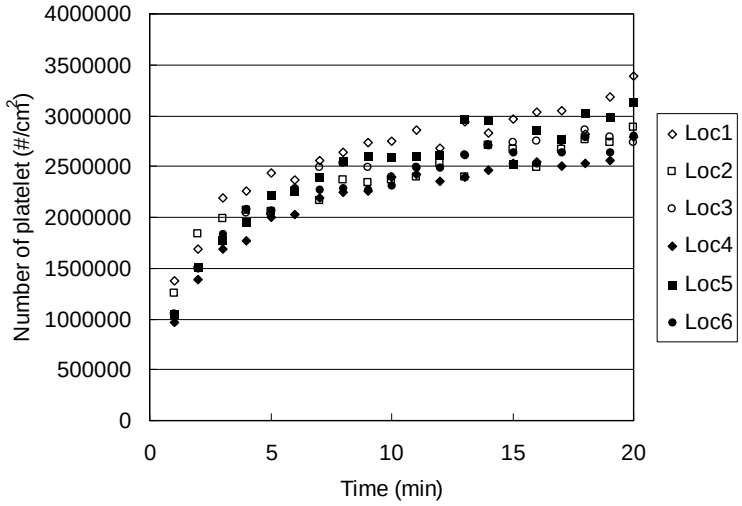

Fig 4-5. (b) Effect of photoactivation on platelet adhesion at shear rate 840 s^{-1}. Location 1, 2, & 3 were exposed to fluorescence for 3 sec, location 4, 5, & 6 for 100 msec.

4.3 Near-Wall Concentration of Platelets in Shear Flow

The experiments in this section were planned to obtain a quantitative evaluation of near-wall concentration of platelets interacting with vWF-coated and BSA-coated surface by using the translating-stage method, to study the effects of platelet adhesion on the flowing blood cells.

Non-Newtonian velocity profiles in the capillary were measured at four different shear rates with the use of fluorescent microbeads, and each profile was evaluated in a function of y, $u(y)$. Since the geometrical shape of actual platelet is not regularly consistent, meaning that the image criteria obtained in section 3.2 cannot be applied, the obtained velocity profile function was used to determine the location of observed platelets flowing near the wall, by measuring velocity of the platelets. In other words, since function $u(y)$ was obtained for each flow rate in Chapter 3, the location of platelets could be determined by $y(u)$ for the same flow rate and hematocrit.

In the present experiment the translating microscope stage was programmed for automatically repeated operation at 1 minute intervals to measure platelet margination, near-wall platelet motion, and platelet transient adhesion. At each observation time, stationary images at 3 capillary positions are recorded to analyze firmly and transiently adherent platelets, which will be discussed in section 4.4, followed by a moving stage image sequence to measure platelet concentration at 3 ± 1 μm from the vessel wall.

4.3.1 Image analysis

To determine the instantaneous local location of the flowing platelets near wall, a Visual Basic program shown in Fig. 4-6 was developed for analysis of image sequences acquired by a SIT camera. By measuring the relative velocity of an individual platelet which is in the focal layer (3 ± 1μm from the capillary wall), actual velocity of the platelet was calculated by summing the relative velocity with the speed of the translating-stage which was set for the experiment. Velocity function $u(y)$ was already determined for different shear rates in Chapter 3, thus the location of the platelets was able to be inversely estimated by $y(u)$. This program automatically generated instantaneous (x, z) coordinates of a platelet by manual selection. With information from two consecutive (x, z) coordinates, a relative velocity was automatically calculated by dividing traveling distance by the time interval between frames, and local location of the platelet in *y* was estimated by the function $y(u)$.

4.3.2 Results

Figure 4-7 shows the platelet near-wall concentration after 20 minutes of blood flow, at depth from 2 to 4 μm from the capillary wall, for vWF and BSA-coated capillaries at various wall shear rates (mean ± SEM, n = 5). This experiment shows the enriched platelet concentration in the near-wall region of the capillary, in both vWF-coated and BSA-coated capillaries. Platelet concentration ranged from 1.9× to 5.3× the bulk average concentration (180,000 platelets/μl) over BSA-coated capillaries, and 1.6×

to 3.2× over vWF coated capillaries. Near-wall concentration increases significantly with wall shear rate for both coatings ($p<0.05$), and at moderate (364 s^{-1}) and high shear rates platelet concentration is significantly lower with vWF coating than with BSA coating ($p<0.05$).

Figure 4-8 (a) represents the dynamics of platelet margination on vWF-coated surfaces for different shear rates. In all cases, margination was observed within 1 minute of flow. On vWF-coated surfaces, platelet concentration does not increase significantly with time, with a slight increasing trend at the highest shear rate. However, platelet concentration increases in terms of shear rate, but not significant for high shear rates: The case for shear rate 364 s^{-1} at each time frame was significantly different from the case for shear rate 612 or 840 s^{-1} ($p<0.05$). However, shear rate 612 s^{-1} case was not different from shear rate 840 s^{-1} at 5 or 20 min. Figure 4-8 (b) represents the dynamics of platelet margination on BSA-coated surfaces. On BSA-coated surfaces, platelet concentration increases significantly with time at shear rates 364 and 840 s^{-1} ($p<0.05$) and with shear rates ($p<0.05$) except between 612 and 840 s^{-1} at 1 or 5 min.

4.3.3 Conclusion

Platelet margination was significantly reduced over vWF at high shear rates, compared to BSA-coated surface. Such a reduction in near-wall platelet concentration has been predicted in a variety of transport-based computational models of platelet thrombosis [Aarts et al., 1986; Eckstein et al., 1991; Sorensen et al., 1999; Turitto et al,

1975 & 1980; Wootton et al., 2001]. This is the first time that the depletion of platelet margination over a platelet-adhesive protein surface has been observed experimentally.

In the referenced models, high rates of platelet adhesion require a high flux of platelets from the flowing blood at the vessel wall to the protein surface. When that high flux is not matched by the rate of transport of platelets from the core flow to the vessel wall, the platelet concentration is depleted within a thin boundary layer near the vessel wall, on the order of 5 to 10 μm thick [Wootton et al., 2001]. The boundary layer depletion mechanism is not completely consistent with our experiments for three reasons. (1) Boundary layer depletion in dispersive transport should lead to non-uniform spatial distribution of platelet adhesion, with higher adhesion upstream and lower adhesion downstream, but no significant axial variation in adhesion density was observed during the experiment. It is possible that persistent drift at steady state over these distances reduces the axial variation of adhesion [Eckstein et al., 1991]. (2) The rate of platelet adhesion in the experiments was on the order of 300 to 1000 platelets/cm^2/s, which gives an adhesion velocity (adhesion rate normalized by platelet concentration) on the order of 10^{-6} to 10^{-5} cm/s, one or two order of magnitude slower than the adhesion velocities associated with moderate boundary layer platelet depletion at these shear rates (10^{-4} to 10^{-3} cm/s) [Wootton et al., 2001]. (3) The temporal pattern of margination observed in the experiments is not consistent with the temporal pattern observed for the platelet adhesion. In the vWF-coated capillaries, margination is rapidly established (within 1 minute) and increases very little thereafter, even though the rate of platelet adhesion decreases significantly toward 20 minutes of flow. In contrast, in the BSA experiments with negligible adhesion platelet flux, margination increases steadily over 20 minutes without

reaching a steady state, especially at the highest shear rate. Furthermore the gap between BSA and vWF experiments grows most rapidly when the rate of platelet adhesion is lowest.

Because the reduction of near-wall platelet concentration in the vWF experiments is greatest when the platelet adhesion is highest and when shear rate is highest, we hypothesize that adherent platelets, which are largely unactivated discoids in these experiments, may cause flow disturbances that repel platelets from the near-wall layers of flow, either through direct hydrodynamic interactions, or indirectly by disturbing RBCs near the wall.

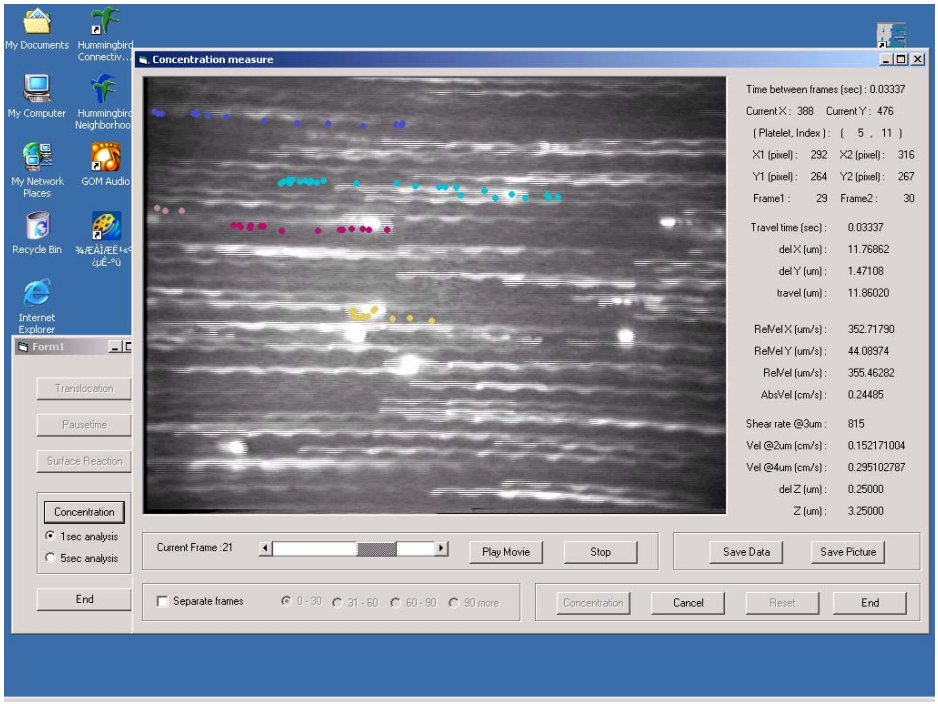

Fig. 4-6. Image analysis program developed for the estimation of near-wall platelet concentration.

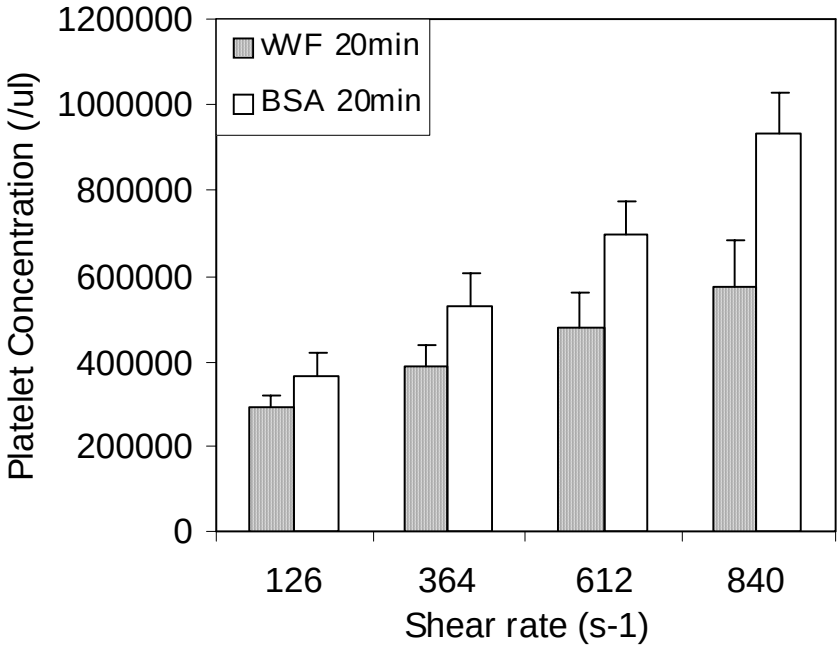

Fig. 4-7. Effect of surface and shear rate on near-wall platelet margination.

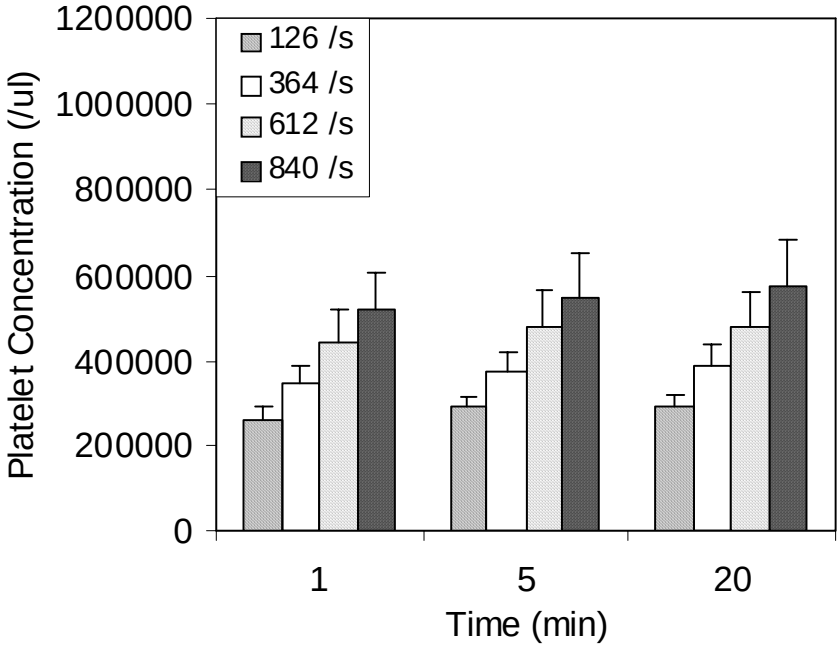

Fig. 4-8. (a) The shear rate effect ($p<0.05$ except between 612 and 840 s^{-1} at 5 or 20 min) and effect of time on near-wall platelet concentration on vWF-coated surface at different time frames (mean ± SEM; n = 5). There was little significant effect of time on platelet concentration over vWF-coated surfaces.

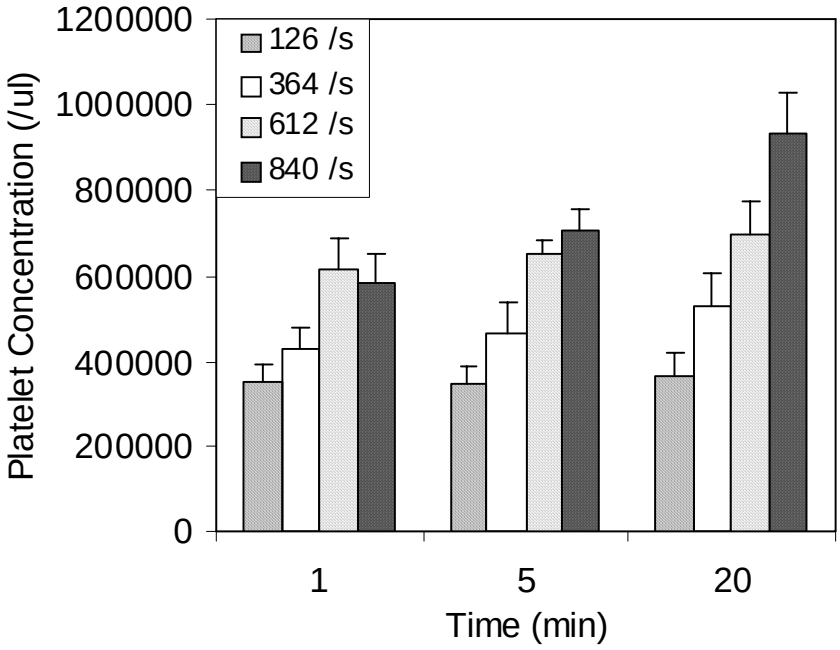

Fig. 4-8. (b) The shear rate effect ($p<0.05$ except between 612 and 840 s^{-1} at 1 or 5 min) and time effect on near-wall platelet concentration on BSA-coated surface at different time frames (mean ± SEM; n = 5).

4.4 Surface Kinetics of Platelets on Immobilized vWF

The ability of platelets to tether to or translocate on injured vascular endothelium depends on the interaction between the platelet glycoprotein (GP) Ibα and the A1 domain of vWF. This receptor-ligand bonding shows similar kinetic characteristics to selectin-like kinetics of leukocyte [Doggett et al., 2002], in other words, the binding interaction has both a fast forward kinetic rate to allow rapid binding, and a fast reverse kinetic rate allowing release of binding and rolling on the surface. A critical level of hydrodynamic shear stress (0.73 dyne/cm^2) is required to initiate platelet adhesion, and there is a short-lived tethering event on an intravascular injury due to a fast intrinsic dissociation rate. As a result of rapid formation and breakage of the adhesive interaction between platelet receptor and ligand on exposed subendothelium, platelets can roll over or translocate on the injury in response to hydrodynamic forces of blood flow. The biological importance of the GP Ibα-vWF kinetics is the fact that these actions can control platelet adhesion, as translocation is a prerequisite for further integrin-mediated stable adhesions and consequent hemostasis or formation of thrombosis.

In this section, detailed kinetic analysis for the GP Ibα -vWF tether bonding was performed by image analysis. The platelet interactions on immobilized vWF were examined over the area of 0.000402 cm^2 during a short time frame (3sec) at 1, 5, and 20 minutes after perfusion of blood suspension. Images were analyzed to determine how many surface-associated platelets (1) remain at the same position, (2) leave the surface, (3) arrive and tether onto the surface, and (4) translocate over the surface. For each analysis, 9 image frames were analyzed that correspond to the image frame acquired at

every 0.333 sec time interval. Intermediate frames (taken at 30 frames/sec) were used to follow platelet motions and categorize platelets in the various groups. All analyzed images were referenced to the first image to determine the change in the behavior of platelets interacting with surface, in other words, how many platelets have kept their initial locations at a later time, how many have moved to another location compared to the initial location, or how many have appeared or disappeared after the initial frame. Even though this analysis was performed for a short time period, the interactions of platelets were obviously in the middle of the long-term accumulation process, and can be described as a representative trend for the whole process.

4.4.1 Image analysis

Figure 4-9 shows a consecutive process of the developed image analysis program running to investigate the kinetics of platelets interacting with vWF-coated surface. This program reads 90 image frames and sets a rectangular region of interest (ROI) in the middle of each image. All platelets interacting with vWF in this area (0.000402 cm^2) were analyzed. The first figure shows the initial position and number of platelets manually selected in the ROI. This program memorizes the (x, z) coordinates of the centroid of each platelet. The second figure designates the platelets which departed from their initial position in the next image frame to be analyzed, the platelets which left the ROI, or the platelets translated within the ROI. Those platelets were indicated by black circle and automatically counted. The remainders were considered as transiently stationary platelets in the image frame, which were indicated by open circles. This

process was performed by multiplying two image frames to compare the intensity values of the same pixel location in the two images. However, the quantitative distinction between leaving and translating platelets was not clear yet, but the summation of two different kinetics was determined. The next step was to determine how many platelets newly arrived into the ROI and tethered on the vWF-coated surface. By selecting new platelets in the ROI of the later image frame and subtracting the first image from the later image, two kinetics involving incoming and translating platelets were estimated. In the third figure, those platelets were indicated by solid blue circles. Thus finally, each quantitative kinetic was estimated by examining the translating platelets: quantitative estimation of transiently stationary, leaving, incoming, and translating platelets.

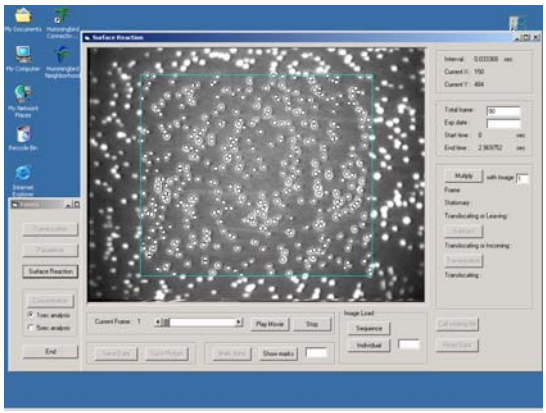

(a) All platelets interacting with vWF-coated surface were selected in the rectangular ROI (open circles). The initial number of transiently stationary platelets in the ROI was counted. Information on the location and pixel intensity data for the all platelets was memorized in the image analysis program.

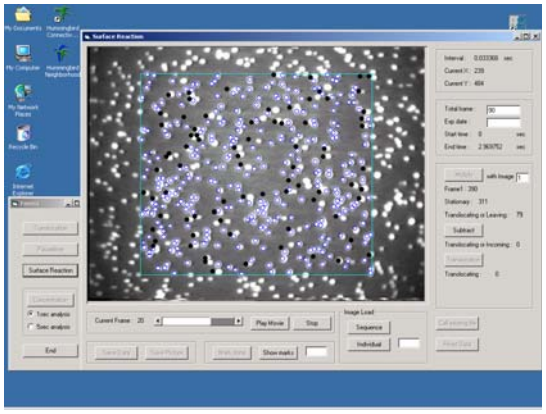

(b) Multiplication of the first image (a) with the current image. The number of translocating or leaving platelets in ROI was counted (black circles). Stationary platelets remain at their original locations (open circles).

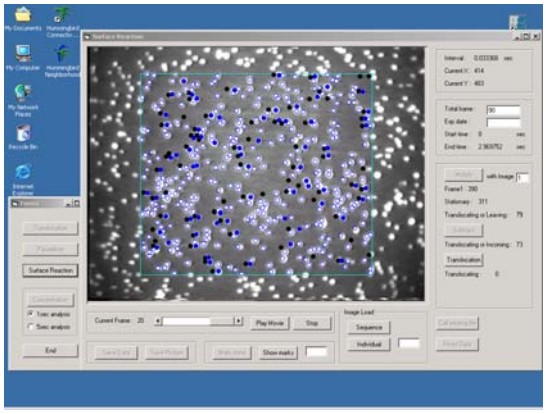

(c) Subtraction of the first image (a) from the current image. The number of translocating or incoming platelets in ROI (blue circles) was counted. Then, translocating platelets among the grey circles were counted. Stationary platelets kept their original locations (open circles).

Fig. 4-9. Image analysis program to quantify surface kinetics of platelet on immobilized vWF surface.

4.4.2 Kinetics of platelets on immobilized vWF

The blood sample used in the present study was treated with four inhibitors to prevent platelet activation by other integrin-ligand interactions except GP Ibα-vWF interaction because the initial tethering of platelets mediated by this interaction and subsequent transient motions on the surface are implicated in the onset of thrombosis and the near-wall platelet concentration. As expected, most platelets interacted with immobilized vWF under various shear rates in the form of stationary, leaving, incoming, or translocation. Platelets translocated on the surface even under the lowest shear rate. Platelets might be rolling over the surface, but rolling could not be distinguished from the translocating platelets. Some platelets just touched the surface and returned to the flow in the next frame; these were not counted in the analysis. A few small aggregates were found at 20 minutes under high shear rates.

Figure 4-10 shows the interactions of platelets with the vWF surface during short time period (3 sec) under the wall shear rate 840 s^{-1}, at time 1, 5, and 20 minutes. Even at 1 min after perfusion of blood suspension, about 300 platelets were interacting with the surface due to the combination of high level of shear-induced dispersion and near-wall margination under high shear rate. Many of those platelets stayed at the initial locations for 3 sec, but about 100 platelets changed their initial locations by the form of translocation or leaving. The change in the absolute number of the transient platelets did not significantly vary with long time period (1, 5, and 20 min), however, there were significant variations in fraction: 35% of adherent platelets left their initial locations at 1 min; at 5 min, 25% left their initial locations, and only 15 % were transient at 20 min.

The number of translocating platelets seemed to be 2.5× as many as any other kinetics such as leaving or incoming platelets. Averaged over 1, 5 and 20 minute time points, the number of platelets translocating, leaving, or incoming after 3 seconds were 73 platelets translocated, and about 30 platelets left and attached. Incoming platelets were slightly more than leaving platelets, which is also reasonable since adherent platelets accumulate over a longer time scale.

Figure 4-11 shows the interactions of platelets with vWF surface during short time period 3 sec under the wall shear rate 612 s^{-1} at time 1, 5, and 20 minutes. At 1min, about 200 platelets were interacting with the surface, and 70 platelets moved from their initial locations by the form of translocation or leaving. There were significant variations in the fraction of moving platelets: 36% of the platelets moved from the initial position at 1 min; at 5 min, 22% moved from their initial locations, and only 13 % were transient at 20 min. The number of translocating platelets seemed to be about twice as many as any other kinetics such as leaving or incoming platelets. There was a slight decrease in the number of platelet leaving or incoming, in terms of long time period. On average, 54 platelets translocated, about 22 platelets left and 28 platelets attached. Incoming platelets were slightly more than leaving platelets, which is also reasonable since adherent platelets accumulate over a longer time scale.

Figure 4-12 shows the interactions of platelets with the vWF surface during short time period 3 sec under the wall shear rate 364 s^{-1} at time 1, 5, and 20 minutes. There were significant variations in fraction of moving platelets: 22% of the platelets moved from the initial position at 1 min; at 5 min, 15% moved from their initial locations, and only 7 % were transient at 20 min. The number of translocating platelets seemed to be

similar to other kinetics such as leaving or incoming platelets. There were slight variations in the number of platelet leaving or incoming, in terms of long time period. On average, 18 platelets showed translocation, about 15 platelets left the surface and 17 platelets came in.

Figure 4-13 shows the interactions of platelet with vWF surface during short time period 3 sec under the wall shear rate 126 s^{-1} at time 1, 5, and 20 minutes: In fraction of moving platelets, at 1 min, 9% moved from their initial locations; at 5 min, 7% moved from their initial locations, and only 2% were transient at 20 min. The number of translocating platelets was smaller than that of leaving or incoming platelets. There were slight variations in the number of platelet leaving or incoming, in terms of long time period. In average, just 1 platelet showed translocation, about 4 platelets left the surface and 6 platelets came in.

4.4.3 The rate of departure

The rate of departure was defined as the time derivative of the ratio of the number of platelets which changed their initial positions to the initial number of platelets in the first image frame. The concept is graphically shown in Fig. 4-14 and mathematically in Eq. 4-1.

$$The\ rate\ of\ \ departure = \frac{\Delta S / S_0}{\Delta t} \times 100\ (\%) \tag{4-1}$$

where,

ΔS = the number of platelets leaving or translocating,

S_0 = the initial number of platelet, and

Δt = the elapsed time.

Figure 4-15 (a) shows the rate of departure for the long time period under various shear rates. The rate of departure shows an increasing trend as the wall shear rate increases, but exponentially decreases in terms of long time period. Being encountered with stronger hydrodynamic resistance at high shear rate, more platelets which have been tethered or adherent were not able to oppose flow forces with the interaction of GP Ibα and vWF. As time elapses, more platelets interacted with the surface, and some platelets seemed to be stably adherent to the surface and some formed small aggregates with each other, thus the rate of departure appears to be an exponentially decreasing function in terms of time. Figure 4-15 (b) shows the rate of departure for the short time period under various shear rates, all had similar trends to those of long time period. Thus, the analysis of short time period could represent whole process of surface kinetics.

4.4.4 Time constant

The characteristic time constant for the platelet transient interaction with human plasma vWF was estimated in this section. The concept of time constant is shown in Fig. 4-16 and mathematically described as follows,

$$S(t) = A(t) + PP, \tag{4-2}$$

where $S(t)$ is the number of transiently stationary platelets, $A(t)$ is the number of stationary platelets that will eventually translate or depart from the surface, and PP is the number of permanent platelets (platelets that will be adherent at infinite time). If any

transient platelet tends to be released from vWF at a constant rate, the rate of change is $S(t)$ or $A(t)$ can be modeled by a first-order process,

$$\frac{dS(t)}{dt} = \frac{dA(t)}{dt} = -\frac{A(t)}{\tau_t} \quad : \quad \frac{dA(t)}{A(t)} = -\frac{dt}{\tau_t} \quad \therefore\ A(t) = AP \cdot e^{-\frac{t}{\tau_t}}, \tag{4-3}$$

where AP is the number of active platelets, and τ_t = the time constants for platelet release.

$$S(t) = AP \cdot e^{-\frac{t}{\tau_t}} + PP\,, \tag{4-4}$$

$$\ln\left(\frac{S(t) - PP}{AP}\right) = -\frac{t}{\tau_t}. \tag{4-5}$$

A numerical iteration method to estimate the optimized values of AP, PP, and τ_t in Eq. 4-4 was used by comparing the measured transiently stationary platelets of each experiment with a numerical result $S(t)$ and by seeking for the minimum sum of squared error between the measured and model values. The method was implemented using the Excel solver function. Figure 4-17 and 18 show the variation of normalized stationary platelets during 3 sec and the characteristic time constant at different shear rates. The measured values show good agreement with the calculated values for each experiment. Even though the wall shear rate varies, the time constant values did not essentially change as a function of wall shear rate (Fig. 4-19) and were on the order of 1 s. Doggett *et al*. (2002) also found that the dissociation rate constant was relatively independent of wall shear stress. Figure 4-20 shows the plots of Eq. 4-5. The slope indicates the negative inverse of the time constant, $-1/\tau_t$. Except for the low shear case at 1 min, shear rate does not have a significant effect on the dissociation rate. Thus, these results suggest that the hydrodynamic forces imposed on the GP Ibα-vWF tether bonding

of platelets may not be sufficient to alter the dissociation of platelets from the immobilized vWF.

Doggett *et al*. (2002) quantified the duration of a transient tether of platelets interacting with vWF-A1 adsorbed surfaces. The transient tether event was defined as a flowing platelet that abruptly halted forward motion for a defined period of time and subsequently released without translocation. In that study, most platelets (>90% of all interactions) were released from the vWF surface in less than 0.7 sec. The dissociation rate constant was 5.23 s^{-1} and time constant was 0.19 sec for wild type vWF-A1 domain. Savage *et al*. (1998) examined the contribution of platelet integrins $\alpha_2\beta_1$ and $\alpha_{IIb}\beta_3$ to stability of adhesion of platelets. Blood containing 5 mM EDTA to inhibit the function of the integrins was perfused on purified vWF-coated surfaces (final concentration 100 μg/ml) at shear rate 1500 s^{-1}, much higher than the present study. Greater than 90 % of all platelets moved on the surface within 3 sec of observation after 2 min perfusion, showing that transient attachment with surface translocation mediated by GP Ibα-vWF is dominant. The time constant was 0.6 sec and rate constant was 1.67 s^{-1}, which means that about 67 % of platelets were displaced from their original positions after 0.6 s. Savage *et al*. (1996) studied the stability of platelet attachment to immobilized plasma vWF. Blood containing PPACK as an anticoagulant was treated with PGE_1 to inhibit platelet full activation and perfused at shear rate 50 s^{-1}. 100 % of all platelets moved on vWF after 40 sec after 5 min perfusion. The time constant was 8 sec, and the rate constant was 0.13 s^{-1}. At shear rate 1500 s^{-1} after 5 min perfusion, untreated blood with PPACK had a time constant of 5 sec and rate constant 0.2 s^{-1}. The time constant was 0.7 sec and rate constant 1.43 s^{-1} for both PGE_1-treated and anti-$\alpha_{IIb}\beta_3$-treated blood.

In the present study, the dissociation rate constant is 0.86 s^{-1} and time constant is 1.17 sec after 5 min perfusion of blood, similar to integrin-inhibited high shear experiments of Savage, and slower than Dogget's experiments. In Doggett's study, a low concentration of recombinant protein (5 μg/ml) was used to estimate the dissociation rate of individual vWF-GPIb bonding, and to better evaluate the effect of flow-induced forces (1.0 – 4.0 dyne/cm^2) on tether bond lifetimes. In this study, the concentration of plasma vWF was 100 μg/ml and the wall shear stress for the current study ranged from 4 to 24 dyne/cm^2. In addition, vWF-A1 domain was used, rather than plasma vWF which is multimeric, leading to clustering of multiple A1 domains near an adherent platelet. These differences may explain the longer time constant derived from our experiments.

While the present and Doggett's study showed the independence of shear rate on the dissociation rate constant, Savage's study did show a dependence on shear rate, over a much wider range of shear rate. By comparison of the present and Savage's study for the treated blood case, the time constant for the present study appears to be in the range of Savage's study (at the higher 1500 s^{-1} shear rate) because the concentration of vWF and the blood perfusion time were under the similar conditions. In Savage's study, the highest shear rate was much higher than in the present study, and the stronger hydraulic force appeared to remove the transiently adherent platelets from the vWF surface somewhat more rapidly (time constant 0.6 s) than in the present experiments (time constant 1.17 s).

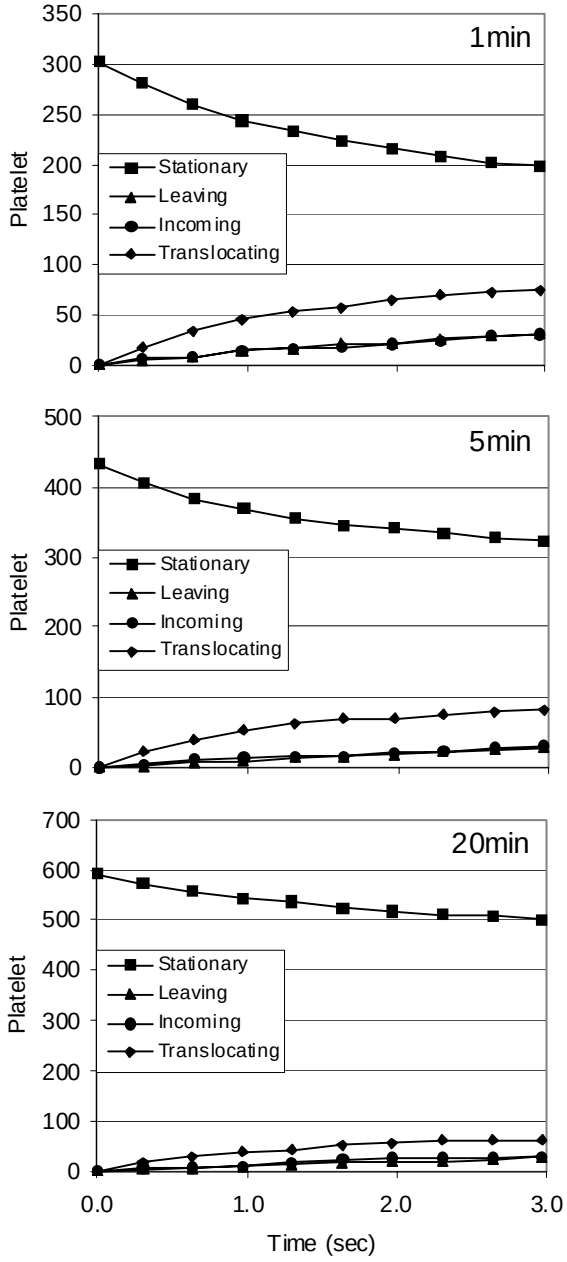

Fig. 4-10. Surface kinetics of platelets interacting with vWF under shear rate 840 s^{-1} at different time frame.

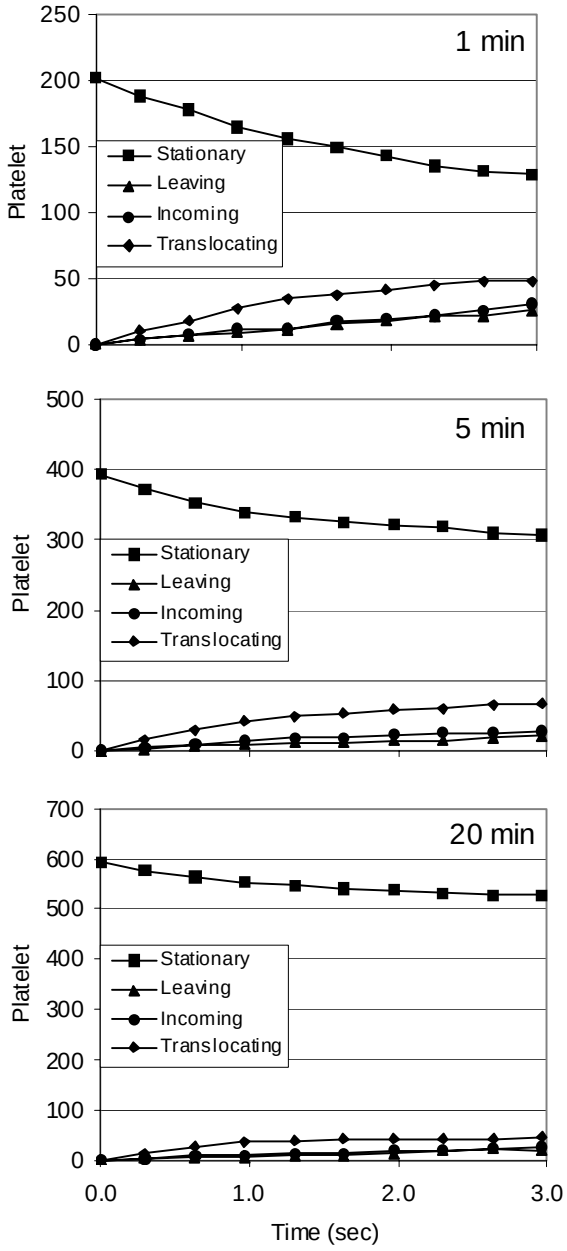

Fig. 4-11. Surface kinetics of platelets interacting with vWF under shear rate 612 s^{-1} at different time frame.

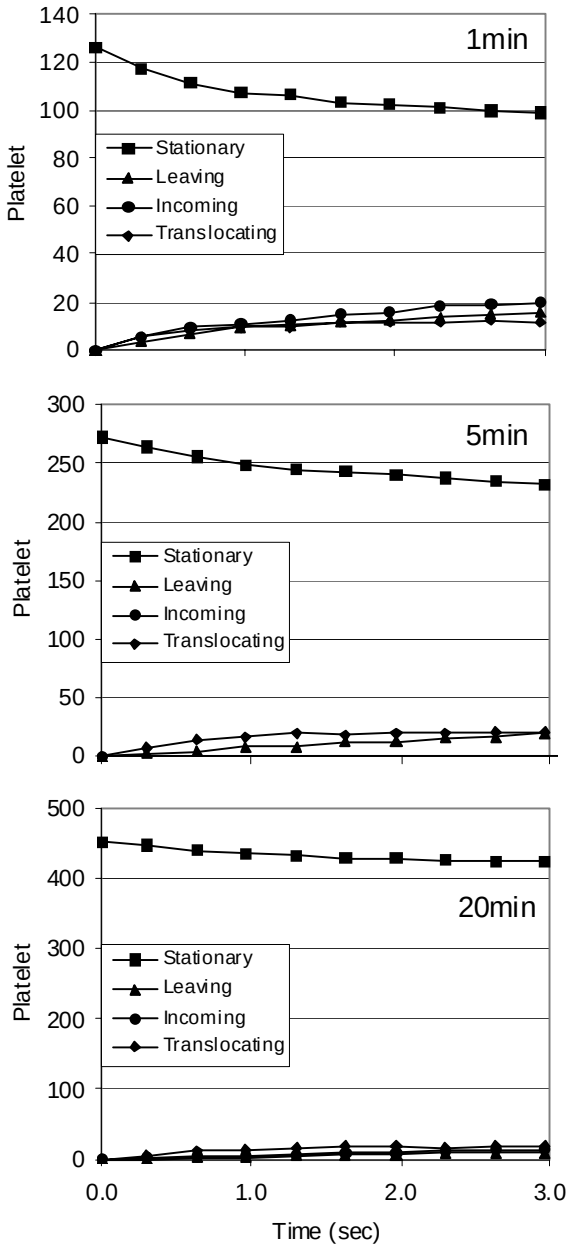

Fig. 4-12. Surface kinetics of platelets interacting with vWF under shear rate 364 s^{-1} at different time frame.

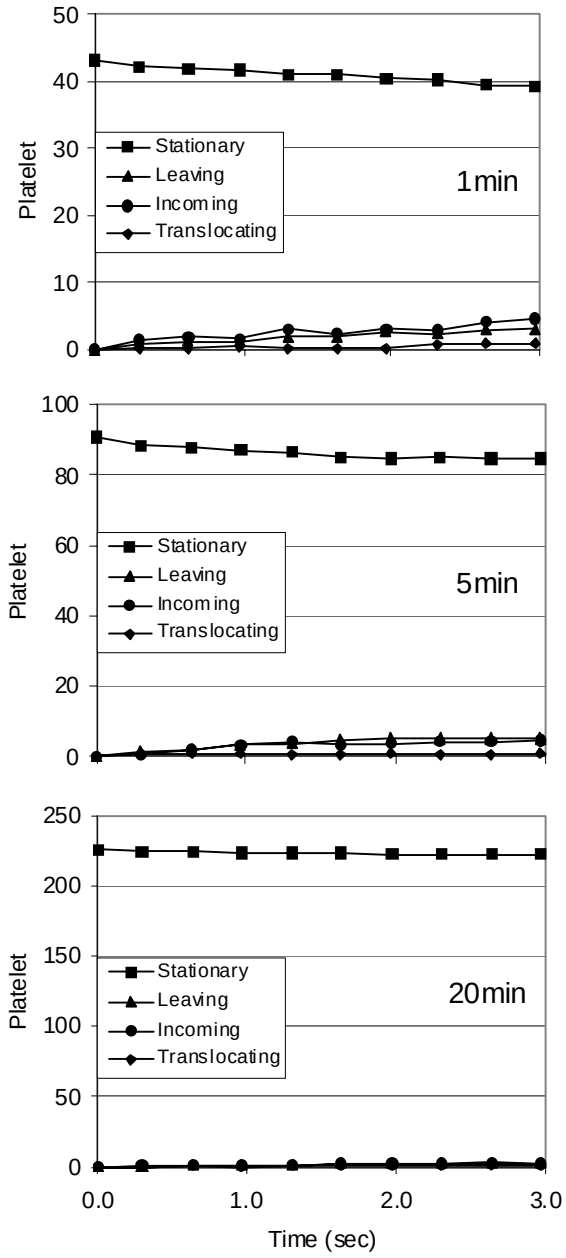

Fig. 4-13. Surface kinetics of platelets interacting with vWF under shear rate 126 s^{-1} at different time frame.

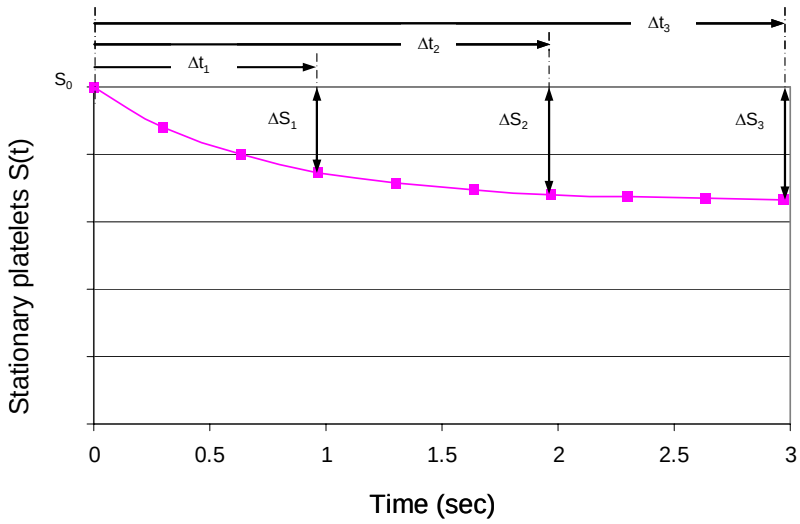

Fig. 4-14. Rate of departure.

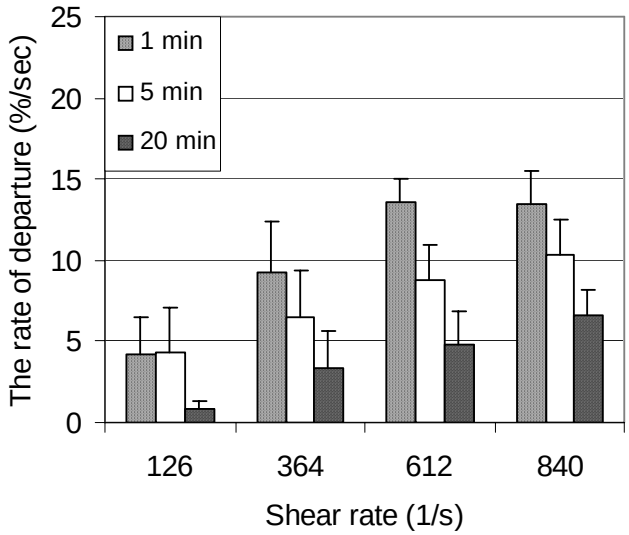

Fig. 4-15. (a) The rate of departure of platelets interacting with vWF for long time period under various shear rates.

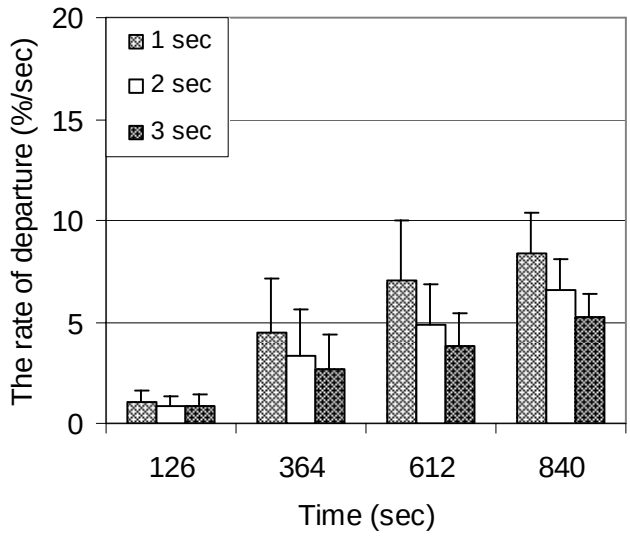

Fig. 4-15. (b) The rate of departure of platelets interacting with vWF for short time period under various shear rates.

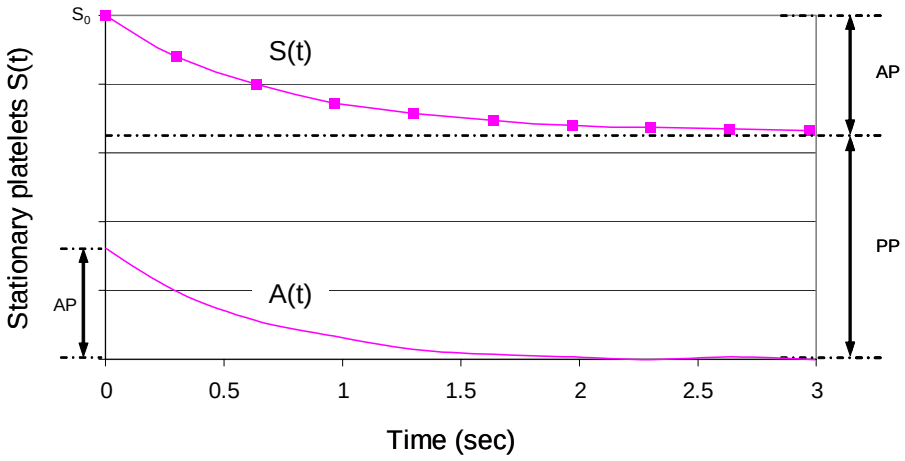

Fig. 4-16. Model of transient platelet binding. Stationary platelets are assumed to be permanently bound (PP) or transiently bound “active” platelets (AP).

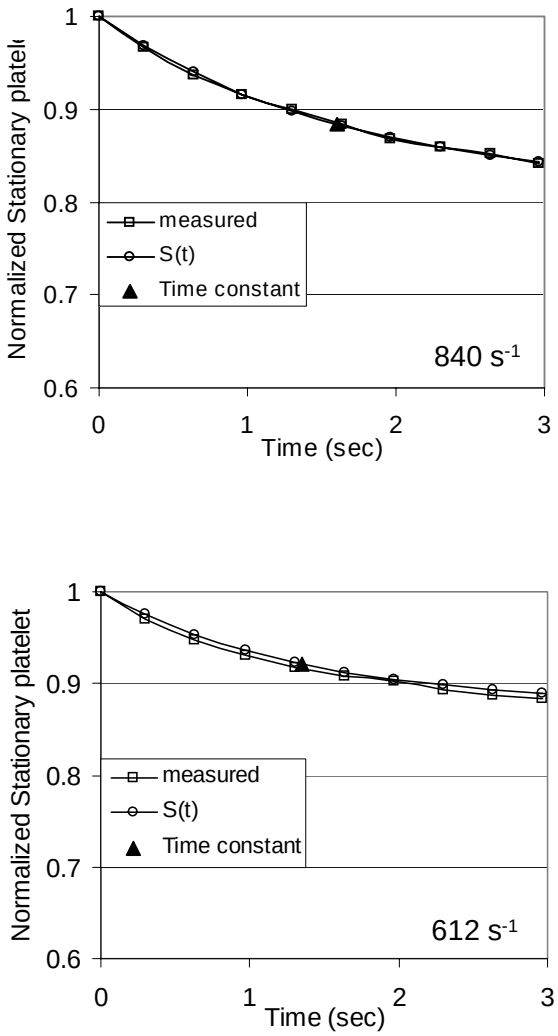

Fig. 4-17. Normalized stationary platelets during 3 sec and the characteristic time constant at shear rates 840 and 612 s^{-1}.

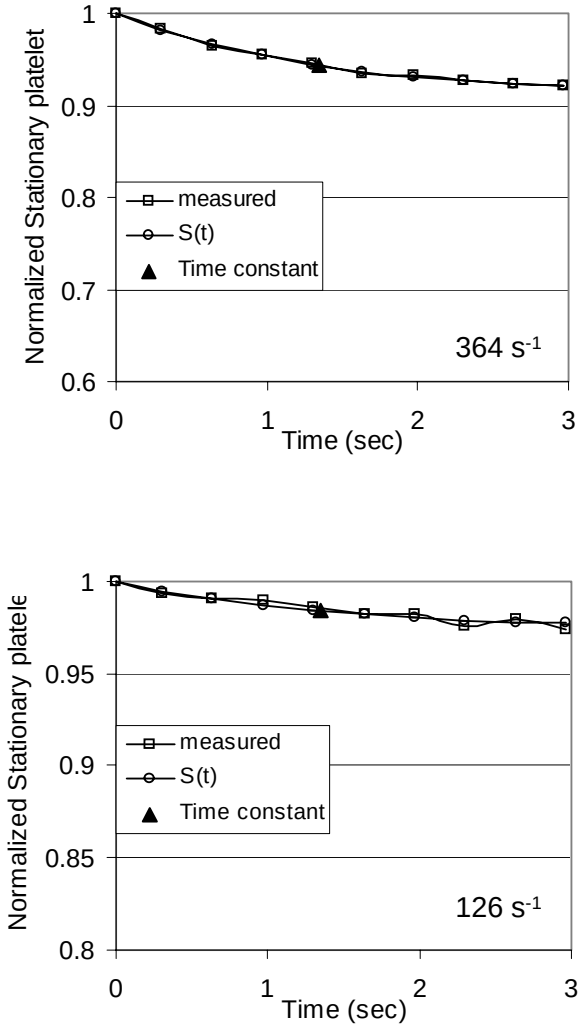

Fig. 4-18. Normalized stationary platelets during 3 sec and the characteristic time constant at shear rates 364 and 126 s^{-1}.

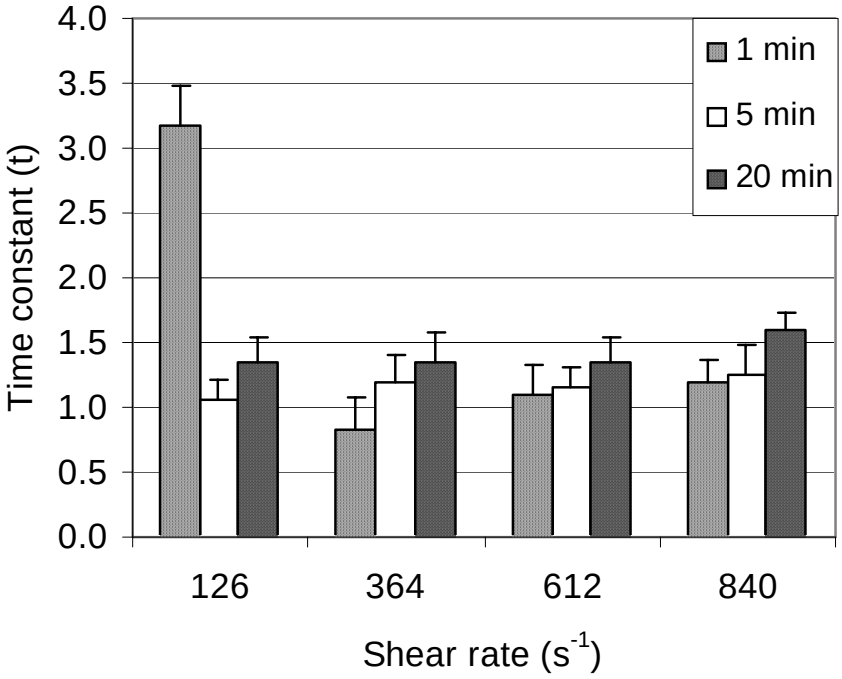

Fig. 4-19. Characteristic time constant at different shear rates (mean ± SEM; n = 5).

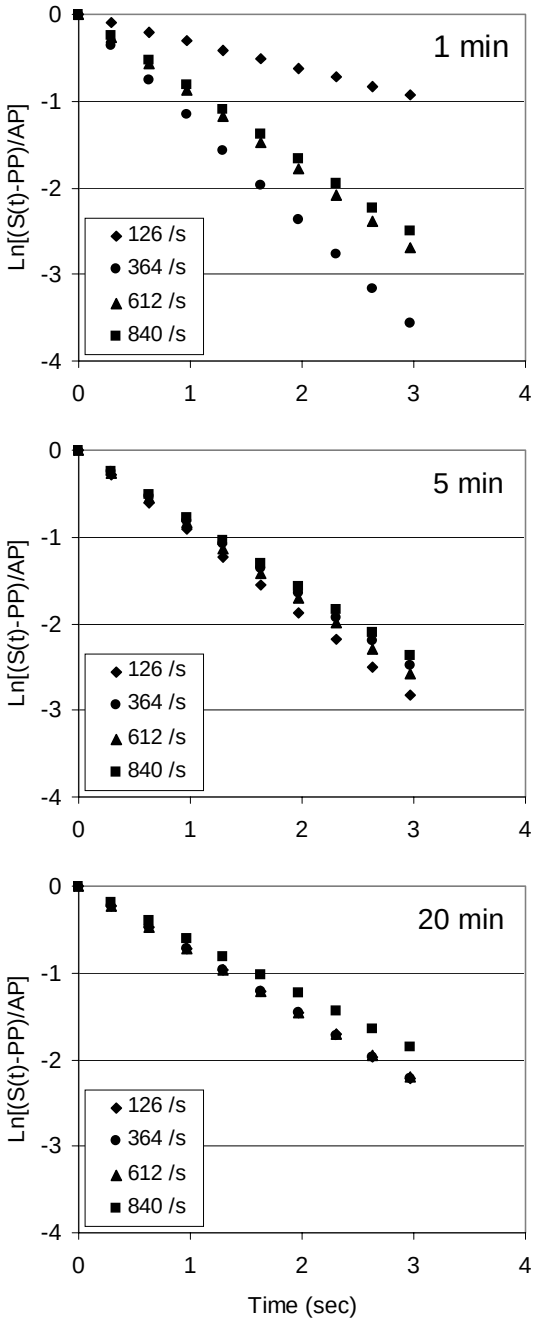

Fig. 4-20. Log plots showing model fit to log-linear equation (Eq. 4-5).

CHAPTER 5. DISCUSSION AND CONCLUSIONS

5.1 Novel Experimental Measurement of Rheologic Parameters in Individual Platelet Adhesion

In Chapter 3, the equations for rheologic parameters in a microscale capillary were mathematically described such as velocity, volume flow rate, wall shear stress, yield shear stress, and wall shear rate, and so forth. Based on the Casson viscosity model, the parameters were described in terms of fluid and flow properties such as η and y_c which are not accurately measurable. This means that the rheologic properties cannot be directly obtained without the knowledge of η and y_c. To numerically estimate these properties which are independent variables in Eq. 3-20, velocity, the dependent variable, was measured by experiment and compared to the theoretical profile for the same volume flow rate. Experimentally, the velocity was measured using the translating stage method and the criteria described in section 3.2. Theoretically, three parameters were used to get a profile and fit the measured profile: the pressure drop, the volume flow rate, and the centerline velocity measured by the translating stage method. After optimization of the velocity profile, the fluid properties were estimated, and therefore the other rheologic parameters were calculated.

Among the rheologic parameters, velocity is the most basic and crucial to describe a flow and induce the expressions for other parameters. Eq. 3-13 and 3-20 represent a velocity equation described with one independent variable and four parameters, which is the eventual goal in chapter 3. Among the four parameters, *h* is a

fixed geometrical dimension, and dP/dx is relatively easy to measure with simple application of a pressure transducer to a flow channel. η is, however, not an accurately-measurable fluid property because it is estimated by asymptotic approach based on other viscosity values measured at finite shear ranges. y_c physically represents a boundary between core and shear region in a flow field, and cannot be precisely measured. Thus, the unknowns are velocity, η, and y_c in the above velocity equation. But, to reduce the number of unknowns, the translating stage method was recruited to experimentally measure velocity values over the cross-section of the capillary. In the measurement of velocity profiles using fluorescent microbeads in chapter 3, the motion of the microbeads flowing in the shear-dominant region was not stable, the microbeads frequently moved forward or backward, or changed the flow direction, which could not be easily defined as a representative value for a focal depth. However, the motion of the microbeads flowing at the centerline was rather stable compared to other focal depth in shear-dominant region, meaning that the centerline velocity is measurable and treated as one of the parameters for the optimization of the theoretical velocity profile. Thus, the iterative process for the estimation of local velocities over the flow field was implemented for two unknowns, η and y_c, which yielded many velocity profiles. In the Casson model, η and τ_y are fixed values for a specific fluid, in other words, fluid properties. With the accurate knowledge for these values, dP/dx, and using Eq. 3-19 to get y_c, an exact velocity profile can be obtained, which is not guaranteed to be accurate. Therefore the volume flow rate was used as an additional parameter for the optimization of velocity profile. The volume flow rate is also measurable and an important flow property. All velocity profiles

numerically obtained by the iterations with η and y_c were integrated over the cross-sectional area of the capillary and compared with the measured volume flow rate. Finally the estimated values for η and y_c that gave an optimal fit to the velocity profile were obtained, which are crucial to calculate other rheologic parameters such as wall shear rate, wall shear stress, and yield stress.

The fluid properties η and τ_y vary for individual donor variations, and possibly change with time or different shear rate or flow rate even for the same blood sample. Among the three optimization parameters, volume flow rate for a syringe pump can be calibrated prior to experiment. dP/dx and centerline velocity can be measured during each individual experiment. Thus, with the measurement of the three parameters, this new method for estimating η and τ_y can be implemented for each individual experimental run, and therefore an accurate velocity profile for each experimental case can be estimated.

5.2 Initial Study toward Fully Automated Rheologic Parameter Identification in Platelet Adhesion Assay

All rheologic parameters were functions of η and y_c. By adequate selection of the properties, proper velocity profile can be obtained, and subsequently volume flow rate and other rheologic parameters can be calculated. We expected that this optimization process could be successfully performed by the Microsoft Excel Solver by iterating η

and y_c. However, the results were not enough to satisfy errors within 0.5 % in volume flow rate. To automate this optimization process, an Excel macro program was programmed, which runs the optimization process shown in Fig. 3-5. After completion of this process, the macro inspects the result to check that the volume flow rate obtained from the theoretical velocity profile satisfies error within 0.5 %, then, sorts out some data satisfying error within 1.0 % for maximum velocity. At this point, a more robust method was used to obtain an optimized velocity profile. Eq. 3-21 shows the root mean square (RMS) error method for this purpose, which includes two normalized terms which are based on quantities that can be measured during individual experiments, and are functions of the unknown parameters η and y_c. With the assumptions that the measured pressure drop and flow rate were accurate, the errors originated from the combination of the calculated flow rate error, which was less than 0.5%, and the calculated maximum velocity error, which ranged from -10% to +3%. Figure 5-1 shows the variation of RMS error in terms of maximum velocity. All of these data have flow rate error less than 0.5 %. The closest value to the measured maximum velocity among the result of numerical iteration appears to decrease RMS error, but there was effect of y_c and η on minimum RMS error.

Figure 5-2 shows (a) the 3-dimensional logarithmic plot for RMS error values with respect to y_c and η, (b) the contour plot of (a), and (c) the zoomed plot of the circled region in (b). Figure 5-2 (a) shows a trough corresponding to an apparently hyperbolic curve in the y_c-η plane shown in Fig. 5-2 (b), along which the RMS error is much lower than other values. In this situation, the Excel Solver function was unable to simultaneously solve for the optimum values of y_c and η, instead holding the value of

y_c fixed and finding the optimum value of η. Figure 5-2 (c) shows that five points satisfied two constraints, flow rate and maximum velocity, but the corresponding y_c and η had different RMS errors. The RMS error approaches a minimum point in the direction of the thick arrows shown in this figure.

In the future, a fully automated parameter optimization method would benefit from using two independent combinations of η and y_c. The first combination should be based on a mathematical analysis of the form $\eta(y_c)$ of the trough and should locate the curve of the trough. The second combination (potentially either η or y_c) should locate the error minimum within the trough.

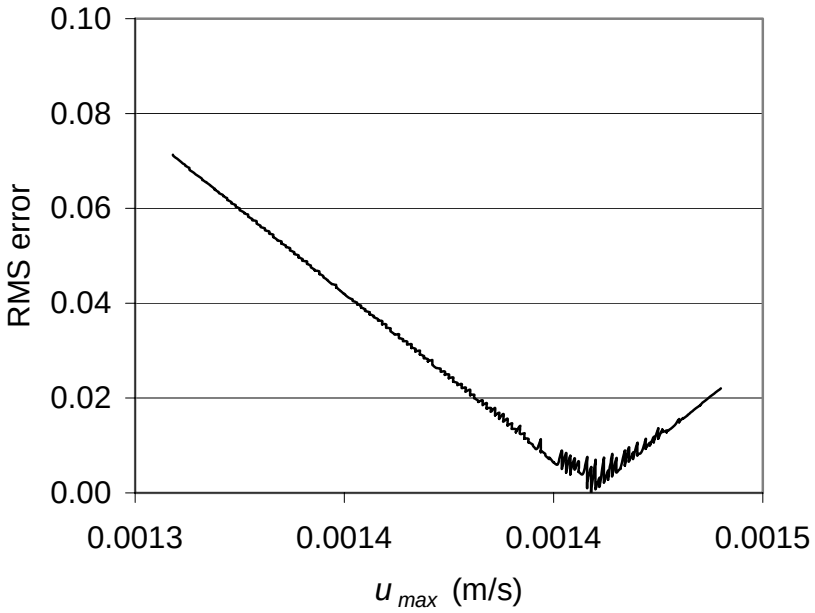

Fig. 5-1. RMS errors with respect to maximum velocity.

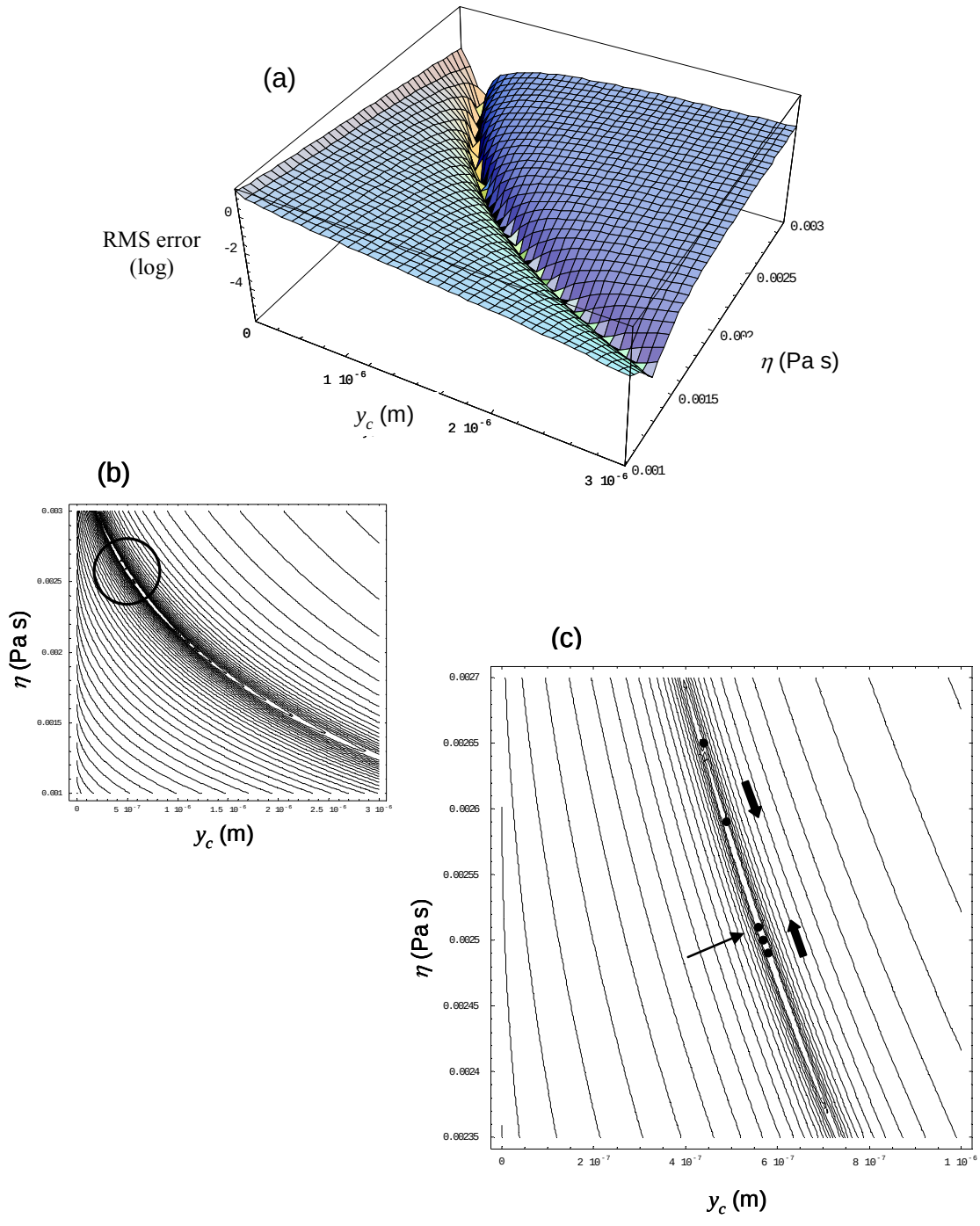

Fig. 5-2. RMS errors with respect to y_c and η:
(a) 3-dimensional plot of log (RMS error), (b) contour plot, (c) zoomed contour plot.

5.3 Platelet Flux Control Volume Analysis

In this section, a control volume was defined in the flow field as shown in Fig. 5-3, and flux of platelets entering or leaving the control volume through boundaries was examined for each flow rate. The platelet balance can be described as follows,

$$\sum F_{in} - \sum F_{out} = \left(F_{conv,in} - F_{conv,out}\right) + \left(F_{d,in} - F_{d,out}\right) = \frac{d(I(t) - L(t))}{dt}, \qquad (5\text{-}1)$$

where

F_{in} = flux of platelets entering the control volume,

F_{out} = flux of platelets leaving the control volume,

$F_{conv,in}$ = convective flux of platelets entering the control volume through the inlet,

$F_{conv,out}$ = convective flux of platelets leaving the control volume through the outlet,

$F_{d,in}$ = dispersive flux of platelets entering the control volume through the top,

$F_{d,out}$ = dispersive flux of platelet leaving the control volume through the top,

$I(t)$ = incoming platelets interacting with the vWF-coated surface, and

$L(t)$ = leaving platelets interacting with the vWF-coated surface.

The dimension of the control volume depends on flow rate. The height of the control volume was set to 2 μm, which is the depth of the lower surface of the region of interest (ROI) for the near-wall concentration analysis. The width of 0.018634 μm was the width of the field of view for the analysis of surface kinetics of platelets. However,

the length of the control volume was defined as the traveling distance of the translating-stage during 9 sec. The stage speed varied with different flow rates: the traveling distance of translating-stage x is equal to the multiplication of translating-stage speed u_{stage} by the elapsed time Δt which is 9 sec, and the control volume length varied from 0.473 cm at the lowest flow rate to 2.018 cm at the highest flow rate.

In Chapter 4, the near-wall platelet concentration between 2 and 4 μm in depth from the surface of capillary was estimated through the field of view (FOV) and averaged for 5 different sites as shown in Fig. 5-3. Defining c1 as the inlet and c5 as the outlet convective flux of platelets for boundary conditions, the numerical iteration using the Excel solver function was implemented assuming that the peak point of near-wall platelet concentration was fixed at 3 μm from the capillary wall [Eckstein et al., 1987]. In this iteration process, the convective mass flux over the half of cross-sectional area of capillary and the platelet concentration between 2 and 4 μm from the capillary wall were examined, and the experiment-based convective platelet flux and concentration were compared to the theory-based values. Originally, the concentration of platelets in the blood suspension was regulated to 180,000 platelets/μl and the volume flow rate through half of the cross-sectional area of capillary was determined based on velocity profiles obtained in section 3.4.2. Thus the experiment-based convective platelet flux was estimated by multiplying the concentration with flow rate. And the concentration between 2 and 4 μm from the capillary wall was measured in section 4.3. Experimental measurements were fit to a theoretical concentration profile, a beta function proposed by Eckstein *et al*. (1991),

$$c(y) = c_0\left[1 + K\left(\frac{y}{h}\right)^{(m-1)}\left[1 - \left(\frac{y}{h}\right)\right]^{(n-1)}\right], \tag{5-2}$$

where

$c(y)$ = platelet concentration profile,

c_0 = centerline platelet concentration,

K = parameter that controls the amplitude of the profile,

h = half of the height of capillary tube, and

m and n = exponents of the beta function.

Once the concentration profile was estimated, the theory-based convective platelet flux was calculated as follows,

$$F_{conv}(y) = \int_0^h u(y)c(y)w dy\,. \tag{5-3}$$

In this numerical process, c_0 and K in Eq. (5-2) were iterated so that at the inlet of the control volume the average of theory-based concentration between 2 and 4 μm from the wall matches the experiment-based concentration c1 shown in Fig. 5-3 and the calculated convective flux matches experiment-based convective flux. At the outlet of the control volume, the average of theory-based concentration between 2 and 4 μm from the wall was compared to the concentration c5 and the convective mass flux was also examined. To obtain optimized values for the two parameters, RMS error minimization method was used based on

$$RMSerror = \sqrt{\left(\frac{c_{\exp} - c_{theo}}{c_{\exp}}\right)^2 + \left(\frac{F_{conv,\exp} - F_{conv,theo}}{F_{conv,\exp}}\right)^2}\,, \tag{5-4}$$

where

$c_{\exp}$ = average of measured near-wall platelet concentration (2 and 4 mm),

c_{theo} = average of calculated near-wall platelet concentration (2 and 4 mm),

$F_{conv,\exp}$ = experiment-based convective flux, and

$F_{conv,theo}$ = theory-based convective flux.

For the dispersive platelet flux entering or leaving through the top boundary of the control volume shown in Fig. 5-3, image sequences for 9 sec recorded for the near-wall concentration analysis were analyzed. Since a function $y(u)$ representing the instantaneous location of platelet in flow was determined in Chapter 3, the number of platelets whose location in the flow changed below 2 μm was counted and considered the dispersive flux entering the control volume through the top boundary. The dispersive platelet flux leaving the control volume through the top boundary was obtained by counting platelets whose location changed from below to above 2 μm. The net accumulation of platelets on the surface of the control volume was estimated by estimating the rate of incoming platelets and the rate of leaving platelets from the analysis of surface kinetics in Chapter 4.

Figure 5-4 and 5-5 show the concentration profile and convective platelet flux at the inlet and outlet of the flow field, respectively. The inlet concentration appears to be similar to the outlet, but convective flux does not have big difference in near-wall region. Figure 5-6 shows quantitative comparison of the calculated net accumulation with the experimentally measured values at different time frames. The calculated net accumulation was obtained by left hand side of the Eq. (5-1), and the experimentally measured values were obtained from the analysis of surface kinetics in Chapter 4. This

figure shows pretty good agreement of platelet balance between calculated and measured values except for the high shear rate case at 20 min. The higher the wall shear rate is, the faster platelets accumulate on the vWF-coated surface. The rate of accumulation is a decreasing function of time at high shear rates. Table 5-1 shows the detailed terms in the flux balance and the rate of accumulation. The platelet flux induced by the dispersive motion appears to be much more than the convective flux, meaning much stronger contribution of shear-induced dispersion to the contact of platelet with thrombogenic surface and furthermore, to the tethering or adhesion, accumulation, and aggregation of platelets than the convective motion. Because the net flux is similar to the platelet accumulation rate and the dispersive flux is an order of magnitude faster than the convective flux, the experiments show that dispersive transport is required for platelet accumulation at these shear rates. The experiments also show that faster adhesion kinetics could allow for more rapid platelet accumulation, since dispersive in flux is much larger than net dispersive flux. Activation by chemical agonists and pseudo pod extension could allow platelets near 2μm to reach the surface.

Table 5-1. Convective and dispersive flux (platelets/sec) under various shear rates at different time frames and the comparison of calculated net accumulation rate with the measured rate.

WSR	Time (min)	$F_{c,in}$	$F_{c,out}$	$F_{c,net}$	$F_{d,in}$	$F_{d,out}$	$F_{d,net}$	*Net*	Net_{exp}
126	1	0.56	0.57	-0.01	115.5	107.2	8.3	8.3	6.6
	5	0.51	0.57	-0.05	94.1	89.9	4.3	4.2	4.4
	20	0.56	0.54	0.01	62.8	56.4	6.4	6.4	4.4
364	1	1.95	1.58	0.37	342.2	288.2	54.0	54.4	46.6
	5	1.92	2.02	-0.10	273.4	260.4	13.1	13.0	14.0
	20	2.23	2.07	0.16	250.7	230.8	19.9	20.1	14.0
612	1	3.83	3.76	0.06	817.3	712.4	104.9	104.9	92.9
	5	4.12	3.88	0.24	737.9	691.6	46.3	46.5	38.7
	20	4.15	4.03	0.12	644.4	603.8	40.6	40.8	15.5
840	1	5.93	6.65	-0.73	1215.1	1099.7	115.3	114.6	121.9
	5	5.64	6.33	-0.68	1098.6	1039.2	59.4	58.7	46.8
	20	6.32	6.35	-0.03	978.7	949.0	29.7	29.7	9.4

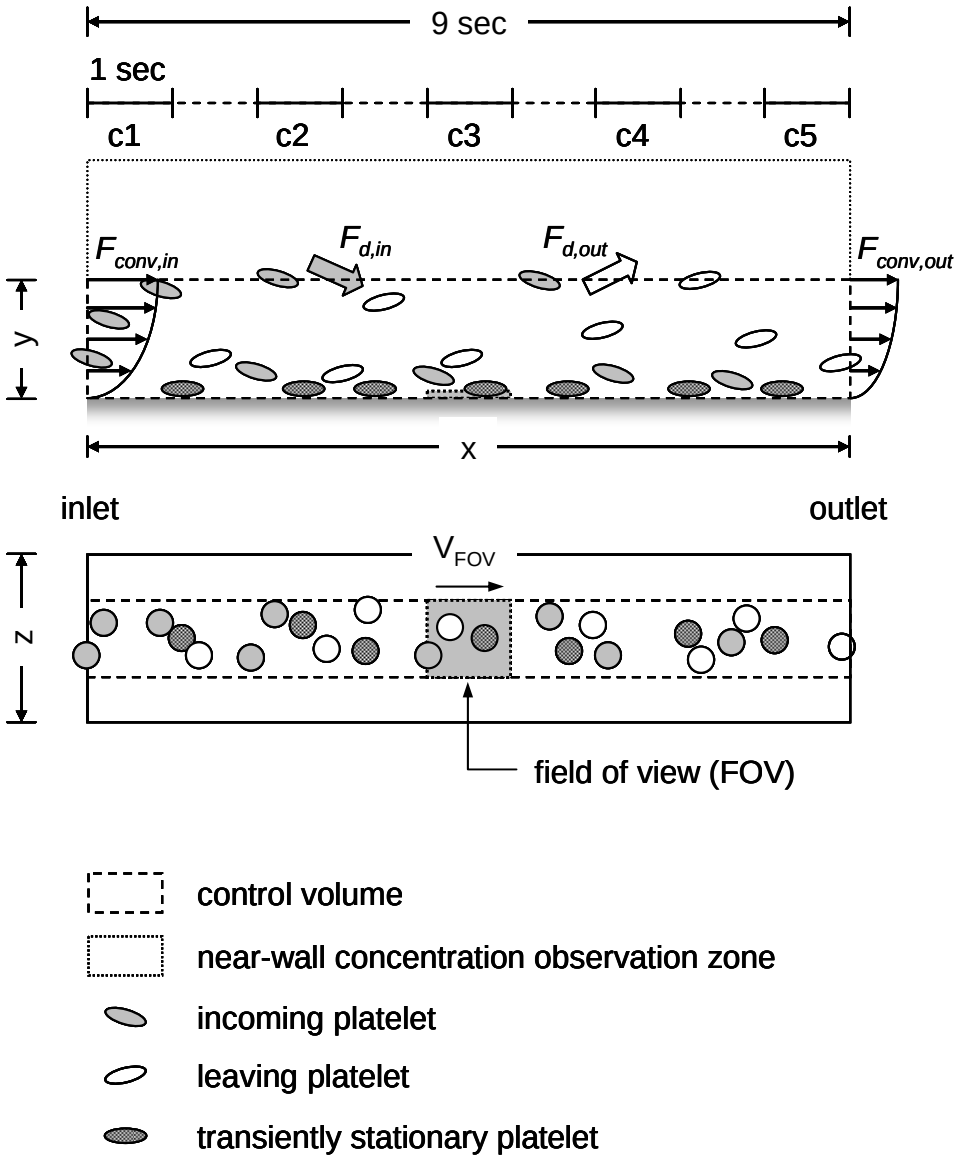

Fig. 5-3. Schematic diagram of the control volume for the flux balance analysis.

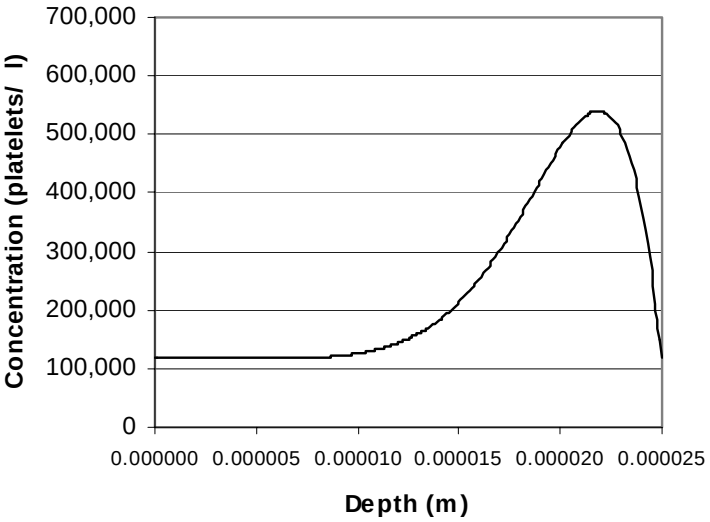

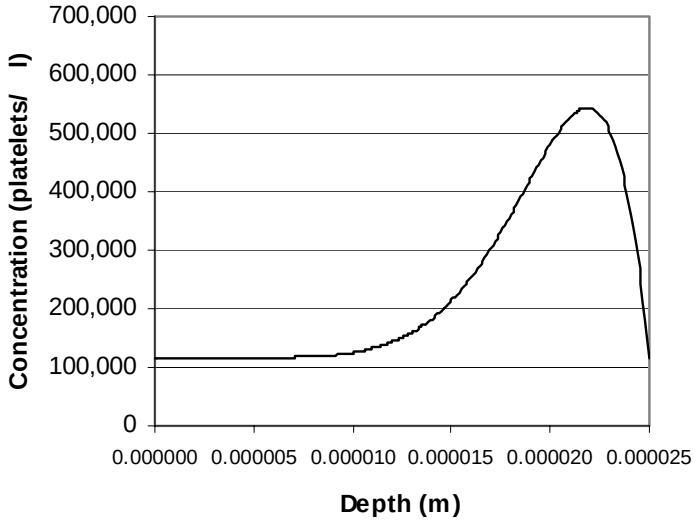

Fig. 5-4. Platelet concentration profiles at the inlet and outlet of the control volume.

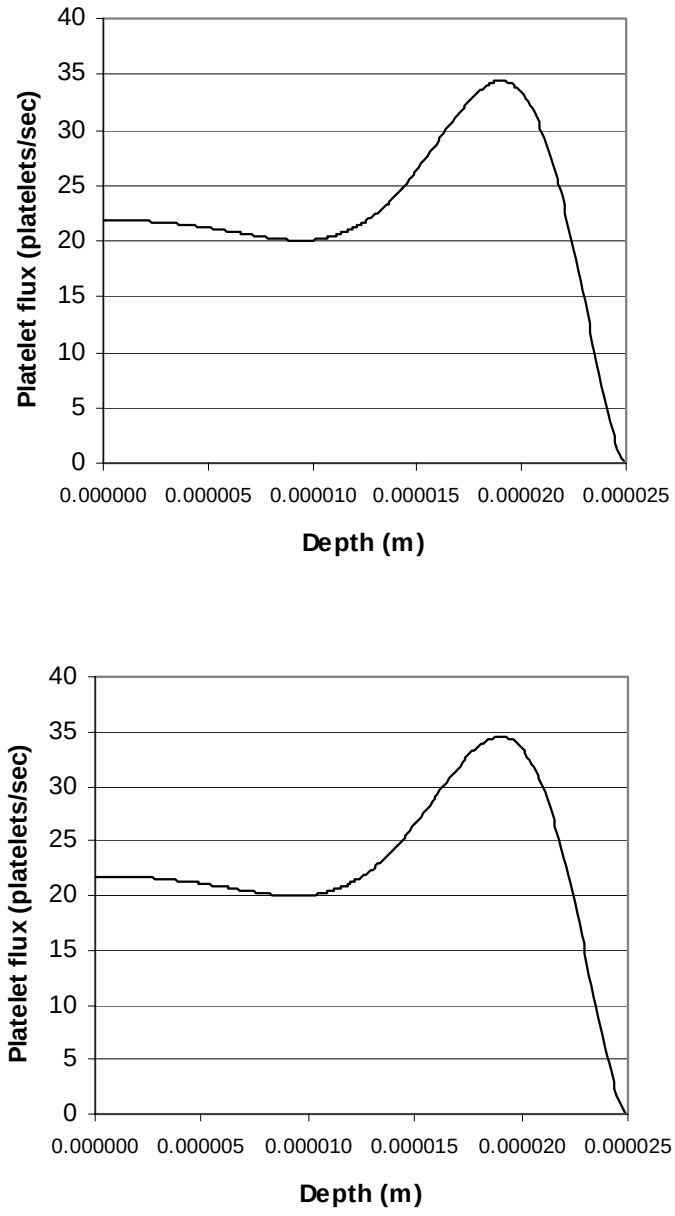

Fig. 5-5. Convective platelet flux profiles at inlet and outlet of control volume.

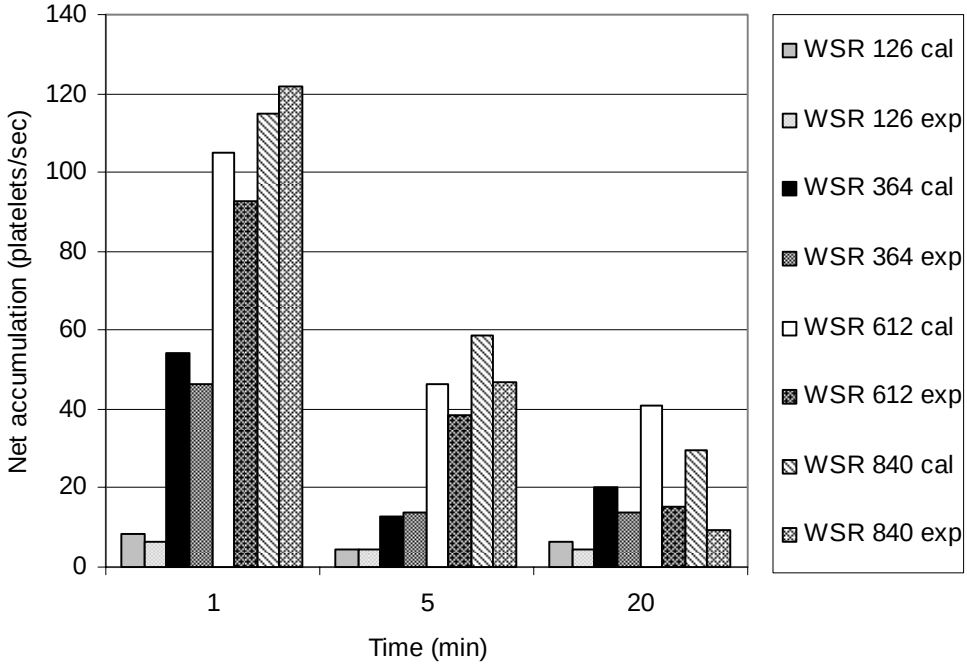

Fig. 5-6. Quantitative comparison of the calculated net accumulation with the experimentally measured values at different time frames.

5.4 Biological and Bioengineering Implications of Results

In the present study, velocity profiles of the blood suspension were investigated to track the flowing platelets and define their locations in a shear flow, and to help establish the concentration of the platelets near wall. Based on the near-wall platelet concentration, the platelet flux over the cross-section of capillary could be estimated. Simultaneously, the kinetic interactions of the platelets on vWF-coated surface were observed during the experiment. And platelet flux balance was performed on a control volume within 2 μm of the vessel wall using the near-wall concentration data, estimated convective flux, and surface net accumulation rate.

Through the experiment of shear dependent adhesion under various shear rates, GP Ibα-mediated interaction with vWF considered as the first step of the process of platelet adhesion was evaluated: The higher the wall shear rate, the more and faster the platelets accumulated on the immobilized vWF surface. This fast rate of bond formation between GP Ibα and vWF A1 domain allows establishment of initial contact even when platelets move at high hydrodynamic speed. Thus the interaction of platelets with vWF appears to be crucial to platelet adhesion especially in high shear flow, and is central to the intriguing phenomena of shear-induced platelet adhesion.

The platelet adhesion affected the near-wall concentration. Platelet margination was significantly reduced over vWF at high shear rates, compared to BSA-coated surface. Because the reduction of near-wall platelet concentration in the vWF experiments is greatest when the platelet adhesion is highest and when shear rate is highest, we hypothesize that adherent platelets, which are largely unactivated discoids in these

experiments, may cause flow disturbances that repel platelets from the near-wall layers of flow, either through direct hydrodynamic interactions, or indirectly by disturbing RBCs near the wall.

In the kinetics analysis, four different types of the platelet behaviors were defined to represent the interaction of platelet with vWF-coated surface: incoming, leaving, translocating, and transiently stationary platelets. With the current optical system, 'rolling' or 'flipping' platelets could not be distinguished from 'translocating' platelets. Through the observation, the GP Ibα-mediated interaction with vWF showed reversible characteristics with fast dissociation rate. This could be caused by the low concentration of vWF used in this study, the number of GP Ibα on the platelet membrane, short residence time for binding, weak attractive forces between GP Ibα and vWF, or inhibited function of $\alpha_{IIb}\beta_3$ which would otherwise lead to stable platelet adhesion.

With the involvement of a control volume near the wall, and as boundary conditions with the combination of the data from the near-wall concentration data, estimated convective flux, and surface net accumulation rate, the cross-streamline dispersion of platelets played a dominant role in the interaction of the platelets near wall. And this could be modeled representing how these relate to vWF surface.

5.5 Experimental Limitations

In the present study, the blood sample was mixed with prostaglandin E_1 (PGE_1) to prevent full activation of platelets and with EDTA to inhibit integrin receptor function of

platelets, and supplemented with apyrase as ADP scavenger. The blood sample was also mixed with abxicimab to inhibit aggregation of platelets in the whole blood. However, even though blood was treated with four inhibitors as soon as collected to prevent full activation of platelet during experiment, the image sequences showed that a fraction of platelets interacting with vWF seem to be activated and firmly adherent to the surface, but a few aggregates formed, which means that 100% of inhibition of activation could not be accomplished. This might be due to the engagement of another activation pathways or the involvement of other molecular binding mechanisms. Other inhibitors, gel-filteration of platelets, and recombinant forms of vWF or vWF domains could be used in future experiments to further inhibit activation, permanent adhesion, and aggregation.

In addition, due to the limited range of speed of the current translating stage as well as the ability of the camera to capture images during experiment, the range of the shear rates was limited from 126 to 840 s^{-1}. The slowest speed of the stage was slightly faster than the velocity at 3 μm from the bottom of capillary at the shear rate 126 s^{-1}. The fastest speed of the stage was 2.0 cm/s, twice as fast as the centerline velocity at the shear rate 840 s^{-1}. However, the images of platelets flowing faster than about 1.0 cm/s (corresponding to the centerline velocity at the shear rate 840 s^{-1}) could barely be obtained with the current camera being operated at a frame rate (30 fps) and with the current concentration of fluorechrome to label platelets. For the latter problem, a higher concentration could not be applied because of a possibility that the natural function of the platelet can be disturbed by high concentration of the chemical. To solve the former problem, several alternative methods trials were tested. A higher frame rate (125 fps) camera was tested with an additional image intensifier, but the recorded images were

poor with low light sensitive and high noisy. Another high speed camera (60 fps) with superior low-light sensitivity was tested but the image window of the resulting digital file was too small to analyze the detail motion of many platelets. Thus, the current camera (30 fps) was used to record the images through a VCR system, then, the images were digitized. In the future, a better optical system needs to be developed to solve the above problems, higher recording rate with low electronic noise and good low-light sensitivity.

5.6 Summary and Contributions of the Thesis

Seven unique contributions to understanding blood flow rheology and platelet biofluid mechanics and kinetics were developed in this research.

1. A novel *in vitro* translating-stage assay was developed that for the first time enables simultaneous measurement of platelet adhesion, platelet margination, wall shear stress, and non-Newtonian flow velocity profile, in blood flow through protein-coated capillaries.
2. A new method was developed to numerically calculate velocity profiles based on the theoretical viscosity model and three parameters that are controlled or quickly measured during experiments: volume flow rate, maximum velocity, and pressure drop. By minimizing the error in flow rate and maximum velocity, accurate estimates of rheological model parameters are obtained. The new method allows accurate estimates of τ_w and $\dot{\gamma}_w$ in each individual run of the translating stage experiment.

3. Quantitative evaluation of shear rate dependence of platelet adhesion on immobilized vWF was performed, and the effect of time on platelet adhesion was investigated. This evaluation confirmed other studies and supported our choice of methods for the sample preparation in the present study.
4. Near-wall concentration of platelets in shear flow was measured for the first time for active thrombogenesis on a protein-coated surface, and supporting image analysis tools were developed for measuring velocity and platelet location. By the adoption of the translating stage method, realistic behavior of the platelets flowing near protein-coated wall under the effect of the dispersive motion of RBCs and the adherent platelets could be observed, and the detail motion of the platelets were analyzed.
5. Surface kinetics of platelets on immobilized vWF was measured, and supporting image analysis tools were developed for quantifying transiently stationary, translocating, incoming, and leaving platelets.
6. A platelet flux balance was performed on a control volume within 2 μm of the vessel wall using near-wall concentration data, estimated convective flux, and surface net accumulation rate. This was the first such experimental flux balance, and supported the importance of dispersive flux in platelet accumulation.
7. Comprehensive image set supports 'data mining' opportunities. Platelet dispersion under the effect of RBCs motion can be estimated by investigating location of the platelets in the images. Drift velocity of the platelet can be estimated using the image analysis tool, and the platelet concentration gradient dc/dy may be estimated based on subdividing the moving volume. We expect other analyses could be performed,

and that this data set will provide a means for validating numerical models of platelet flow and accumulation.

5.7 Future Work

In this study, only one layer was investigated for the concentration of platelet flowing near vWF-coated wall. By examining other deeper layers (toward the centerline) based on the velocity optimized in Chapter 3, quantitative estimation of the platelet concentration profile over the entire flow field will be investigated and modeled.

Future work will focus on additional experiments studying the simultaneous characterization of both platelet and RBC motion in a shear flow using the present translating stage method with two-color tracers and the quantitative estimation of the effect of RBC motion on platelet dispersion by examining the interaction of the cells. Furthermore, the effective dispersion rate of RBC or platelets will be estimated by determining the location of cells in a shear flow.

Finally, improved imaging methods using higher-speed camera (60 fps) will be used to observe more detail motion of the platelets.

LIST OF REFERENCES

Aarts, P.A., Steendijk, P., Sixma, J.J., Heethaar, R.M., Fluid shear as a possible mechanism for platelet diffusivity in flowing blood. J. Biomech, 19 (1986) 799-805.

Aarts, P.A. M.M., van den Broek, S.A.T., Prins, G.W., Kuiken, G.D.C., Sixma, J.J., Heethaar, R.M., Blood platelets are concentrated near the wall and red blood cells, in the center in flowing blood, Arteriosclerosis, 8 (1988) 819-824.

Back, C.H., Radbill, J.R., Crawford, D.W., Analysis of pulsatile viscous blood flow through diseased coronary arteries of man, J. Biomech., 10 (1977) 339-353.

Baker, M., Wayland, H., On-line volume flow rate and velocity profile measurement for blood in microvessels, Microvascular Research, 7 (1974) 131-143.

Barbee, J.H., Cokelet, G.R., The Fahraeus effect, Microvascular Research, 3 (1971) 6-16.

Barnes, H.A., Thixotropy-a Review, J. Non-Newtonian Fluid Mech., 70 (1997) 1-33.

Basheer, A.R., El-Asmar, M.F., Soslau, G., Characterization of a potent platelet aggregation nducer from *Cerastes cerastes* (Egyptian sand viper) venom, Biochimica et Biophysica Acta, 1250 (1995) 97-109.

Benis, A.M., Usami, S., Chien, S., Effect of hematocrit and inertial losses on pressure-flow relations in the isolated hind paw of the dog, Circulation Research, 27 (1970) 1047-1068.

Bennett, J.S., Vilaire, G., Cines, D.B., Identification of the fibrinogen receptor on human platelets by photoaffinity labeling, J. Biol. Chem., 257 (1982) 8049-8064.

Bilsker, D.L., Waters, C.M., Kippenhan, J.S., Eckstein, E.C., A freeze-capture method for the study of platelet-sized particle distributions, Biorheology, 26 (1989) 1031-1040.

Bird, R.B., Armstrong, R.C., Hassager, O., Dynamics of Polymeric Liquids, Vol. 1, Wiley, New York, 1987.

Bishop, J.J., Nance, P.R., Popel, A.S., Intaglietta, M., Johnson, P.C., Effect of erythrocyte aggregation on velocity profiles in venules, Am J Physiol. Heart Circ Physiol, 280 (2001) H222-H236.

Braunwald, E., Zipes, D.P., Libby, P., Heart Disease, 6th ed, Saunders, 2001.

Bugliarello, G., Hayden, J.W., High-speed microcinematographic studies of blood flow in vitro, Science, 138 (1962) 981-983.

Bugliarello, G., Hayden, J.W., Detailed characteristics of the flow of blood in vitro, Trans Soc Rheology, 7 (1963) 209-230.

Bugliarello, G., Sevilla, J., Velocity distribution and other characteristics of steady and pulsatile blood flow in fine glass tubes, Biorheology, 7 (1970) 85-107.

Coller, B.S., Interactions of normal, thrombasthenic, and Bernard-Soulier platelets with immobilized fibrinogen: defective platelet-fibrinogen interaction in thrombasthenia, Blood, 55 (1980) 169-178.

Colman, R.W., Hirsh, J., Marder, V.J., Salzman, E.W., Hemostasis and Thrombosis: Basic Principles and Clinical Practice, 3rd ed., J.B. Lippincott Company, 1994.

Colman, R.W., Rao, A.K., Platelets in health and disease, Hematology/Oncology Clinics of North America, 4 (1990) 107-128.

Corattiyl, V., Eckstein, E.C., Technical reports: regional platelet concentration in blood flow through capillary tubes, 32 (1986) 261-270.

Cruz, M.A., Diacovo, T.G., Emsley, J., Liddington, R., Handin, R.I., Mapping the glycoprotein Ib-binding site in the von Willebrand factor A1 domain, The Journal of Biological Chemistry, 275(2000) 19098-19105.

Davies, M.J., Thomas, A., Thrombosis and acute coronary-artery lesions in sudden cardiac ischemic death, The New England Journal of Medicine, 310 (1984) 1137-1140.

De Groot, P.G., The role of von Willebrand factor in platelet function, Seminars in Thrombosis and Hemostasis, 28 (2002) 133-138.

De Marco, L., Girolami, A., Zimmerman, T.S., Ruggeri, Z.M., von Willebrand factor interaction with the glycoprotein IIb/IIIa complex. Its role in platelet function as demonstrated in patients with congenital afibrinogenemia, The Journal of Clinical Investigation, 77 (1986) 1272-1277.

Doggett, T.A., Girdhar, G., Lawshe, A., Schmidtke, D.W., Laurenzi, I.J., Diamond, S.L., Diacovo, T.G., Selectin-like kinetics and biomechanics promote rapid platelet adhesion I flow: the GPIba-vWF tether bond, Biophysical Journal, 83 (2002) 194-205.

Eckstein, E.C., Tilles, A.W., Millero III, F.J., Conditions for the occurrence of large near-wall excesses of small particles during blood flow, Microvascular Research, 36 (1988) 31-39.

Eckstein, E.C., Koleski, J.F., Waters, C.M., Concentration profiles of 1 and 2.5 m beads during blood flow: Hematocrit effects, ASAIO Transactions, 35 (1989) 188-190.

Eckstein, E.C., Belgacem, F., Model of platelet transport in flowing blood with drift and diffusion terms, Biophys. J., 60 (1991) 53-69.

Frenette, P.S., Johnson, R.C., Hynes, R.O., Wagner, D.D., Platelets roll on stimulated endothelium in vivo: An interaction mediated by endothelial P-selectin, Proceedings of the National Academy of Sciences of the United States of America, 92 (1995) 7450-7454.

Friedman, R.J., Moore, S., Signal, D.P., Repeated endothelial injury and induction of atherosclerosis in normolipemic rabbits by human serum, Lab. Invest.,32 (1975) 404-415.

Fujimoto, T., Hawiger, J., Adenosin diphosphate induces binding of von Willebrand factor to human platelets, Nature, 297 (1982) 154-156.

Fung, Y.C., Biomechanics: Mechanical Properties of Living Tissues, Springer, New York, 1993.

Fuster, V., Stein, B., Ambrose, J.A., Badimon, L., Badimon, J.J., Chesebro, J.H., Atherosclerotic plaque rupture and thrombosis, Circulation, 82 (1990) II47 – II59.

Fuster, V., Badimon, L., Badimon, J.J., Chesebro, J.H., The pathogenesis of coronary artery disease and the acute coronary syndromes (1), N. Engl. J. Med., 326 (1992) 242-250.

Fuster, V., Badimon, L., Badimon, J.J., Chesebro, J.H., The pathogenesis of coronary artery disease and the acute coronary syndromes (2), N. Engl. J. Med., 326 (1992) 310-318.

Gibson, M.C., Diaz, L., Kandarpa, K., Sacks, F.M., Pasternak, R.C., Sandor, T., Feldman, C., Stone, P.H., Relation of vessel wall shear stress to atherosclerosis progression in human coronary arteries, Arterioscl. Thromb., 13 (1993) 310-315.

Goldman, L., Textbook of Medicine, 21st ed., Saunders Company, 2000.

Gogstad, G.O., Brosstad, F., Krutnes, M. Hagen, I., Solum, N.O., Fibrinogen-binding properties of the human platelet glycoprotein IIb-IIIa complex: a study using crossed-radioimmuno-electrophoresis, Blood, 60 (1982) 663-671.

Goldsmith, H.L, Red cell motions and wall interactions in tube flow, Federation Proceeding, 30 (1971) 1578-1590.

Goldsmith, H.L., Marlow, J.C., Flow behavior of Erythrocytes II. Particle motions in concentrated suspensions of ghost cells, Journal of Colloid and Interface science, 71 (1979) 383-407.

Goldsmith, H.L., Turitto, V.T., Rheological aspects of thrombosis and haemostasis: basic principles and applications. ICTH-Report-Subcommittee on rheology of the international committee on thrombosis and haemostasis. Thrombosis and Haemostasis, 55 (1986) 415-435.

Goto, S., Ikeda, Y., Saldivar, E., Ruggeri, Z.M., Distinct mechanisms of platelet aggregation as a consequence of different shearing flow conditions, The Journal of Clinical Investigation, 101 (1998) 479-486.

Harker, L.A., Ross, R., Slichter, S.J., Scott, C.R., Homocystine-induced arteriosclerosis: the role of endothelial cell injury and platelet response in its genesis, The Journal of Clinical Investigation, 58 (1976) 731-741.

House, S.D., Lipowsky, H.H., Microvascular hematocrit and red cell flux in rat cremaster muscle. Am. J. Physiol. Heart Circ Physiol., 252 (1987) H211-H222.

How, T.V., Advanced in Hemodynamic and Hemorheology, Vol. 1, JAI Press, London, 1996.

Italiano, J.E., Jr., Lecine, P., Shivdasani, R.A., Hartwig, J.H., Blood platelets are assembled principally at the ends of the proplatelet processes produced by differentiated megakaryocytes, J. Cell Biol., 147 (1999) 1299-1232.

Keller, K.H., Effect of fluid shear on mass transport in flowing blood, Fed. Proc., 30 (1971) 1591-1593.

Kiserud, T., Hellevik, L.R., Hanson, M.A., Blood velocity profile in the ductus venosus inlet expressed by the mean/maximum velocity ratio, Ultrasound in Med. & Biol., 24 (1998) 1301-1306.

Koleski, J.F., Eckstein, E.C., Near wall concentration profiles of 1.0 and 2.5 mm beads during flow of blood suspensions, ASAIO Transactions, 37 (1991) 9-12.

Kulkarni, S., Dopheide, S.M., Yap, C.L., Ravanat, C., Freund, M., Mangin, P., Heel, K.A., Street, A., Harper, I.S., Lanza, F., Jackson, S.P., A revised model of platelet aggregation, The Journal of Clinical Investigation, 105 (2000) 783-791.

Lee, R., Libby, P., The unstable atheroma, Arterioscler Thromb Vasc Biol, 17 (1997) 1859-1867.

Mayrovitz, H.N., Brief communications: An optimal flow-radius equation for microvessel non-newtonian bblood flow, Microvascular Research, 34 (1987) 380-384.

Mazzucato, M., Spessotto, P., Masotti, A., De Appollonia, L., Cozzi, M.R., Yoshioka, A., Perris, R., Colombatti, A., De Marco, L., Identification of domains responsible for von Willebrand factor Type VI collagen interaction mediating platelet adhesion under high flow, The Journal of Biological Chemistry, 274 (1999) 3033-3041.

McClung, W.G., Feuerstein, I.A., Epifluorescent video microscopy (EVM) for platelet-biomaterial interactions: elimination of photoactivation and dye effects, Biomaterials, 13 (1992) 871-877.

More, S., Thromboatherosclerosis in normolipemic rabbits: a result of continued endothelial damage, Lab. Invest., 29 (1973) 478.

Munson, B.R., Young, D.F., Okiishi, T.H., Fundamentals of Fluid Mechanics, Wiley, New York, 1998

Mustard, J.F., Packham, M.A., Kinlough-Rathbone, R.L., Perry, D.W., Regoeczi, E., Fibrinogen and ADP-induced platelet aggregation, Blood, 52 (1978) 453-466.

Nachman, R.L., Leung, L.L.K., Complex formation of platelet membrane glycoproteins IIb and IIIa with fibrinogen, The Journal of Clinical Investigation, 69 (1982) 263-269.

Reinhart, W.H., Haeberli, A., Stark, J., Straub, P.W., Influence of blood withdrawal and anticoagulant on clotting activity, hematologic data, and certain rheologic measurements, The Journal of Laboratory and Clinical Medicine, 115 (1990) 98-103.

Ribes, J.A., Francis, C.W., Wagner, D.D., Fibrin induces release of von Willebrand factor from endothelial cells, The Journal of Clinical Investigation, 79 (1987) 117-123.

Robbins, S.L., Cotran, R.S., Pathologic Basis of Disease, 2nd ed., Saunders, 1979.

Ruggeri, Z.M., Bader, R., De Marco, L., Glanzmann thrombasthenia: deficient binding of von Willebrand factor to thrombin-stimulated platelets, Proc. Natl. Acad. Sci., 79 (1982) 6038-6041.

Ruggeri, Z.M., De Marco, L., Gatti, L., Bader, R., Montgomery, R.R., Platelets have more than one binding site for von Willebrand factor, The Journal of Clinical Investigation, 72 (1983) 1-12.

Ruggeri, Z.M., Dent, J.A., Saldivar, E., Contribution of distinct adhesive interactions to platelets aggregation in flowing blood, Blood, 94 (1999) 172-178.

Ruggeri, Z.M., Old concepts and new developments in the study of platelet aggregation, The Journal of Clinical Investigation, 105 (2000) 699-701.

Sarelius, I.H., Duling, B.R., Direct measurement of microvessel hematocrit, red cell flux, velocity, and transit time, Am. J. Physiol. Heart Circ Physiol., 243 (1982) H1018-H1026.

Savage, B., Saldivar, E., Ruggeri, Z.M., Initiation of platelet adhesion by arrest onto fibrinogen or translocation on von Willebrand Factor, Cell, 84 (1996) 289-297.

Savage, B., Almus-Jacobs, F., Ruggeri, Z.M., Specific synergy of multiple substrate-receptor interactions in platelet thrombus formation under flow, Cell, 94 (1998) 657-666.

Savage, B., Sixma, J.J., Ruggeri, Z.M., Functional self-association of von Willebrand factor during platelet adhesion under flow, Proceedings of the National Academy of Sciences of the United States of America, 99 (2002) 425-430.

Shepard, B.L., French, J.E., Platelet adhesion in the rabbit abdominal aorta following the removal of the endothelium: a scanning and transmission electron microscopical study, Proc. R. Soc., 176 (1971) 427-432.

Sixma, J.J., Wester, J., The hemostatic plug, Semin. Hematol., 14 (1977) 265-299.

Sorensen, E.N., Burgreen, G.W., Wagner, W.R., Antaki, J.F., Computational simulation of platelet deposition and activation: II. Results for Poiseuille flow over collagen. Ann Biomed Eng, 27 (1999) 449-458.

Stemerman, M.B., Ross, R., Experimental arteriosclerosis. I. Fibrous plaque formation in primates, an electron microscope study, J. Exp. Med., 136 (1972) 769-789.

Tangelder, G.J., Slaaf, D.W., Teirlinck, H.C., Alewijnse, R., Reneman, R.S., Localization within a thin optical section of fluorescent blood platelets flowing in a microvessel, Microvascular Research, 23 (1982) 214-230.

Tangelder, G.J., Teirlinck, H.C., Slaaf, D.W., Reneman, R.S., Distribution of blood platelets flowing in arterioles, Am. J. Physiol. Heart Circ Physiol., 248 (1985) H318-H323.

Tangelder, G.J., Slaaf, D.W., Muijtjens, M.M., Arts, T., oude Egbrink, M.G.A., Reneman, R.S., Velocity profiles of blood platelets and red blood cells flowing in arterioles of the rabbit mesentery, Circulation Research, 59 (1986) 505-514.

Tangelder, G.J., Slaaf, D.W., Arts, T., Reneman, R.S., Wall shear rate in arterioles in vivo: least estimates from platelet velocity profiles, Am. J. Physiol. Heart Circ Physiol., 254 (1988) H1059-H1064.

Tilles, A.W., Eckstein, E.C., The near-wall excess of platelet-sized particles in blood flow: its dependence on hematocrit and wall shear rate, Microvascular Research, 33 (1987) 211-223.

Turitto, V.T., Benis, A.M., Leonard, E.F., Platelet diffusion in flowing blood, Ind. Eng. Chem. Fundam., 11 (1972) 216-223.

Turitto, V.T., Baumgartner, H.R., Platelet interaction with subendothelium in flowing blood in a perfusion system. Physical role of red blood cells, Microvascular Research, 9 (1975) 335-344.

Turitto, V.T., Baumgartner, H.R., Platelet deposition on subendothelium exposed to flowing blood: mathematical analysis of physical parameters. Trans Am Soc Artif Intern Organs, 21 (1975) 593-601.

Turitto, V.T., Baumgartner, H.R., Platelet interaction with subendothelium in flowing rabbit blood: effect of blood shear rate, Microvascular Research, 17 (1979) 38-54.

Turitto, V.T., Weiss, H.J., Baumgartner, H.R., The effect of shear rate on platelet interaction with subendothelium exposed to citrated human blood, Microvascular Research, 19 (1980) 352-365.

Wang, N.H., Keller, K.H., Solute transport induced by erythrocyte motions in shear flow, Trans. Am. Soc. Artif. Intern. Organs, 25 (1979) 14-18.

Waters, C.M., Eckstein, E.C., Concentration profiles of platelet-sized latex beads for conditions relevant to hollow-fiber hemodialyzers, Artificial Organs, 14 (1990) 7-13.

Wayland, H., Johnson, P.C., Erythrocyte velocity measurement in microvessels by a two-slit photometric method, J. Appl. Physiol., 22 (1967) 333-337.

Weiss, H.J., Turitto, V.T., Baumgartner, H.R., Further evidence that glycoprotein IIb-IIIa mediates platelet spreading on subendothelium, Thromb. Haemost., 65 (1991) 202-205.

Woldhuis, B., Tangelder, G.J., Slaaf, D.W., Reneman, R.S., Concentration profile of blood platelets differs in arterioles and venules, Am. J. Physiol. Heart Circ Physiol, 262 (1992) H1217-H1223.

Wootton, D.M., Markou, C.P., Hanson, S.R., Ku, D.N., A mechanistic model of acte platelet accumulation in thrombogenic stenoses, Annals of Biomedical Engineering, 29 (2001) 321-329.

Xu, C., Wootton, D.M., Platelet near-wall excess in porcine whole blood in artery-sized tubes under steady and pulsatile flow conditions, Biorheology, 41 (2004) 113-125.

Yeh, C., Calvez, A.C., Eckstein, E.C., An estimated shape function for drift in a platelet-transport model, Biophysical Journal, 67 (1994) 1252-1259.

Yeh, C., Eckstein, E.C., Transient lateral transport of platelet-sized particles in flowing blood suspensions, Biophysical Journal, 66 (1994) 1706-1716.

Zydney, A.L., Colton, C.K., Augmented solute transport in the shear flow of a concentrated suspension, Physico Chemical Hydrodynamics, 10 (1988) 77-96.

APPENDIX A. Nomenclature

English letters

$\vec{a}$	acceleration [$m \cdot s^{-2}$]
A	number of stationary platelets that eventually translate or depart from vWF-coated surface
AP	number of transiently bound “active” platelets on vWF-coated surface
C_1	coefficient of y^2 term of theoretical nonNewtonian velocity profile [$m^{-1} \cdot s^{-1}$]
C_2	coefficient of $y^{3/2}$ term of theoretical nonNewtonian velocity profile [$m^{-1/2} \cdot s^{-1}$]
C_3	coefficient of y term of theoretical nonNewtonian velocity profile [s^{-1}]
C_4	coefficient of constant term of theoretical nonNewtonian velocity profile [$m \cdot s^{-1}$]
c	concentration [platelets$\cdot \mu l^{-1}$]
c_0	centerline platelet concentration [platelets$\cdot \mu l^{-1}$]
d	diameter [μm]
D	displacement [μm]
$\vec{F}$	force [N]
F	platelet flux [platelets$\cdot sec^{-1}$]
h	height between centerline and bottom surface of capillary tube [m]
H	height of capillary tube [μm]
I	number of incoming platelets interacting with vWF-coated surface
K	parameter that controls the amplitude of concentration profile [dimensionless]

L	number of leaving platelets interacting with vWF-coated surface
M	mass [kg]
m	consistency index in Power-law [$Pa \cdot s^n$]
n	Power-law index [dimensionless]
P	pressure [Pa]
PP	number of permanently bound platelet on vWF-coated surface
Q	volume flow rate [$m^3 \cdot s^{-1}$]
S	number of transiently stationary platelets on vWF-coated surface
ΔS	number of platelets leaving or translocating on vWF-coated surface
S_0	initial number of platelet interacting with vWF-coated surface
Δt	elapsed time [sec]
u	flow velocity [$m \cdot s^{-1}$]
V	velocity [$m \cdot s^{-1}$]
v/v	volume ratio
w	width of capillary tube [m]
W	width of capillary tube [μm]
WSR	wall shear rate [s^{-1}]
x	x-direction coordinate in image
x	x-direction variable [m]
y	y-direction variable [m]
y_c	half-width of plug flow zone [m]
z	z-direction coordinate in image

Greek letters

ε	tolerance in iteration process
$\dot{\gamma}$	shear rate [s^{-1}]
$\dot{\gamma}_w$	wall shear rate [s^{-1}]
η	constant viscosity near infinite shear rate [Pa·s]
μ	Newtonian fluid viscosity [Pa·s]
τ	shear stress [Pa]
τ_t	time constant [sec]
τ_w	wall shear stress [Pa]
τ_y	yield shear stress [Pa]

Subscripts

c	core region
cal	calculated
conv	convective
d	dispersive
exp	experimental
FOV	field of view
in	entering

m	measured
max	maximum
out	leaving
shear	shear region
theo	theoretical
w	wall
x	x-direction
y	yield stress

APPENDIX B. Calibration Data

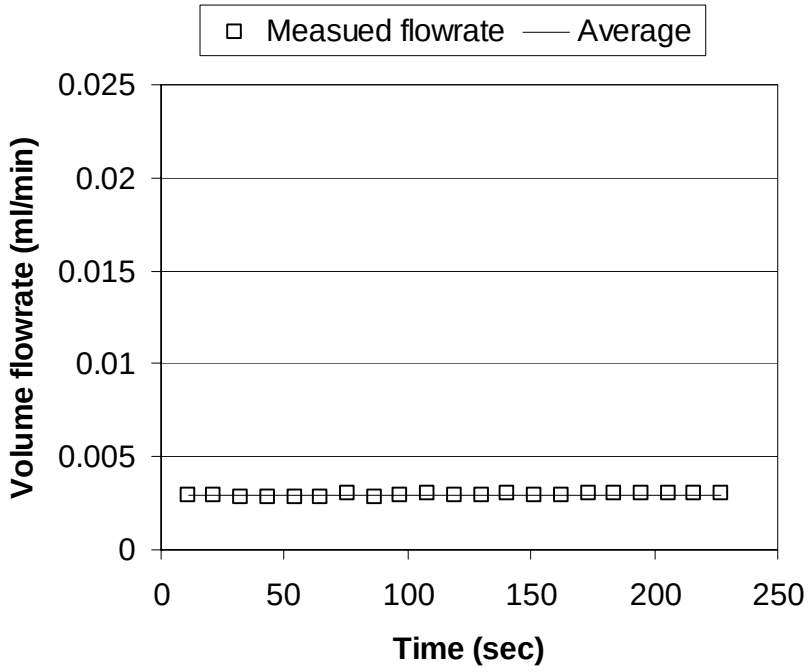

Fig. B-1. Volume flow rate calibration for wall shear rate 126 s^{-1}.

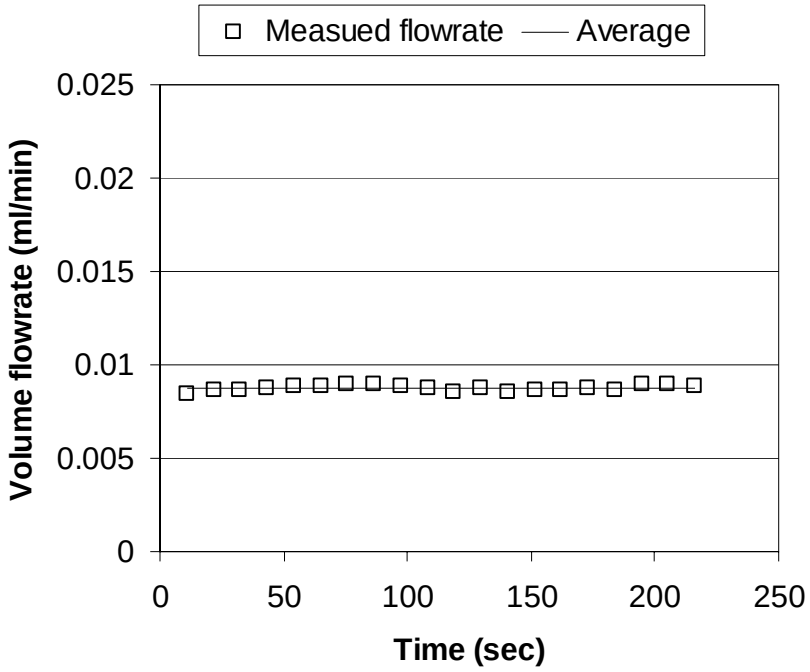

Fig. B-2. Volume flow rate calibration for wall shear rate 364 s^{-1}.

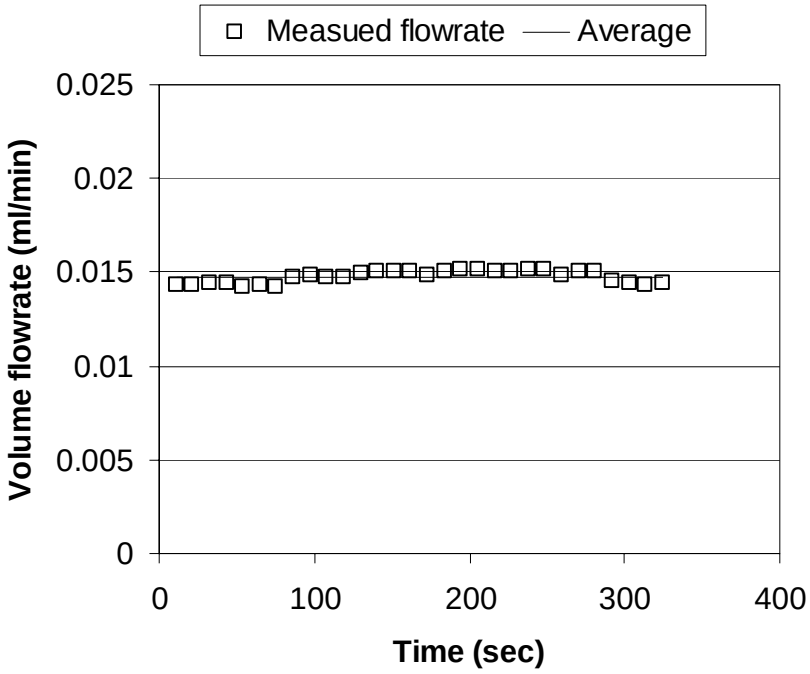

Fig. B-3. Volume flow rate calibration for wall shear rate 612 s^{-1}.

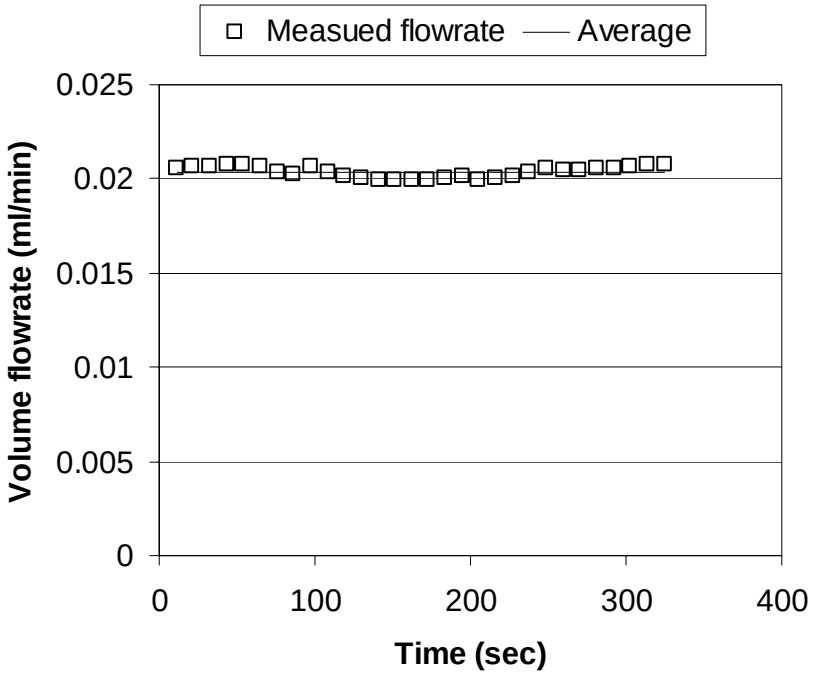

Fig. B-4. Volume flow rate calibration for wall shear rate 840 s^{-1}.

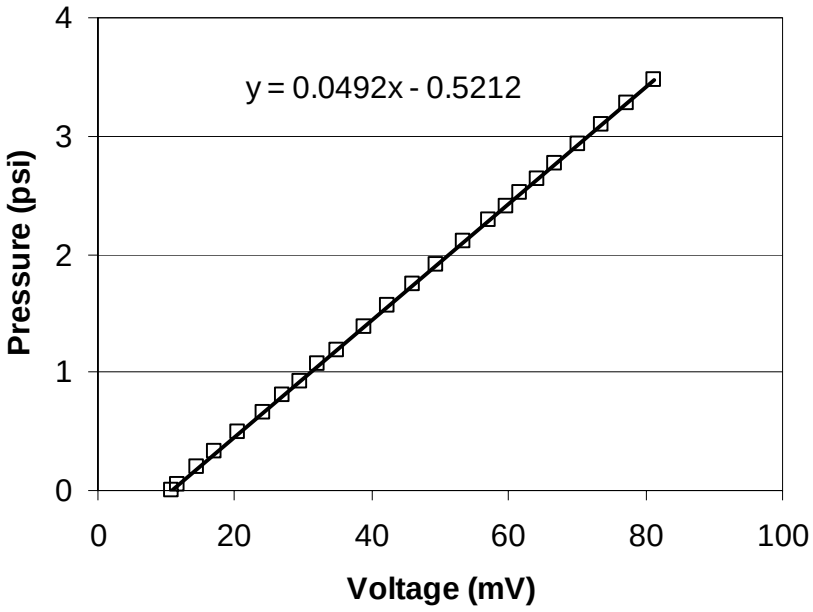

Fig. B-5. Pressure transducer calibration.

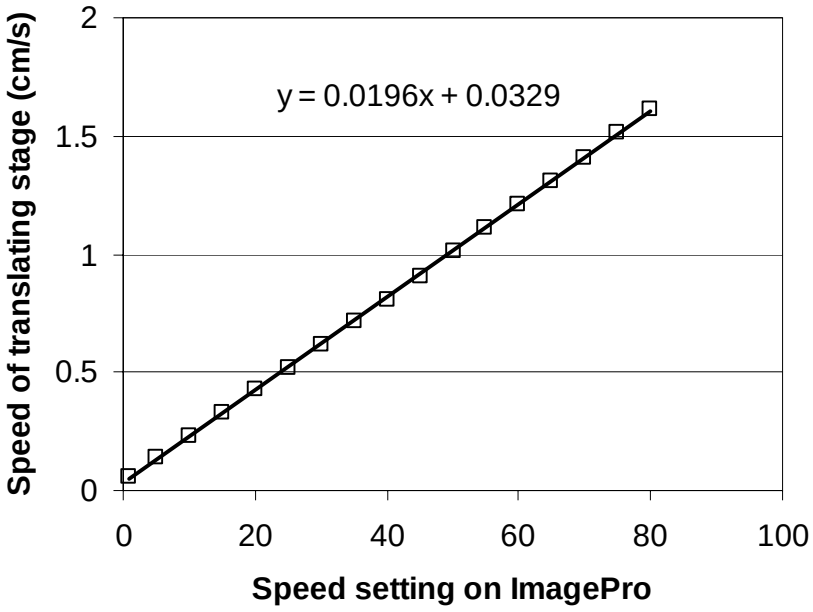

Fig. B-6. Translating-stage speed calibration.

APPENDIX C. Velocity Raw Data

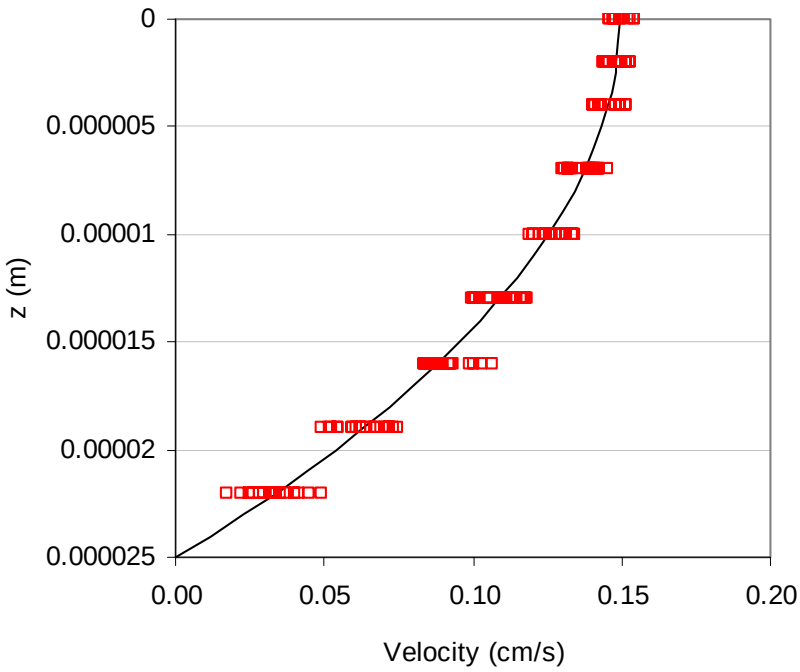

Fig. C-1. Water velocity profile at wall shear rate 120 s^{-1}.

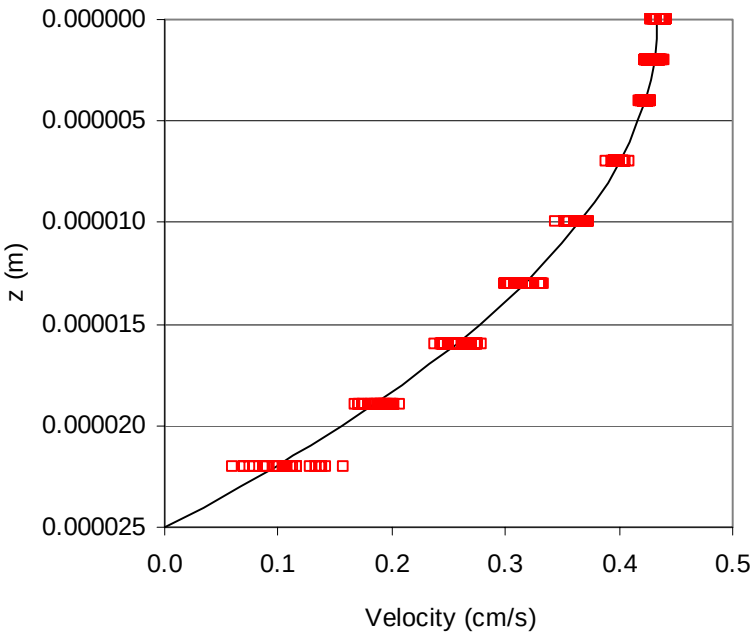

Fig. C-2. Water velocity profile at wall shear rate 350 s^{-1}.

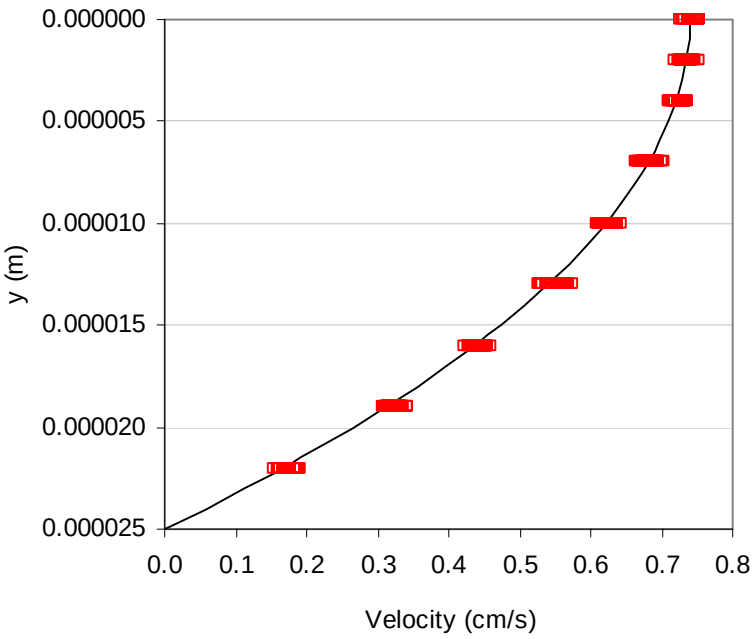

Fig. C-3. Water velocity profile at wall shear rate 590 s^{-1}.

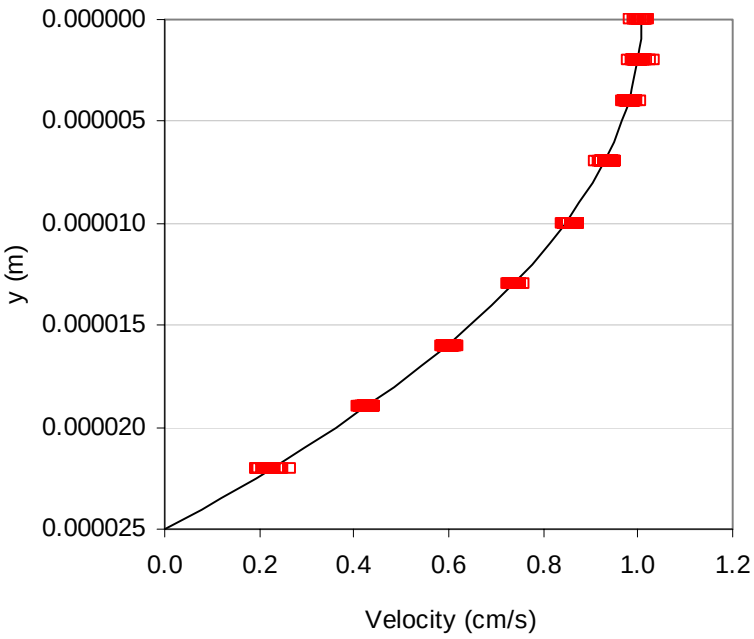

Fig. C-4. Water velocity profile at wall shear rate 815 s^{-1}.

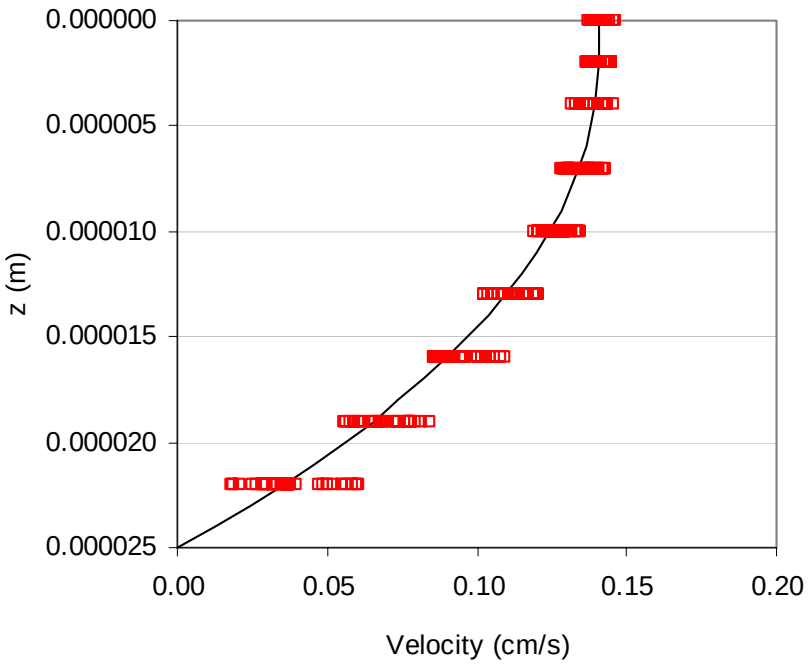

Fig. C-5. non-Newtonian Casson velocity profiles at wall shear rate 126 s^{-1}.

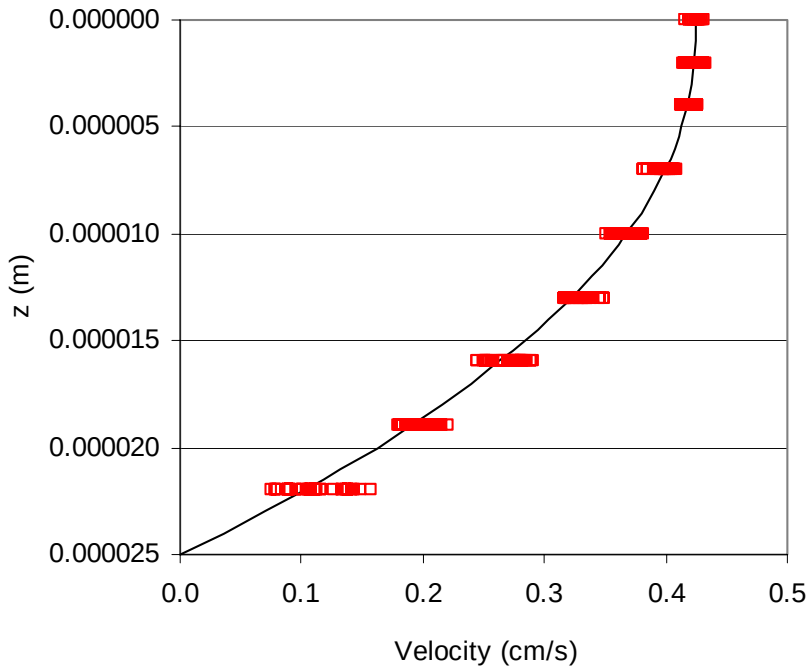

Fig. C-6. non-Newtonian Casson velocity profiles at wall shear rate 364 s^{-1}.

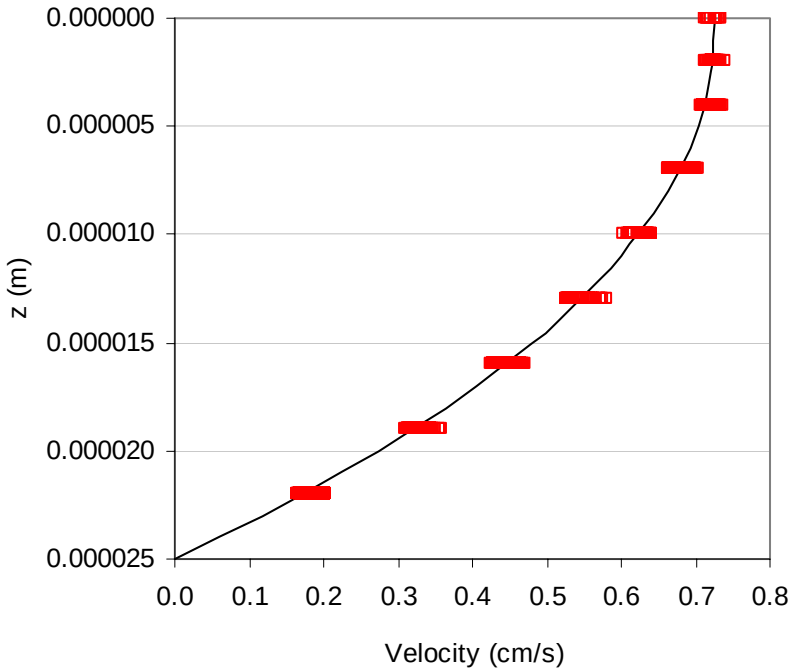

Fig. C-7. non-Newtonian Casson velocity profiles at wall shear rate 612 s^{-1}.

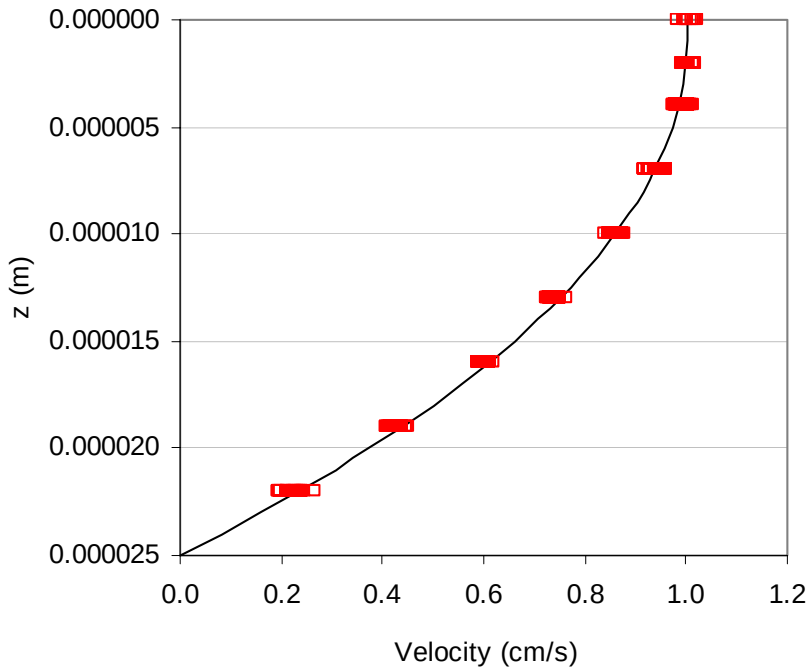

Fig. C-8. non-Newtonian Casson velocity profiles at wall shear rate 840 s^{-1}.

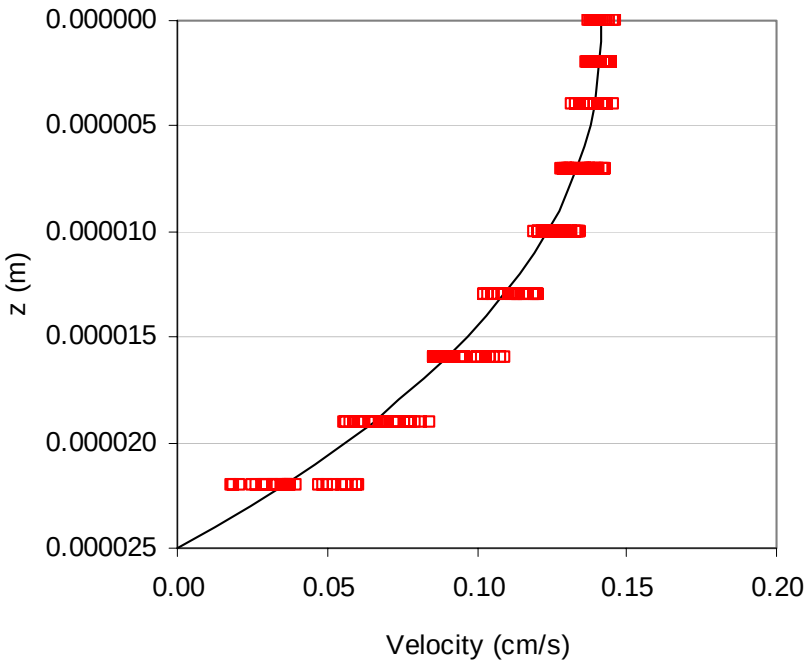

Fig. C-9. non-Newtonian Power-law velocity profiles at wall shear rate 127 s^{-1}.

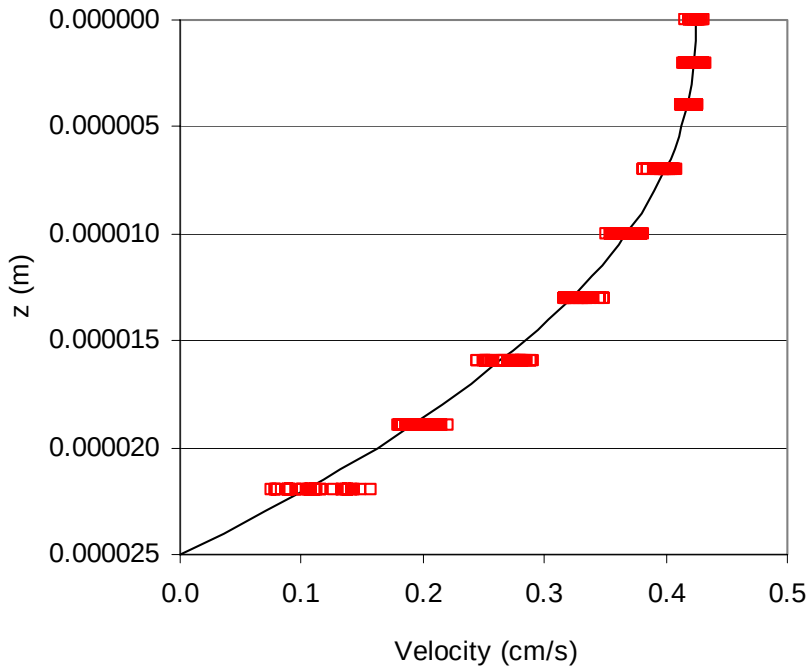

Fig. C-10. non-Newtonian Power-law velocity profiles at wall shear rate 363 s^{-1}.

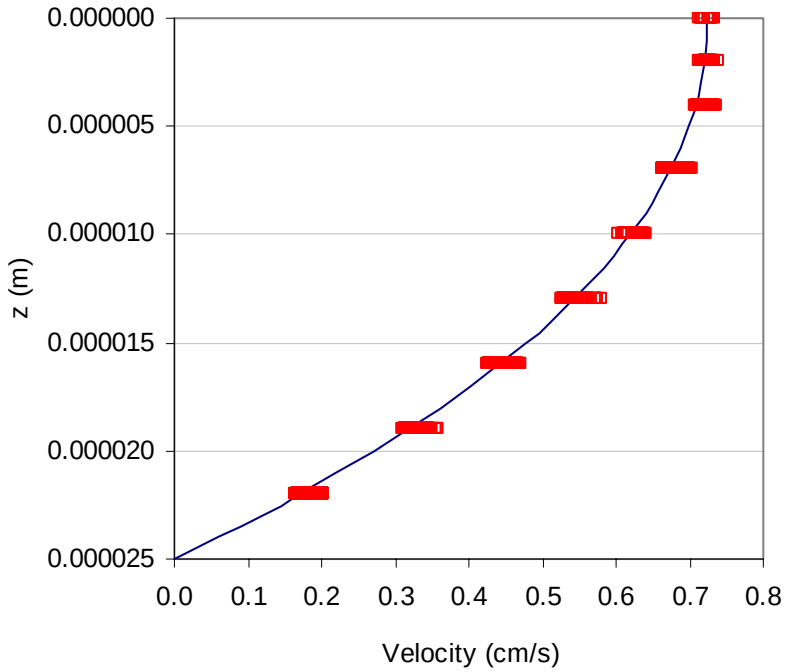

Fig. C-11. non-Newtonian Power-law velocity profiles at wall shear rate 612 s^{-1}.

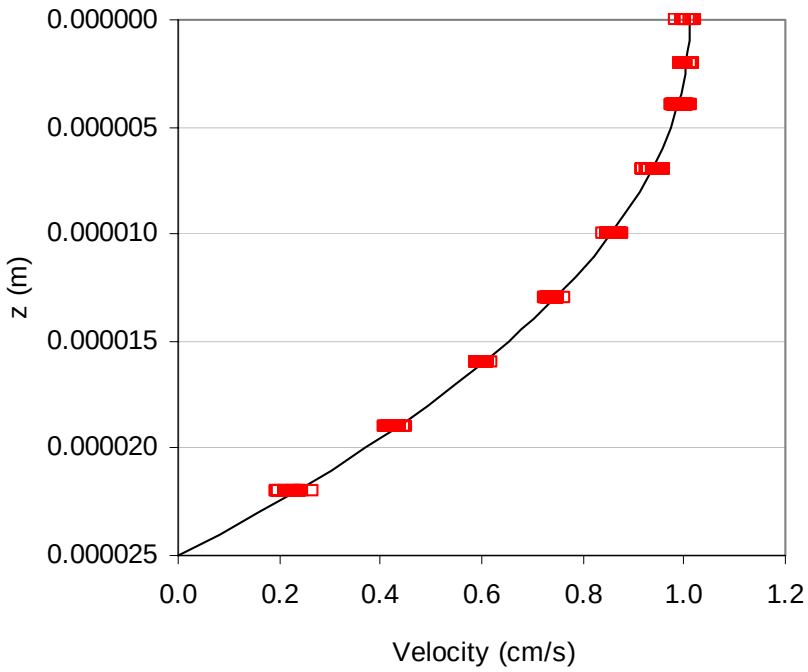

Fig. C-12. non-Newtonian Power-law velocity profiles at wall shear rate 827 s^{-1}.